

Ionization within a Plasma for the Purpose Investigating Space Propulsion and the Vasimr Plasma Rocket Engine

A project present to
The Faculty of the Department of Aerospace Engineering
San Jose State University

in partial fulfillment of the requirements for the degree
Master of Science in Aerospace Engineering

By

Jeffrey Meadows

May, 2016

approved by

Dr. Marcus Murbach
Faculty Advisor



Abstract

This paper investigates 2 key methods of ionization; Electron bombardment and RF bombardment, for plasma production in space as it relates to propulsion applications. The Paschen curve for air was measured experimentally and a 2mm wide region of <10% error was measured from those results. Ionization costs of between 8,000 and 15,000 electron Volts were calculated within the 2mm gap region. From these results, it was determined that electron bombardment could not provide efficient ionization for thrusting applications above 0.1 Newtons. From previously published data the ratio of ionization potential to atomic mass was determined to be a key design parameter limiting propellant selection to the noble gases. The elements specifically investigated were Argon, Xenon & Krypton. More importance was placed on investigating Argon owing to the abundance of previously published data. Furthermore, a novel solution was proposed relying on published data and experimental investigation, to fill the design space between VASIMR and ion/hall thrusters. The theoretical results of this solution are a thrust of 0.6 N operating on 25 kW of power at total efficiency of just 10%. A future experiment was proposed for investigating RF bombardment ionization efficiencies of the 3 elements to better estimate their ionization efficiencies within the Helicon antenna to improve this 10% total efficiency.

Table of Contents

Page

Introduction	8
1. Background	9
2. Brief History of	
2. Rocketry	1
1	0
Space	
Propulsion	1
3. Rocket	
3. propulsion	1
1	6
Chemical	
3. Propulsion	1
2	7
3.2.1 Solids, liquids &	1
hybrids	8
3.2.2 The Aerospike	2
nozzle	0
Nuclear	
3. Propulsion	2
3	1
Electric	
3. propulsion	2
4	2
3.4.1 The Ion	
thruster	2
VASIMR	
Engine	2
4. Plasma	5
4.1	
Plasma	2
4.2 Components of the VASIMR	2
engine	7
4.2.1 Propellant	
Ionization	2
4.2.2 Ion Cyclotron Resonance Heating	2
(ICRH)	8
4.2.3 Plasma acceleration within an expanding magnetic	2
field	9
Design Iterations on	
5. VASIMR	1
5. VASIMR iteration VX-	
1 10	3
5. VASIMR iteration VX-	
2 50	3
5.3 VASIMR iteration VX-	3
200	5
5.4 Mars Mission profile utilizing VASIMR	3
engines	9

7.	Discussion.....	5
3	5
8	Electromagnetism	5
8.	Investigation of charged particle trapping within the ICRH of VASIMR	6
1	modeled by a uniform magnetic field	5
8.	Investigation of charged particle trapping in a non-uniform magnetic field	5
2	BOOM	8
	Novel	
9	Design	6
	3
	9.1	
	Purpose	6
	3
9.	Novel Solution Design	6
2	Analysis	3
9.	Mission profile Design	6
3	process	5
	Novel solution	
9.	comparison	6
4	5
	9.4.1 Propellant	
	selection	6
	6
	9.4.2	
	Design	6
	6
	9.4.3	
	Solution	6
	6
	Conclusive	
	Remarks	6
10.	8
	10.1 Project	
	Conclusion	6
	8
	10.2 Future	
	Plans	6
	9
	Citations	6
11.	9

Table of Figures

[Figure 2.1 Chinese “arrows of flying fire”, such as might be expected to have been used at the battle of Kai-Keng.](#)

.....
[10](#)

[Figure 2.2 \(left\); Sir Isaac Newtown \[24\]](#)

.....
[11](#)

[Figure 2.3 left to right: Konstantin Tsoilkovsky \[24\], Robert Goddard \[25\], Hermann Oberth \[26\]](#)

.....
[11](#)

[Figure 2.4 The VfR, Society for Space Travel; from left to right: Rudolf Nebel, Franz Ritter, unknown, Kurt Heinisch, unknown, Hermann Oberth, unknown, Klaus Riedel \(holding the early version of the “Mirak”, Wernher Von Braun, unknown \[23\]](#)

.....
[12](#)

[Figure 2.5 \(2.1.5\); The V2 ballistic missile \[27\]](#)

.....
[13](#)

[Figure 2.6 Wernher Von Braun\(left\) \[26\], Sergei Korolev\(right\) \[27\]](#)

.....
[13](#)

[Figure 2.7 Juno 1 \(Jupiter-C\) rocket before its successful launch of the first US satellite in 1958 \(left\) \[28\]; The launch of Sputnik\(right\) \[30\]](#)

.....
[14](#)

[Figure 3.1Figure \(left\); The velocity step was set at 5,700 m/s; the approximate velocity budget of a Hohmann transfer from LEO to LMO, and iterated over MR values from 0.05 to 0.95. see appendix for details. \[Appendix A\]](#)

.....
[17](#)

[Figure 3.2 4. Figure \(3.2.1\) \(left\); combustion chamber and convergent-divergent rocket cross-section; from now on the subscripts for rocket nozzle parameters will be assigned according to this figure. P is pressure, T is temperature, v is velocity, and A is cross](#)

.....
[18](#)

[Figure 3.3 Figure 3.4 \(right\) Each contour is a successive burning surface for a fixed time step. \[3\]](#)

.....
[19](#)

[Figure 3.5Figure 3.6 low altitude \(left\) \[3\] and high altitude \(bottom\) aerospike operational schemes \[3\]](#)

21

Figure 3.7 (left); schematic of a nuclear pulse engine similar to the Orion project. [34]

.....
21

Figure 3.8 Schematic of an Ion Thruster [38]

.....
23

Figure 3.9 (left); Schematic of a Hall thruster [39]

.....
24

Figure 4.1 The experimental VX -200 rocket engine [5].

.....
25

Figure 4.2 (left); Thrust-test results for 16 run cases of various iterations of the VASIMR engine [6]

.....
26

Figure 4.3 VASIMR power flow diagram [40]

.....
27

Figure 4.4 (left); Helicon antenna with a quartz tube running through it. [2]

.....
28

Figure 4.5 (left); ICRH antenna. [43]

.....
28

Figure 4.6 Ambipolar acceleration in VX-200i exhaust field[5]

.....
30

Figure 5.1 (right); VX -10 design schematic from ASPL [40]

.....
31

Figure 5.2 (left); Performance parameters as functions of I_{sp} for Lithium, Helium, Deuterium, Hydrogen & other unnamed elements. The system efficiency η , the RF booster power partition f are dimensionless, the thrust F has units of Newtons [40]

.....
31

Figure 5.3 (left); plasma ion flux versus helium flow rate [40]

.....
32

Figure 5.4 VX-10 ion velocity exhaust distributions for 0,216 & 1444 W of RF booster power [40]

.....
33

Figure 5.5 (right); isotropic of the VX-50 showing key component parts and magnetic field flux as a function of distance along the thrusting axis [41]

.....
33

Figure 5.6 (left); The derivative of the RPA characteristic for three different ICRF power levels. This

indicates the ion energy distribution acceleration. Preliminary impact target experiments confirm a significant momentum flux in the flow due to the action of

.....
34

[Figure 5.7 a\) ICRF antenna plasma loading measurements for a range of frequencies, 4 MHz at the center of the antenna. Indicates the loading point where high power was applied. b\) Antenna circuit efficiency for coupling power to the plasma, exceeding 90 %.](#)

.....
[35](#)

[Figure 5.8 \(left\); optimization of ionization cost versus RF power input \[42\]](#)

.....
[36](#)

[Figure 5.9 Schematic of the test section from the 2011 analysis. \[44\]](#)

.....
[36](#)

[Figure 5.10 \(left\) force density measured as a function of radial distance. \(right\) confirmation of the linear relationship between total power and total thrusting force. \[44\]](#)

.....
[37](#)

[Figure 5.11 Thrusting efficiency as a function of power ratio\(a\) and as a function of specific impulse \(b\).](#)

[Figure b uses a superimposed, least-squares fit. \[44\]](#)

.....
[38](#)

[Figure 5.12 \(left\)\); Mission duration I_Sp profile \[43\]](#)

.....
[39](#)

[Figure 5.13 mission duration I_sp profile \[43\]](#)

.....
[40](#)

[Figure 5.14 Mission profile for the CTV \(left\), 7 day spiral orbit Martian capture of the CTV\[43\]](#)

.....
[40](#)

[Figure 5.15 Two abort mission profiles for aborts on days 8 and 9 respectively. \[43\]](#)

.....
[41](#)

[Figure 6.1 Theoretical Paschen curves for various elements \[49\].](#)

.....
[45](#)

[Figure 7.1 my own experiemental apparatus set up, for a gap of 3 mm](#)

.....
[51](#)

[Figure 7.2 theoretical Paschen prediction, atmospheric air. The linear fit equation \$V_{bd}=3363*d+2319\$ was solved for in matlab utilizing \$y=mx+b\$ to generate the linear fit curve.](#)

.....
[52](#)

[Figure 7.3 measurement oscilloscope for vreakdown voltages. Equipment owned by L3 communications.](#)

[53](#)

[Figure 8.1 Result of equation 6.5.1 simulated in MATLAB for a uniform magnetic field of .05 Tesla](#)

.....
[57](#)

Figure 8.2 XZ plane results beginning at the origin and progressing in the positive x direction with constant x velocity.....**Error! Bookmark not defined.**

Figure 8.3 Simulation Isometric View.....**Error! Bookmark not defined.**

Figure 9.1 Results of equations 8.2 & 8.3. Plot taken from appendix. This figure is a display of the power cost as a function of the ionization cost of the propellant.....**Error! Bookmark not defined.**

Figure 9.2 modification of the design space of figure 9.1 around the estimated parameters; thrust = 0.8

N, m_i propellant= .679E-4,.....**Error! Bookmark not defined.**

NOMENCRALTURE

μ_0 magnetic field	
	Effective exhaust velocity
d	gap distance
	Velocity step
E	electric field
	Thrusting force
G gravitational constant ($9.81 \text{ / } ^2$)	
ICRF	Ion Cyclotron Radio Frequency emitter (aka ICRH)
ICRH	Ion Cyclotron Resonance Heating
ISS	International Space Station
	specific impulse
	total impulse
j	current
LEO	Low earth orbit
LMO	Low mars orbit
	final stage mass
	initial stage mass
	stage propellant mass
	Ratio of wet to dry, stage masses
	equilibrium ion density
n	perturbed ion density
1 Helicon power	
2 ICRH power	

.....power dissipated

RF..... Radio Frequency

..... anode/cathode electron transit time

T kinetic energy

U potential energy

..... average anode/cathode electron transit velocity

Wpower required for each electron pair

..... electron cyclotron frequency

1. Introduction

The purpose of this paper is for the experimentation and potential development of a magneto-plasma rocket engine for satellite orbit maintenance. Since the only company developing electrodeless plasma propulsion is VASIMR, its history and test data are central to this report. This paper discusses the Variable Specific Impulse Magneto Plasma Rocket engine (VASIMR) and provides necessary background on rocketry history and rocketry principles in order to show the need for VASIMR in terms of deep space propulsion. This paper also attempts to show the logical flow of space craft design from chemical combustion through to electric propulsion in order to explain the necessity of the latter. This investigation will culminate in a novel solution to the electric propulsion regime between 0.1 and 6 Newtons.

2. Background

2.1 Brief History of Rocketry

Although the action-reaction principle which serves as the basis of rocketry can be found as far back as 500 B.C in which directed steam vapor was the primary propellant to drive a spinning metal sphere to rotate about a singular axis. The first instance of modern rocketry comes from China and the year 1232 A.D; when, during the battle of Kai-Keng, the Chinese were able to fight off a Mongolian army by using a barrage of, “arrows of flying fire”. These devices were extra-long arrows which had attached to them bamboo tubes which were capped off at one end and filled with a sulfur-charcoal base propellant. These devices, once ignited, would then be propelled by the expanding gases from the open end of the tube; effectively creating the first solid-propellant fueled rockets. [20]



Figure 2.1 Chinese “arrows of flying fire”, such as might be expected to have been used at the battle of Kai-Keng.

By the 13th century rockets had spread to Europe where they were used mainly in military applications. Experimentation in Europe resulted in improvements to the solid propellant (gunpowder) for the purpose of increasing range although gunpowder itself comes from Asia. It was eventually discovered that accuracy could be improved by providing a tube within which the rocket could begin burning, yet this development was still not enough to produce a military advantage. Rockets gradually fell into disuse in the military theatre since their introduction to Europe because of their inefficiency as a killing weapon. However, scientific experimentation did not cease due to the popularization of fireworks. In the 16th century a German Firework maker named Johann Schmidlap invented the, “step rocket” which was the first documented time a multi-stage rocket was used for anything. It consisted of two rockets, a small one on top of a larger one and when the large one burnt out the smaller one would ignite and carry the explosive firework to greater altitudes; and thus the modern Multistage launch vehicle was born. [20]

Sir Isaac Newton is responsible for the modern scientific aspect of rocketry. Newton proposed, after his publication of *Philosophiæ Naturalis Principia Mathematica* (Mathematical principles of natural philosophy) and as a theoretical extension of it, that if you were to launch a cannon ball from the top of the earth, and parallel to the ground at that point, it would travel some distance before eventually hitting the ground. Yet, if launched faster it would travel further, and if the launch velocity were continually increased (and friction were ignored) eventually the falling path of the object would mirror the curvature of a spherical earth, and so theoretically the object would continually “fall” around the earth. In this theoretical experiment, Newton brought the dream of space travel into the realm of mathematics and science. In addition, Newtons’ three laws of motion explain the action-reaction principle which identifies how rockets could work in the vacuum of space [20].



Figure 2.2 (left); Sir Isaac Newtown [24]

Even with hundreds of years of development leading to advancements in rocketry accuracy for the purposes of war rockets were finally phased out with the development of the rifled barrel and exploding cannon rounds which proved to be far more effective killing mechanisms. It was not until 1898 that a Russian professor named Konstantin Tsoilkovsky proposed the concept of space exploration by rocket, and in 1903 he published a report suggesting the use of liquid propellants in order to achieve greater range. Tsoilkovsky correctly recognized that, “the velocity and range of a rocket were only limited by the velocity of the exhaust gases”. Tsoilkovsky died in 1935 and has since been called the father of modern Astronautics for his research and vision [20].

Meanwhile In the early 20th century in the United States, the American Robert Goddard became interested in achieving greater altitudes than were possible for lighter-than-air balloons. During testing with solid propellant rocket engines, Goddard became convinced that much greater exhaust velocities could be achieved by using liquid propellants. On March 16, 1916 Goddard conducted the first successful test flight of a liquid fueled rocket engine which used liquid oxygen and gasoline and flew for 2.5 seconds, reaching a height of 12.5 meters. In subsequent flights Goddard employed gyroscopes for flight path control and employed the use of a parachute for safe return of scientific instruments. Goddard is today recognized as the father of modern rocketry.

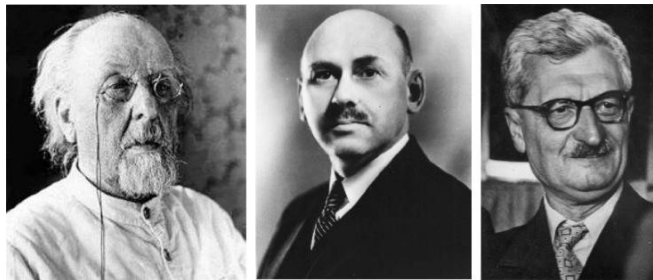


Figure 2.3 left to right: Konstantin Tsoilkovsky [24], Robert Goddard [25], Hermann Oberth [26]

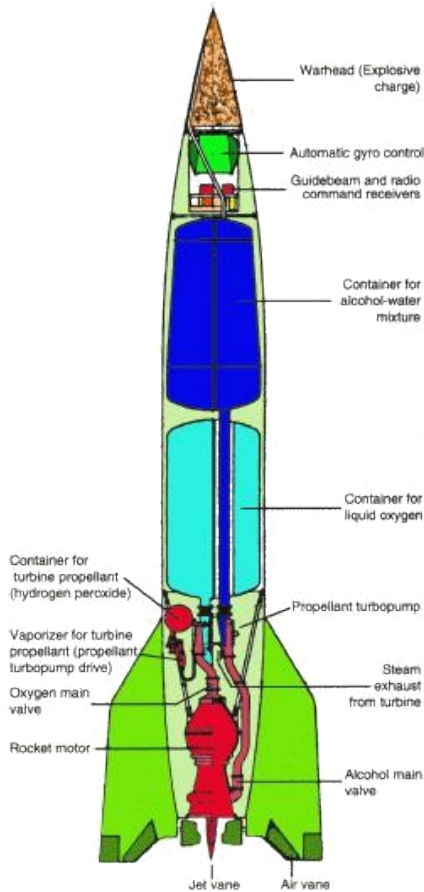
Possibly inspired by the liquid fuel developments of Goddard a few years earlier or possibly inspired by the liquid propellant theories of Tsoilkovsky; in 1923 a Transylvanian Scientist named Hermann Oberth published a book entitled, “*Die Rakete zu den Planetenräumen*” (The Rocket into Planetary Space) which received wide publication across post-war Europe and is credited with inspiring the formation of many rocketry societies therein [21]. One of these societies was called the Verein fur Raumschiffahrt (VfR, Society for Space Travel), founded in 1927 by church administrator Johannes Winkler. Beginning in 1930 several members of VfR conducted liquid-fueled rocket tests until in 1934 the Nazi government closed the testing facility located in Berlin [22]. During its time of operation, the society advanced liquid rocket propulsion experimentation in the interest of reaching ever greater altitudes; yet perhaps the most important thing the society did was introduce a 19-year-old Wernher von Braun to the military who were so impressed by him that he was invited to do his graduate thesis on chemical rocket propulsion at Kummersdorf [22].



Figure 2.4 The VfR, Society for Space Travel; from left to right: Rudolf Nebel, Franz Ritter, unknown, Kurt Heinisch, unknown, Hermann Oberth, unknown, Klaus Riedel (holding the early version of the "Mirak", Wernher Von Braun, unknown [23]

In 1937 German scientists, including Von Braun and Oberth, assembled at Peenemunde to develop the V-2 under the directorship of Von Braun. The V-2 was the first supersonic ballistic missile to be mass produced and used during war [20]. The V-2 ("A-4", as it was known in Germany) was fueled on liquid Oxygen and alcohol which it consumed at ≈ 1000 g/s. So, it was small by today's standards yet had a modest range of 320 km and a maximum velocity of $1,600$ m/s ($h \approx 4.7$). The development of the V-2 was the first step in a major turning point in modern warfare. It was the beginning of ballistic missile development and production. After the development of nuclear weapons, it would become the deadliest weapon mankind has ever produced. The V-2 was a single-stage liquid rocket that had a warhead on top and fuel and oxidizer tanks below, respectively. It operated a turbine powered compressor on the monopropellant hydrogen peroxide. A schematic is pictured below in figure (2.1.5).

By the end of the failed German siege of Stalingrad in 1942, it was a forgone conclusion that Germany was eventually going to lose the war. FDR and Churchill knew, after their meeting with Stalin at the Tehran conference in December 1943, that conflict with the USSR would become inevitable after the fall of Germany as the presiding governments fought over the nature of governance that would develop in post-war Europe. From the Russian perspective, so much treasure and blood was spent defending themselves and reconquering half of Europe with little assistance from the US or the UK that they believed they should be rewarded for this effort with control over the newly conquered European territories such as Poland, Lithuania, Romania, Austria and Germany, while France and Belgium could be left to the directorship of the US and the UK. From the American perspective, a communist Europe did not promise economic, social or domestic security at home; and thus, the cold war began. This bit of history is important because this conflict is the only reason development of the science of rocketry was funded by government.



German V-2 (A-4) Missile

Figure 2.5 (2.1.5); The V2 ballistic missile [27]

It was because of the development of the V-2 that both the USSR and the United States realized the strategic importance of rockets as a military weapon and so at the end of WW2 both countries tried to capture as many rocket scientists as each could. The two competing premier rocket scientists of the time were Wernher von Braun for the United States and Sergei Korolev for the USSR. Wernher Von Braun surrendered to the Americans and in addition to being allowed to come to the United States, his past as a NAZI party member of the SS was forgiven on the condition that he build rockets for the US Government. Sergei Korolev spent the war in the Gulag, a sort of Russian work camp for political enemies and anyone unlucky enough to be deemed a danger to the government. Even though the two men never met (Von Braun never learned Sergei Korolev's name) they spent their adult lives competing with one another on the national stage; first, to get to space and then to put a man on the moon.

On October 4th, 1957, the USSR announced that it had successfully placed a man-made satellite into orbit around the earth with the launch of the Russian modified R-7. The satellite, named "Sputnik", got its unique shape from an issue that arose when various scientific organizations provided so many instruments that the payload became too heavy make it into orbit, and so Korolev's satellite design team stripped all scientific equipment and placed a simple transceiver and a small

battery which weighed just 83 kilograms within an aluminum ball [29]. Sputnik was delivered into low earth orbit (LEO) where it continued to transmit a steady stream of beeping noises for 21 days until it finally burnt up in the earth's atmosphere after a total of 3 months in orbit. Then, less than a month later than Sputnik 1's launch, the Russians launched Sputnik 2, which was even larger than sputnik 1 and carried the first dog into space. [31].



Figure 2.6 Wernher Von Braun(left) [26], Sergei Korolev(right) [27]

The R7 which delivered Sputnik's 1 & 2 is a massive rocket consisting of 4 strap-on boosters and a two-stage main-rocket. The News of a Russian satellite reaching orbit shocked the rest of the

democratic world. The fact that an “adversary” such as the USSR could have achieved this feat first freighted many people in a world which largely believed it was on the brink of nuclear war. As a consequence of the successful Russian launch the United States finally approved Von Braun’s team to develop the Jupiter-C for satellite delivery (a task which they had already secretly done). After the failure of the Navy’s Vanguard rocket Von Braun’s Redstone rocket program launched, on January 31st 1958, the Jupiter-C (renamed Juno-1), a relatively small two-stage rocket, successfully delivering the Explorer 1 satellite into earth orbit. The Explorer 1 had a mass of only 13.97 kg which was a requirement because of the small size of the Juno 1 rocket. Yet still, the satellite was able to carry a Geiger-Mueller Detector, for the purpose of detecting cosmic rays. The Jupiter-C was also the first rocket to launch and subsequently successfully test an ablative nose-cone upon reentry. This meant that for the first-time objects launched into space could be returned safely [28].

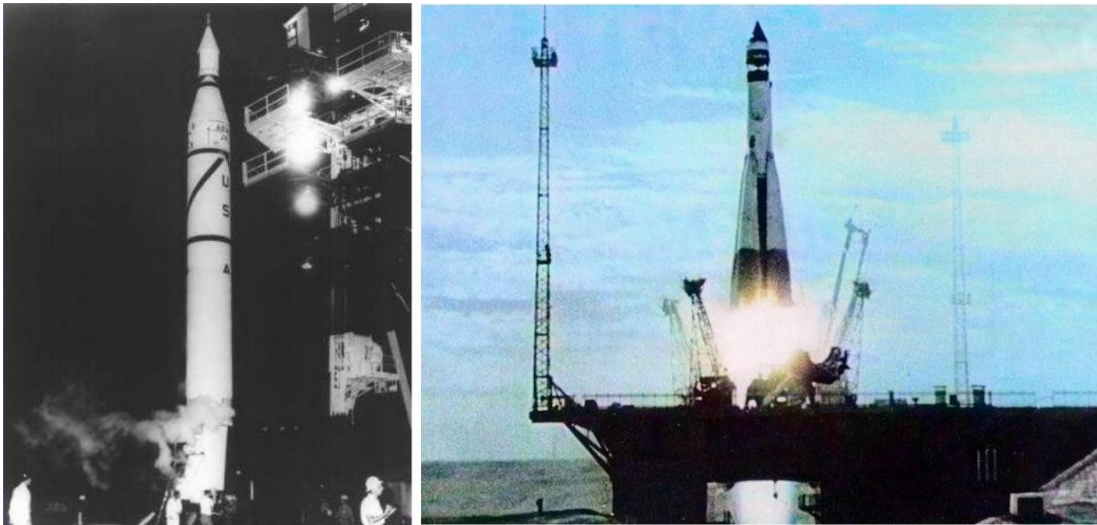


Figure 2.7 Juno 1 (Jupiter-C) rocket before its successful launch of the first US satellite in 1958 (left) [28]; The launch of Sputnik(right) [30]

At this point it is necessary to introduce the concept of specific impulse defined below, where v_e is the exhaust velocity of the combustion products, g_0 is 9.81 m/s^2 and \dot{m} is the mass flow rate of the propellant.

$$I_{sp} = v_e / g_0 \quad (2.1.1) [3]$$

$$I_{sp} = \frac{F}{\dot{m} g_0} \quad (2.1.2) [3]$$

The limiting factor in the production of thrust, as noted by Tsoilkovsky 50 years earlier, is the exhaust velocity of the propellants. This property can be measured and is also defined as the product of the acceleration of gravity and the specific impulse of a rocket engine (I_{sp}). So intuitively, if the I_{sp} is increased then the exhaust velocity and thus the thrust (F) are likewise increased. This relationship serves as part of the foundation of rocket design and development in that it is used to size a rocket for a specific payload. When combined with the rocket equation (2.1.3), below, it becomes clear that the I_{sp} of a rocket serves as the corner stone of the entire rocket development.

$$\Delta v = \frac{v_e}{I_{sp}} \ln \left(\frac{m_0}{m_f} \right) \quad (2.1.3) [3]$$

The equation above relating thrust (F) and is derived from the basic momentum equation laid out by Newton's third law. This equation means two things; first, that mass flow rate is linearly proportional to thrust, and second that is also linearly proportional to thrust. Intuitively, this relationship provides two means of increasing thrust. Either increase the quantity of mass flowing out of a given nozzle per unit time or increase the velocity the given mass which is exiting that nozzle. The mass flow rate of a given rocket is limited by the ability of the rocket nozzle materials to withstand the temperatures of combustion and confinement in the throat region of the nozzle. For this reason, increasing the specific impulse of the reactants has been the main focus of rocket propulsion research. The table below shows comparisons of various propellant-oxidizer combinations and their approximate . From this table, it is apparent that the best is occurs when Fluorine is combined with liquid Hydrogen.

Table 2.1 various oxidizer-fuel configurations [3]

Oxidizer	Fuel	Mixture Ratio		Average Specific Gravity	Chamber Temp. (K)	Chamber c^* (m/sec)	SR (kg/mol)	I_s (sec)		k
		By Mass	By Volume					Shifting	Frozen	
Oxygen	Methane	3.20	1.19	0.81	3526	1835			296	
		3.00	1.11	0.80	3526	1853		311		
	Hydrazine	0.74	0.66	1.06	3285	1871	18.3		301	1.25
		0.90	0.80	1.07	3404	1892	19.3	313		
	Hydrogen	3.40	0.21	0.26	2959	2428	8.9		389.5	1.26
		4.02	0.25	0.28	2999	2432	10.0		285.4	
	RP-1	2.24	1.59	1.01	3571	1774	21.9		300	1.24
UDMH	2.56	1.82	1.02	3677	1800	23.3		295	1.25	
Fluorine	Hydrazine	1.39	0.96	0.96	3542	1835	19.8			
		1.65	1.14	0.98	3594	1864	21.3	310		
	1.83	1.22	1.29	4553	2128	18.5	334		1.33	
	2.30	1.54	1.31	4713	2208	19.4		365		
	Hydrogen	4.54	0.21	0.33	3080	2534	8.9		389	1.33
Nitrogen tetroxide	Hydrazine	7.60	0.35	0.45	3900	2549	11.8	410		
		1.08	0.75	1.20	3258	1765	19.5		283	1.26
	1.34	0.93	1.22	3152	1782	20.9	292			
	50% UDMH- 50% hydrazine	1.62	1.01	1.18	3242	1652	21.0		278	1.24
	RP-1	2.00	1.24	1.21	3372	1711	22.6	289		
Red fuming nitric acid	MMH	3.4	1.05	1.23	3290		24.1		297	1.23
		2.15	1.30	1.20	3396	1747	22.3	289		
	1.65	1.00	1.16	3200	1591	21.7		278	1.23	
	RP-1	4.1	2.12	1.35	3175	1594	24.6		258	1.22
	4.8	2.48	1.33	3230	1609	25.8	269			
Hydrogen peroxide (90%)	RP-1	1.73	1.00	1.23	2997	1682	20.6		272	1.22
		2.20	1.26	1.27	3172	1701	22.4	279		

Notes:
 Combustion chamber pressure—1000 psia (6895 kN/m²); nozzle exit pressure—14.7 psia (1 atm); optimum expansion.
 Adiabatic combustion and isentropic expansion of ideal gas.
 The specific gravity at the boiling point was used for those oxidizers or fuels that boil below 20°C at 1 atm pressure.
 Mixture ratios are for approximate maximum value of I_s .

Sergei Korolev knew this yet neither he nor Von Braun decided to go with Fluorine as an oxidizer because it is extremely toxic and reactive. Fluorine will react with anything willing to give it a spare electron including even water molecules in the air at sea level. Obviously, this is significantly problematic for storage and transportation of the oxidizer. The next best oxidizer-fuel combination is liquid hydrogen and liquid oxygen which has an approximate of 389.5 seconds, according to the table above. Liquid oxygen is very reactive, but not as much so as liquid fluorine, in addition it does not produce toxic fumes and is easier to transport and store for moderate periods of time of 2 weeks. So, for instances when very large amounts of thrust are required and volume considerations are not a limiting factor, liquid Oxygen and liquid Hydrogen are typically the chosen propellants. The issue many rocket designs have with using liquid hydrogen is that it has a specific gravity of 26 % that of water meaning that it's energy content per volume is much lower than most other fuels. In cases where volume is a critical parameter RP-1 might be used because it's specific gravity is slightly greater than that of water. However, typically a parametric study will need to be done between RP-1, methane and hydrazine fuels around the thrusting, volumetric and velocity requirements for each rocket and each engine to determine the optimum oxidizer-fuel combination.

Chemical methods of propulsion have been pushed to their limit to get a man to the moon in 1969 and then to deliver rovers carrying imaging and scientific equipment to the surfaces of Mars and Venus in the decades that have followed. In the progress of these great achievements it has become clear that in order to get payloads as large as 150,000 kg into interplanetary space more efficient methods of space travel will have to be employed.

3. Space Propulsion

3.1 Rocket propulsion

While Newton's third law serves as the guiding principle of rocket propulsion, the rocket equation which is derived from it is still regarded as the key to rocket development.

$$\Delta v = c \ln \left(\frac{m_0}{m_f} \right) \quad (2.1.3)[3]$$

Equation 2.1.3 is appropriate for single stage rockets since it only outlines one mass ratio. This section of the report concerns interplanetary travel using only chemical propulsion and so for the purposes of this report the more general, multi-stage, form of the rocket equation is appropriate. Equations 3.1.1, and 3.1.2 are the general form of the rocket equation in explicit and in suffix notation, respectively. The terms are the effective exhaust velocities of the individual stages, the mass ratios of the individual stages and 'n' is the number of stages. There are two common ways of solving this equation. The first controls the design so that the individual stages have the same mass. This method is appropriate for rockets designed for mass production applications where the mass of propellant is not so critical; simplifying the manufacturing process. The second method is to fix the mass ratios so that they are all equal ($r_1 = r_2 = r_3 \dots$). This second method is appropriate for larger rockets because it serves as an optimization of a rocket's mass about its payload mass and is hence the most efficient method, but more expensive to build.

$$\Delta v = v_1 \ln \left(\frac{m_0}{m_1} \right) + v_2 \ln \left(\frac{m_1}{m_2} \right) + v_3 \ln \left(\frac{m_2}{m_3} \right) + \dots \quad (3.1.1)[3]$$

$$\Delta v = c \ln \left(\frac{m_0}{m_f} \right) \quad (3.1.2)[3]$$

Space exploration revolves around the exchange of momentum between a spacecraft and its chosen propellant. This means that the faster a propulsion system can eject mass in a given direction the more total thrust will be generated in the opposite direction and the further, and faster, a given spacecraft can travel. The ejection of mass in space propulsion is a function of many design properties of a rocket engine in relation to its utilization of propellant. However, generally speaking these things are: the molecular chemistry of the propellants, the temperature of the exhaust gases (hotter gases expand at faster rates thus generating more thrust) and the combustion pressure of the reactants.

All of these characteristics ultimately result in an effective exhaust velocity of the gas as it exits the rocket nozzle and this is incorporated in to the rocket equation as, 'c'. When this value of c is multiplied by the acceleration of gravity g_0 , the result is an important property called specific impulse

(Δv), (measured in seconds), previously defined by equation 2.1.1 and further defined by equation 3.1.3, below.

$$I_{sp} = \frac{F_{thrust}}{m_0 g_0} \quad (3.1.3) [3]$$

The purpose of the rocket equation is to relate the efficiency of a given rocket engines' exchange of momentum and a desired change in velocity to determine the required mass ratio to accomplish the task. Thus, the rocket equation provides approximate quantities of fuel necessary to meet whatever the mission requirement may be. The best way to increase the velocity of the payload and/or the size of the payload in proportion to the rest of the rocket, is to increase the Specific impulse, I_{sp} , of the rocket. Equations 3.1.3 through 3.1.6 are combined to form equation 3.1.7, which is an explicit expression for in terms of for a single stage rocket.

$$\Delta v = I_{sp} g_0 \ln \left(\frac{m_0}{m_f} \right) \quad (3.1.4) [3]$$

$$m_0 = \frac{m_f}{\left(\frac{\Delta v}{I_{sp} g_0} \right)^{-1}} \quad (3.1.5) [3]$$

$$m_0 = m_f \left(\frac{I_{sp} g_0}{\Delta v} \right)^{-1} \quad (3.1.6) [3]$$

$$MR = \frac{m_0}{m_f} = \left(\frac{I_{sp} g_0}{\Delta v} \right)^{-1} \quad (3.1.7) [3]$$

The result of equation 3.1.7 is represented graphically by figure 3.1.1, directly below, in order to demonstrate the relationship between increasing I_{sp} and mass ratio. The velocity step somewhat arbitrarily selected as 5,700 m/s, since that is the required velocity step to complete a Hohmann transfer from 300 km earth altitude to 300 km Martian altitude.

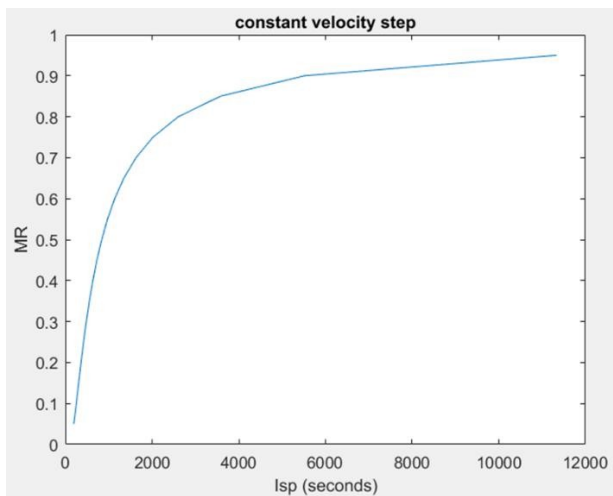


Figure 3.1.1 (left); The velocity step was set at 5,700 m/s; the approximate velocity budget of a Hohmann transfer from LEO to LMO, and iterated over MR values from 0.05 to 0.95. see appendix for details. [Appendix A]

3.2 Chemical Propulsion

The limit of chemical propellant is less than 500 seconds and values above 400 seconds are only typically observed in a vacuum environment with the obvious exception being for Liquid Fluorine & liquid Hydrogen. This creates a problem if you want to go further into space because as you add fuel to a rocket you increase the mass of that rocket thus increasing further the amount of fuel required. If you instead add stages to the rocket, then the amount of payload you can deliver to some specific velocity and altitude in space gained per stage decreases exponentially. Intuitively from figure 3.1.1 it can be observed

that for an of 400 seconds the corresponding is somewhere around 0.15. This means that the mass of the payload maxes out at about 15% of the mass of the total rocket forcing either the payload to be very small or the rocket to be very large. Adding stages to the rocket can increase in the vicinity of 30%, however when more than three stages are added the benefit per stage drops to less than 2% for that 4th stage and cost begins to outpace effectiveness [3]. These percent changes are variable and are functions of the velocity change required for the orbital maneuver.

The difficulties related to relatively inefficient fuel consumption associated with low values less than 500 seconds, have been the subject of much research and innovation. One issue with the convergent-divergent nozzle section shown below in figure 3.2.1 is that it does not allow for consistent ideal expansion (the condition where $p_2 = p_3$) of the flow exiting the nozzle. In other words, p_2 will only be equal to p_3 (atmospheric pressure) for one specific altitude where that happens to be the case. This reality is addressed by the Aerospike nozzle covered in section 3.2.2.

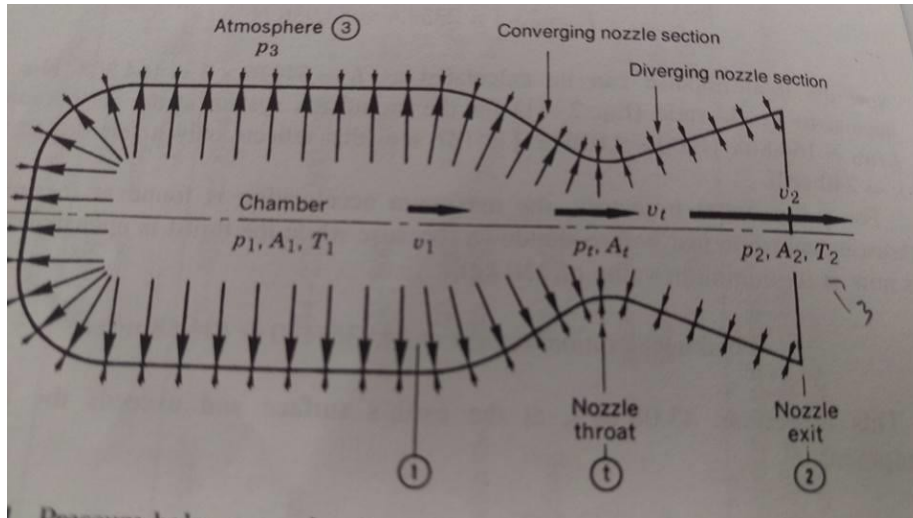


Figure 3.2 4. Figure (3.2.1) (left); combustion chamber and convergent-divergent rocket cross-section; from now on the subscripts for rocket nozzle parameters will be assigned according to this figure. P is pressure, T is temperature, v is velocity, and A is cross

3.2.1 Solids, liquids & hybrids

Solid propellant of a sulfur base was the first rocket propellant and was mentioned in chapter 2. As mentioned it dominated the field of rocketry until the early 20th century when experiments with liquid propellants yielded greater range and increased dynamic controllability. Today solid propellants are used mostly in smaller rocket applications such as weapons delivery systems and smaller rockets for delivering satellites to LEO. They are also the preferred propellant of booster rockets. This is because, even though the typical range of solid propellants places them mostly below 300 seconds (See figure below), they are still widely preferred for their increased reactive stability, reduced expense and superb storage capability. Not only do solid propellants store better but because of their simplistic design there is some reduced risk during launch as well as illustrated by the subsequent figure 3.2.1.1.

Solid propellant fueled rocket engines have a 98.7% success rate as compared with a 97.7 % success rate for liquid fueled engines in the United States. Internationally the failure rate of solids is 2.27 % compared with 2.72 % for liquids.

Table 3.1 Table 3.1 Figure (3.2.1.1); comparison of solids and liquids in terms of failure rate during launch [33]

Country	Propulsion			
	Solid		Liquid	
	Succ	Fail	Succ	Fail
USA	462	6	518	12
CIS/USSR	6	0	1557	41
Europe	101	0	173	9
China	0	2	95	3
Japan	54	2	37	2
India	19	1	15	0
Israel	5	1	0	0
Brazil	0	2	0	0
N. Korea	0	1	0	0
Total	647	15	2395	67
80-08 (%)	97.73		97.28	

In a solid propellant rocket a primary design feature is the grain configuration. The goal of a grain configuration is to allow the fuel to burn in a manner which does not rapidly increase the empty volume of the propellant chamber, since this chamber also serves as the combustion chamber a larger chamber would mean a lower combustion pressure resulting in a loss of thrust with time. This is achieved by choosing grain configurations such as the one below which reduce the change in burning surface area to less than 15% [3].

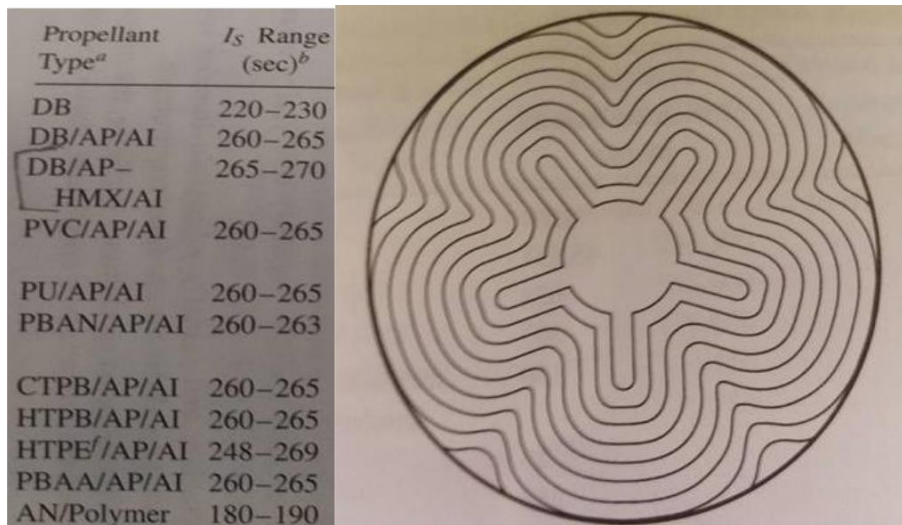


Table 3.2 Table 3.3 Various solid propellants and corresponding I_{sp} ranges

Figure 3.3 Figure 3.4 (right) Each contour is a successive burning surface for a fixed time step. [3]

A main application of solid propellants is for weapons systems. Weapons systems typically require long storage life and instant “readiness” in addition to moderate durability. These requirements rule out using liquid fuels and oxidizers which have short shelf-lives (2 → 15 days for liquid oxygen

[32]). Solid propellants are much lower risk because they can store very well and unless exposed directly to flame or extreme heat, are not very reactive. Solids used in spacecraft applications such as were used in strap-on boosters for the space shuttle program had lower than liquid fuels but were still preferred because of reduced risk and reduced production cost. The space shuttle had a maximum altitude of about 600 km, so using solids in primary stages was not unacceptable but was near the limit of the technology.

Since the beginning of the 20th century the pursuit of rocket science has been measured in terms of maximizing and has been focused on improving methods of liquid propulsion to do so. While solid fuels are good for initially getting a rocket off of the ground, getting small satellites up to LEO altitudes and reducing the overall riskiness of a rocket, solids are incapable of getting a spacecraft to sufficient velocities needed for interplanetary travel. This is because of the lack of control over the combustion process associated with solid fuel propulsion. Currently liquid propulsion is also limited but here it is limited by rocket engine construction materials. Thrust is dependent on combustion temperature and combustion pressure and mitigating the effects of these things on a rockets engine has been the focus of materials science and research in regards to rocketry. Until stronger and more ablative materials are invented capable of withstanding higher temperatures and pressures the ability of chemical propulsion to produce additional thrust and get payloads further into interplanetary space will likewise be limited.

Hybrid rocket engines were developed for the purpose of reducing the cost of launches as well as the risk while improving on the controllability problem inherent to solid propellants. One of the issues with solid propulsion is the inability to shut down and/or restart an engine once it has begun firing and one issue with liquid propellants is their poor storage capability. Hybrids meet these two demands with varying degrees of success. A hybrid rocket engine works by flushing a gaseous oxidizer over the surface of the solid fuel within the rocket. This way the engine thrust duration can be controlled by controlling the flow of oxidizer to the solid fuel, thus solving one of the problems of solid propulsion. While the cryogenic liquid oxidizer does not store well since it is a pressurized & corrosive liquid; There are storable options when it comes to oxidizers with boiling points in excess of the freezing point of liquid water by as much as 150°C. however, even if a cryogenic oxidizer is used, it still is a less risky configuration for a rocket than having both a liquid oxidizer and fuel on a rocket. In addition, the rocket can be prepped for launch faster than a liquid only rocket since only the oxidizer tank would have to be filled before launch.

3.2.2 The Aerospike nozzle

The problem of a lack of non-ideal expansion for conical and bell-shaped nozzles, mentioned at the beginning of section 3.2, has led to the development of the Aerospike nozzle for allowing ideal expansion at all altitudes. Figure 3.2.2.1 shows the radial aerospike nozzle for both theoretical high back pressure and theoretical low back pressure configurations, illustrating the fact that the diameter of the exhaust flow plumes increase with altitude.

For this configuration, the aerospike nozzle has separate combustion chambers and features a low expansion ratio, comparatively to a comparable bell-shaped nozzle. The base of the nozzle is porous for the ejection of low pressure gas (often pressure cycle exhaust), which adds a small amount of thrust to the rocket engine. Some advantages of the aerospike with regards to conventional bell & conical nozzles are first and foremost, ideal expansion at all altitudes of operation, allowing for the highest possible nozzle efficiency (η). This means also, an increase in thrust (see equation 3.2.2.1).

$$= \dot{m} \cdot v_e + (p_e - p_a) A_e \quad (3.2.2.1) [3]$$

Second, a shortened nozzle length (about 1/3 the length of a bell comparable nozzle) conveniently reduces the overall structural mass of the rocket. Finally, because of separate combustion chambers individual nozzles can be operated independently, allowing for differential thrust vectoring eliminating the need for additional stabilization systems. [3]

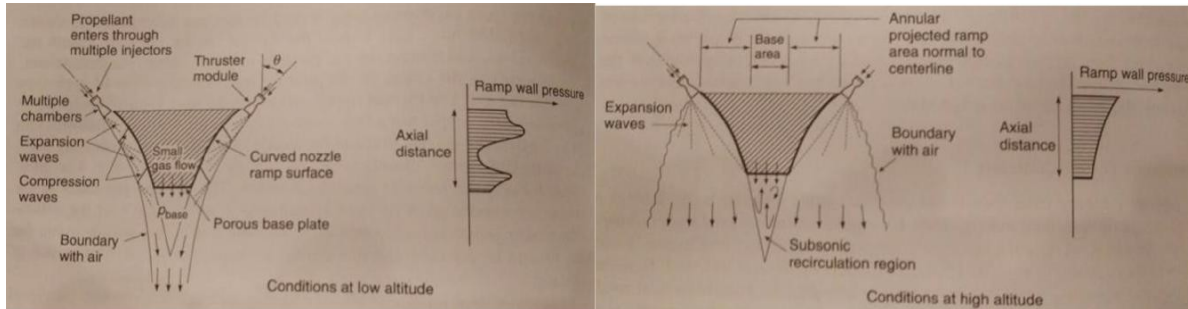


Figure 3.5 Figure 3.6 low altitude (left) [3] and high altitude (bottom) aerospike operational schemes [3]

The disadvantages of the nozzle include a significant lack of flight-test data and the fact that the nozzle has a larger surface area which is subject to high levels of heat transfer in comparison to bell and conical nozzles. There are small performance losses as well when the supersonic gas flow exits the convergent-divergent axial-symmetric portions of the nozzle, as well as losses due to the subsequent turning of the flow. [3]

3.3 Nuclear Propulsion

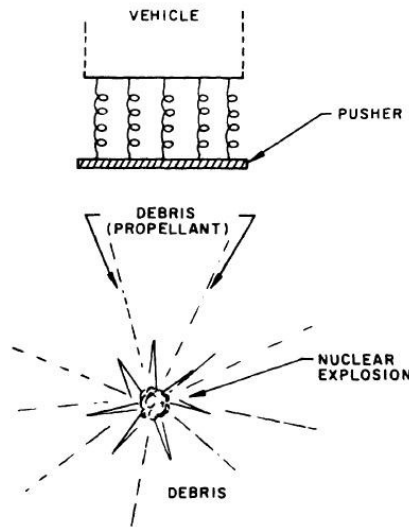


Figure 3.7 (left); schematic of a nuclear pulse engine similar to the Orion project. [34]

The Nuclear test ban treaty, signed in 1963, bans the detonation of nuclear weapons in the earth's atmosphere and so today research into using nuclear material for space travel has focused on using nuclear energy to power electric propulsion systems. This will be discussed in subsequent chapters. Before JFK signed that treaty, in the late 1940's the concept of a Nuclear pulse rocket engine was proposed. The idea was for a spacecraft which would ride a shockwave generated by subsequent nuclear explosions aft of the space craft, propelling it faster and further in to space. The estimated of this technology was well in excess of 200,000 seconds according to a paper published in 1965 by, The General Atomic division of General Dynamics Corporation. The technology would prevent the astronauts from being killed by the shockwave generated from hundreds of nuclear blasts by a large spring-like device between the spacecraft and the detonation site.

The main drawback of nuclear propulsion is the unacceptable fact that it would rain nuclear fallout down upon the earth, not only near the ground where it would cause devastation locally but in the upper atmosphere where it would be carried by the jet stream, all over the earth. Not only is such

detonation banned but, as alluring as an of 200,000 seconds is, the creation and application of such a spacecraft is morally irresponsible.

3.4 Electric propulsion

The final section on propulsion systems involving the application of Newton's third law are electric propulsion systems. These systems utilize an easily ionized propellant and accelerate small quantities of this propellant to velocities in excess of 1% the speed of light ($> \approx 300 \text{ km/s}$). The three types discussed here are the Ion thruster, the Russian Hall-effect thruster (both of which operate on the principal of the Hall Effect) and finally the VASIMR engine. The key design parameter of electric propulsion systems is the electrical efficiency of the electrical system itself. The availability of electrical power drives everything about these types of propulsion systems from propellant selection and sizing to thrust production and payload sizing. In all electric propulsion systems ionization cost is the key figure of merit in design because it directly relates input power requirements to plasma energy for both electron bombardment and RF wave bombardment processes.

The Hall effect was discovered by Edwin Hall in 1879. The Hall effect is the separation of positively charged and negatively charged particles within a conducting plate that has an established electrical current going through it being subjected to a uniform magnetic field. This separation of positive and negative charges then creates an electric potential across the plate. This concept is used to create the electric potential gradient used in ion and Hall thrusters to accelerate ions and thus generate thrust.

3.4.1 The Ion thruster

The ion thruster is a technology which began to be investigated in the 1940's. Since the ion thruster was first tested in space on July 20th, 1964 by NASA's Glenn Research Center, the development of ion thrusters with regards to available thrust has proceeded at the pace of developments in available electrical power systems. In 1999 Deep Space 1 became the first spacecraft to use ion propulsion for interplanetary travel, a feat made possible by developments in solar-cell energy capture technology. Today ion thrusters are currently being used to keep over 100 geosynchronous satellites in orbit. [35]

Typical ion thrusters work by first ionizing a propellant using a process called, "Electron bombardment" in which the propellant atoms are bombarded with high energy (negatively charged) electrons which knock electrons of the propellant atoms loose, forming positively charged ions. This process results in what is called a Plasma, which has some of the properties of a gas, however because of the movement within it of free electrons and ions, it is affected by magnetic and electric fields, while on the whole remaining inert. The most common propellant for Ion propulsion systems is Xenon. This is because of its storability and high atomic mass which both produces more thrust when accelerated and is easily ionized [35]. A process known as Thermionic emission, in which electrons are emitted from the surface of a heated metal, is responsible for generating the electrons used in the bombardment process [37]. The electrons produced in this process are attracted to the highly, positively charged discharge chamber walls because of the thrusters' discharge power supply. Into this chamber is injected neutral propellant and it is subsequently bombarded by electrons; releasing more electrons and creating ions, resulting in a plasma. A magnetic field insulates the discharge chamber walls in order to prevent any of the electrons, which are attracted to it, from colliding with it. This both prolongs the life of the propulsion system and extends the time the electrons spend within the discharge chamber meaning that they will

continue to circle around the magnetic field lines until collision with propellant atoms, thus increasing the overall efficiency of the thermionic process and saving energy. Then, the ions make their way to a positively charged electrode grid via the electric potential gradient induced by the Hall effect. As ions pass between the oppositely charged grids they are accelerated up to 90,000 mph toward a negatively charged electrode and out of the thruster, producing a small amount of thrust, typically on the order of less than 100 mN. In order that all of these electrons do not build up on the surface of the spacecraft, which among other problems would attract all of the ions back to the thruster cancelling any thrust being generated; the electrons are injected into the exhaust flow of the ions [35].

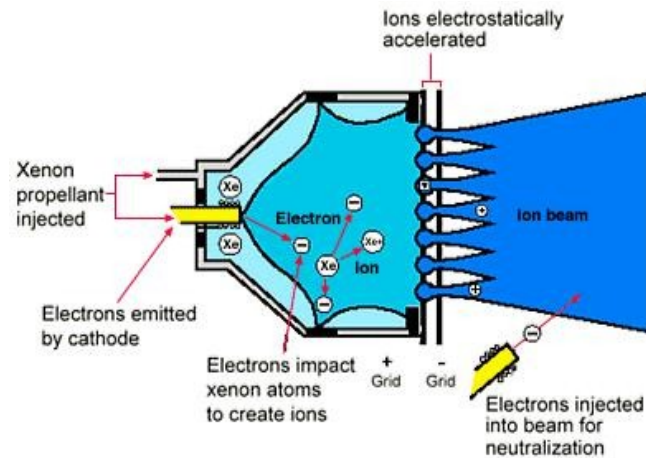


Figure 3.8 Schematic of an Ion Thruster [38]

The ion propulsion system on Deep Space 1, which utilized Xenon and electron bombardment, operated on 2.3 kW to produce 92mN of thrust (40 /) at peak operation. Comparatively that is slightly less per kW than the force of a piece of computer paper under gravity on the surface of the earth (≈ 45). At the ion propulsion systems' lowest power setting (525 W) it produced just 19 of thrust [36].

Ion thrusters are relatively simple propulsion systems which generate ions and then push them out of a thruster providing an opposing negatively charged cathode grid to give the ions a uniform direction and increase thrusting efficiency. The ion thruster is an American invention which has been under development since the 1950's but has yet to achieve greater levels of thrust on the order of 1 N because of the corrosion caused by interactions between the ions and the cathodes. This corrosion is the limiting factor of thrust generation and applicability when it comes to this type of electric propulsion. The major drawbacks of Ion propulsion include: low thrust per unit area and a heavy power supply.

3.4.2 Hall Thruster

Due to the cold war, scientific exchange between the United States and the USSR unfortunately did not take place, yet, because the rocket equation clearly lays out the benefit of increasing the ejection velocity of propellants it comes as no surprise that the Russian Space program developed their own Ion thruster which operates on the Hall effect and is aptly named the Hall Thruster. Although in principal the hall thruster and the ion thruster consist of the same processes (ionization & acceleration via an electrical potential gradient) the principal difference between the Hall thruster and the Ion thruster is the hall

thruster lacks a negatively charged cathode grid for acceleration and directing of the ions, instead relying on a simpler yet less efficient means of using a general electrical potential gradient.

A Hall thruster consists of a discharge anode, cathode, a magnetic field generator and the discharge region. Electrons are fed via a cathode into the discharge region where they are attracted to the anodes which conveniently happen to be supplying the non-ionized propellant. On their way to the anode they encounter, within the cylindrical region, a transverse magnetic field which both prevents them from reaching the anode and causes them to circle about the thrusting axis [39].

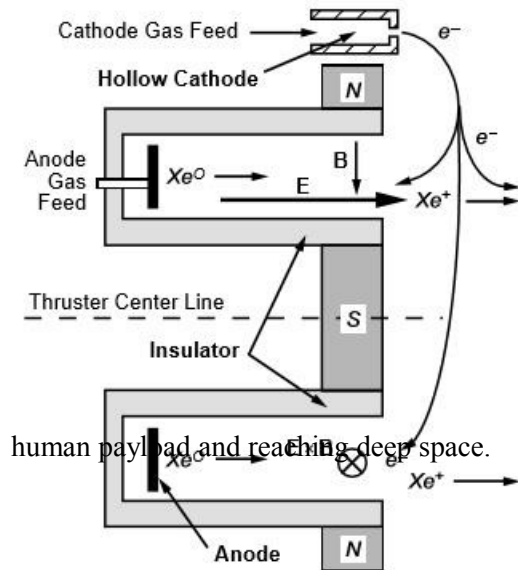


Figure 3.9 (left); Schematic of a Hall thruster [39]

The electrons in this region collide with the propellant gas producing a plasma of ions and electrons which are then accelerated via an electrical gradient, generating thrust and dragging free electrons along with them to neutralize the exhaust. The Hall thruster is less efficient than the ion thruster, where the Ion thruster used on board Deep space 1 was generating $40mN/kW$, the average Hall thruster generates about 60% of that, or ≈ 24 , owing to a maximum of 2000 seconds [39]. The primary advantage of the Hall thruster is its cheaper to manufacture per Newton of thrust delivered, than an ion thruster. For deeper space applications, however, neither is capable of producing more than a single Newton of thrust at any one time nor an in excess of 3600 seconds, and so neither technology is very appealing for the application of taking a

4. VASIMR Engine

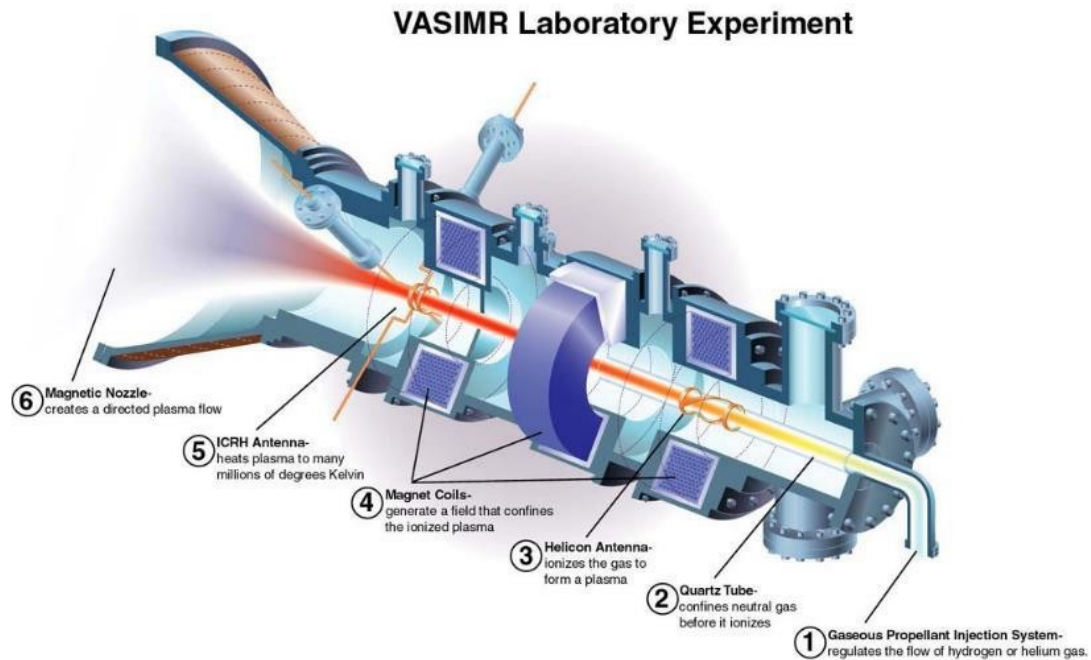


Figure 4.1 The experimental VX -200 rocket engine [5].

The Variable Specific Impulse Magneto-plasma Rocket engine (VASIMR engine) was proposed by NASA astronaut Cheng-Diaz, in its present form, in the early 1990's as a means of faster space travel for larger payloads. The concept addresses a few issues raised by previous forms of electric propulsion.

The application of the VASIMR engine is at high power, >100 kW, due to its high power-density RF coupling to a magnetized plasma stream and its lack of necessity for electrodes [41]. Specifically, it avoids all contact between the plasma which is generated and the rocket engine materials containing it. Thus, avoiding the potential corrosion that occurs between the anode grid and the ions in ion propulsion. Second, it uses radio frequency waves emitted at the harmonic frequency of the propellant to rapidly ionize the propellant; meaning that more propellant can be ionized in less time without emitting electrons from a cathode, increasing simplicity and decreasing risk. Thirdly, acceleration of the entire plasma (not just ions) results in additional mass being ejected and thus additional thrust. Finally, because the plasma never contacts the materials of the rocket engine the plasma can be heated rapidly to temperatures greater than the surface of the sun without exceeding the thermal limit of the engine materials, allowing for additional thrust to be generated by more rapid expansion as the plasma exits the magnetic rocket engine nozzle.

Although thrust output in regards to the VASIMR engine appears to be linearly proportional to kW input, there seems to be a physical limit to how small a VASIMR engine can be because of the size of the superconducting magnets which are required to insulate the plasma from the rocket wall materials. The superconducting magnets are too large for this type of propulsion system to be used for orbit maintenance for smaller satellites. The Hall and Ion thrusters are better designed for those purposes. However, for a satellite such as the International Space Station (ISS) this technology is ideally suited. Periodically the International space station needs a boost to maintain its altitude within the thermosphere at 400 km. The VX-200 version of the VASIMR, in 2010 produced 1 lb. of thrust while operating at 200

kW, making it the most powerful electric propulsion engine in existence. Currently the ISS uses chemical propulsion with an in the vicinity of 400 seconds to boost the ISS. The VX-200 at its lowest efficiency (highest thrust) setting has an of 3000 seconds, approximately 7.5 times that of the current chemical method of re-boosting the ISS. This could save in yearly operational costs for the ISS or it could be the primary re-boosting system for the next ISS after the current one is set to de-orbit in 2024. The other application of a VASIMR engine is interplanetary travel. Proposals by Ad Astra, which is the developing company and was founded by Cheng-Diaz, estimate earth-mars transit times of as little as 90 days for human carrying payloads, saving on-board mass required for life support systems.

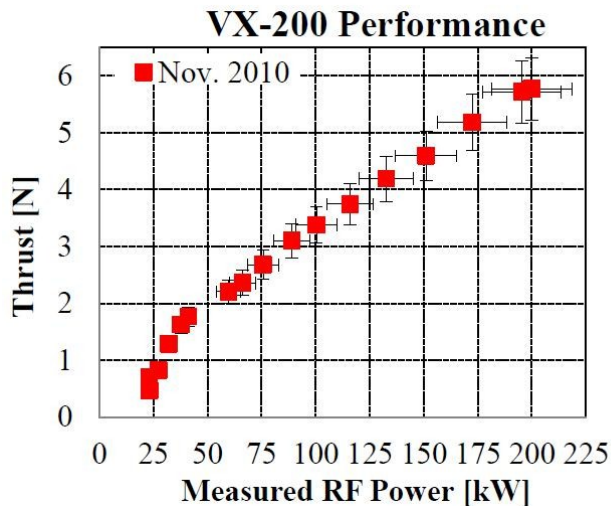


Figure 4.2 (left); Thrust-test results for 16 run cases of various iterations of the VASIMR engine [6].

VASIMR exhaust gases are hotter than the VASIMR engine materials can tolerate and VASIMR solves this design problem by taking advantage of the way a plasma interacts with a magnetic field. Plasmas, being internally charged gases, follow magnetic field lines; VASIMR exploits this relationship to prevent the charged gas from interacting with the walls of the rocket engine allowing for much greater plasma temperatures without causing a critical failure.

A VASIMR engine operates on a constant power supply and varies that power supply manually between two sections; 1) plasma production and 2) plasma heating, in order to manually control the specific impulse of the rocket engine. Providing more of the available power to the plasma heating process results in hotter exhaust gases which will expand faster and result in greater efficiency; meaning higher at the cost of reducing thrust. Conversely, if more of the available power is diverted to the plasma production process and less to the heating then the result will be an increased mass flow and more thrust at the expense of reduced .

4.1 Plasma

This section will briefly provide a background of plasma, the fourth state of matter, since its gaseous and magneto-electric interactions are the subject of the VASIMR engine and this paper. Plasma is the fourth state of matter. It occurs after the gaseous state when an electron from each atom within the inert gas is forced free producing an overall inert gas comprised of positively charged ions and negatively charged free electrons. In a VASIMR engine ionization is done using radio waves when they are emitted at appropriate resonant frequencies.

The relationship between plasmas and magnetic fields, was first theorized by Kristian Birkeland in 1908 when he concluded from observations of the deflection of a compass needle whenever the Aurora Borealis would appear that it was actually a small visible part of the product of a highly charged gaseous electrical current because the relationship between electric currents and magnetic fields described by

Gauss had been previously well documented. His observations were widely rejected since it was believed impossible that electrical currents could travel through the vacuum of space.

Anyone who has ever clipped an electrical wire in a simple circuit has no doubt noticed that the current does not jump the connection freely post clipping; and that whatever was being operated by the closed circuit no longer functions properly. So naturally it was believed that Birkland's currents were an impossibility since space was known to be an effective insulator. For this reason, Birkeland was ostracized by the scientific community, who refused to accept his conclusions on the existence of electrical currents travelling through the vacuum of space. It was not until 1967 when a satellite was flown through the Aurora's that the existence of the current predicted by Birkeland was confirmed.

The glow that is seen in figure 1.4 is caused by high energy plasmas which are emitted by the sun and then captured by the magnetic field lines produced by the earth colliding with air molecules in the upper atmosphere. The color of the Aurora as seen from the earth's surface depends both on which atoms it is colliding with and the altitude where the majority of the collisions are taking place. For example, in figure 1.4 greenish yellow auroras are produced by plasma colliding with oxygen at about 60 miles above the earth's surface and the green color is then emitted when the excited atmospheric electrons return to their previous stable state [8].

4.2 Components of the VASIMR engine

Conceptually A VASIMR engine can be divided in to three parts; 1) gas ionization, 2) plasma heating and finally 3) plasma acceleration via RF resonance heating and expanding magnetic field.

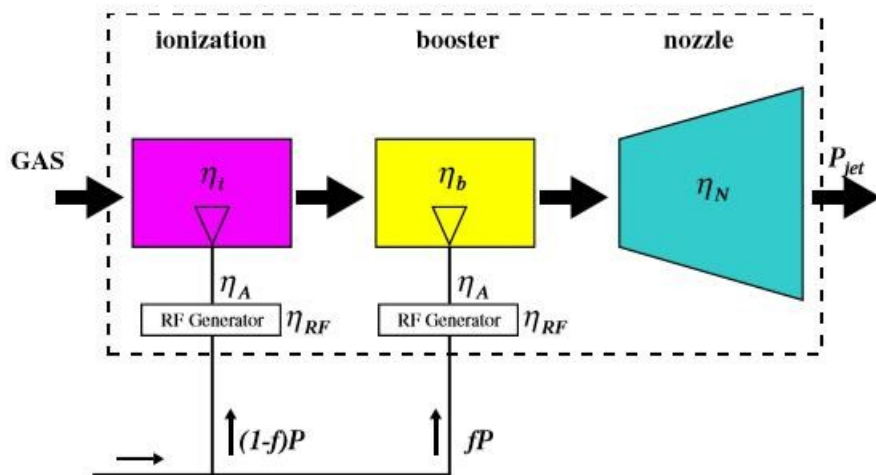


Figure 4.3 VASIMR power flow diagram [40]

4.2.1 Propellant Ionization

An inert gas can be ionized relatively easily if it has a lot of free electrons, or as is the case with VASIMR, which is designed to run on helium or hydrogen or argon (elements with not so many free electrons), ionization is produced by helicon waves [2]. When the helicon waves are emitted in the direction of the gyration of the plasma particles about the induced magnetic field lines, i.e the opposite

direction of the thrust, illustrated by the pink colored lines and the red arrow in figure 1.3, respectively, resonance occurs within the inert gas and the electrons are freed. Ionization is an efficient process, with as much as 98 % energy conversion efficiency [2].

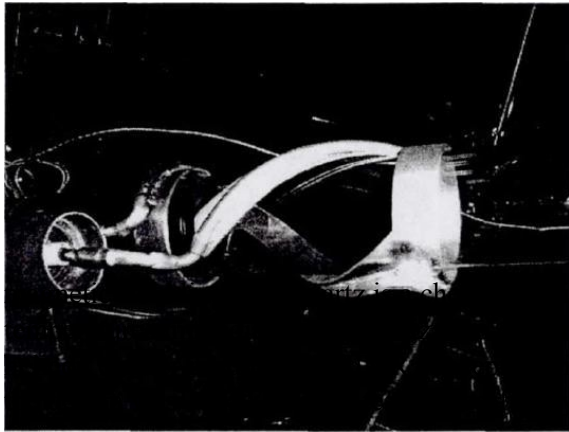


Figure 4.4 (left); Helicon antenna with a quartz tube running through it. [2]

Gas is introduced into the ionization chamber via a cylindrical, quartz tube and ionized by a radio frequency (RF) driven helicon wave which boosts the velocity of the ions to approximately 10^7 / [2]. The purpose of the quartz cylinder is two-fold; first the cylindrical shape has been shown to maximize the efficiency of the helicon ionization process, second, this part of the internal structure is not protected by a material that has demonstrated great resiliency to the heat, such as 5800 K [10]. Figure 1.4, below, shows the antenna published in 2000. The total operational kW usage of the antenna yielded thrusts of between 5,000 and 10,000 seconds.

The helicon in the ionization chamber has three components; An RF field which has a structure dependent upon the excited Eigen mode of the antenna (which itself is a property of the propellant selection), power balance and particle balance. The helicon Antenna in figure 1.4 is water-cooled and of a half-turn geometry. It operates between 7 and 50 MHz under 3 kW of power to completely ionize 1.5 mg/s of hydrogen propellant [2].

4.2.2 Ion Cyclotron Resonance Heating (ICRH)

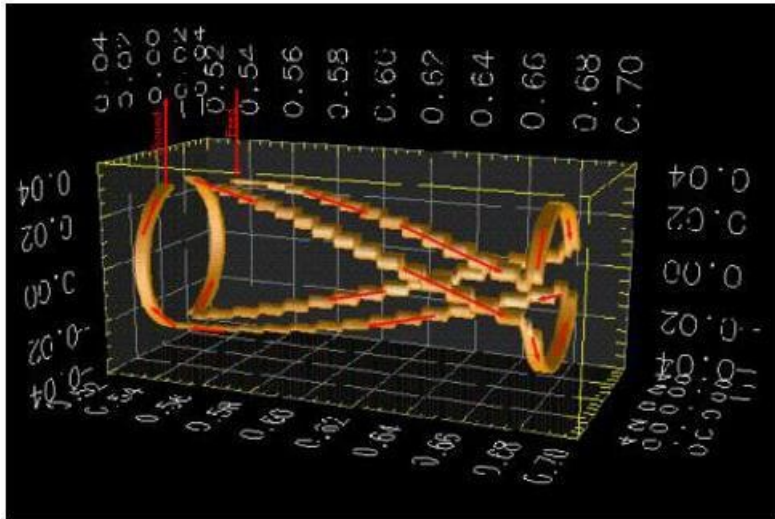


Figure 4.5 (left); ICRH antenna. [43]

Ion Cyclotron Resonance Heating is the second stage of thrust production for a Variable Specific Impulse Magneto-plasma rocket engine. It is important to remember that even though the gas post ICRF ionization is about the same temperature as the surface of the sun [11], it is still considered a “cold gas”. This is important to remember in order to keep the efficiency of the

VASIMR engine in context of modern chemical propulsion engines, which do not often exceed the cold gas temperature of the plasma at any one point. For example, the Saturn V, which is the engine that launched astronauts to the moon during the Apollo missions had an exhaust temperature of only 2600 K

[12]

and a peak combustion temperature of

3500 K [13]. The Wave amplitude is

proportional to plasma 28

diameter and density. When the ICRH frequency matches the applied frequency, ions are accelerated and wave energy is transferred into ion kinetic energy [43].

ICRH is a technique of heating plasma using RF waves that is borrowed from nuclear fusion experiments involving tokamak reactors. In VASIMR engines the temperature within the ICRH was measured at, in the latest iteration (VX – 200), 7 eV (about 81,700 K). The ICRH works by emitting RF waves at resonance from a circular antenna toward the plasma which flows through it. The plasma absorbs the RF waves when they are emitted at the proper frequency. The proper frequency for most efficient absorption is determined by the propellant and the strength of the magnetic field. It has been experimentally proven through use in nuclear fusion experiments that this frequency is the characteristic frequency of the ion gyration about the magnetic field lines [15]. The difference in ion and electron response to the RF waves emitted by the ICRH results in perpendicular electric field lines that rotate at a frequency equivalent to the input power frequency [43].

Referring to figure 4.1, the ICRH is seen as number 5 and it is labelled “booster” in figure 4.2.1. The great benefit of ICRH over the comparable method in ion propulsion engines is that the ICRH in VASIMR does not require the use of electrodes to energize the plasma flow. This is a major advantage of VASIMR in comparison with Ion propulsion. It is the electrodes which wear out first in Ion propulsion engines due to the highly corrosive nature of plasmas; and it is therefore the electrodes which have ultimately been responsible for not a single Ion propulsion engine used in orbit, outperforming or even reaching its design life expectancy goal [14].

4.2.3 Plasma acceleration within an expanding magnetic field

Plasma's are charged gases, and because of their heat they will “want” to expand, especially in the vacuum of space. In addition, when a charged particle, positive or negative, is confronted with an expanding magnetic field it too will accelerate. A plasma, being both a collection of charged particles and a gas reaps the benefit of both of these characteristics. When a charged electron “see's” an expanding magnetic field it translates some of its gyrational momentum into axial momentum, producing an acceleration and thus a thrust in the opposite direction of motion.

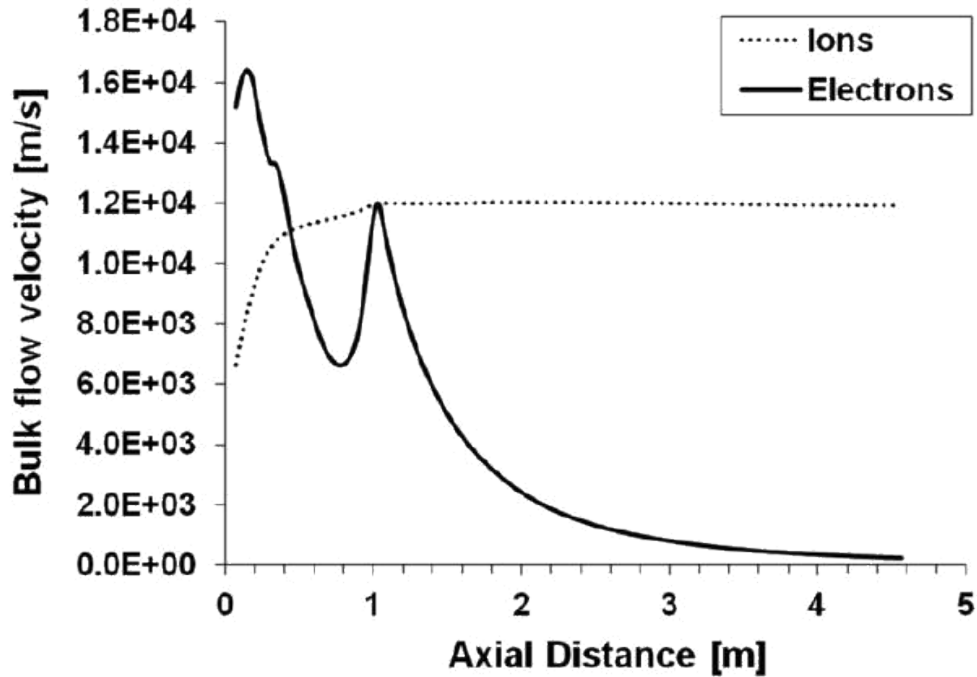


Figure 4.6 Ambipolar acceleration in VX-200i exhaust field[5]

What is even more interesting is that because the electrons are so much smaller than the ions (on the order of 3.6 thousand times smaller), they are accelerated faster under the influence of an identical magnetic field than are the ions. This primary flow of large numbers of electrons creates an electric current which then pulls on the ions behind them causing additional acceleration of the ions in a process known in plasma physics as ambipolar ion acceleration [17]. Figure (), above, is a measurement of this relationship taken during a verification-based experiment of the effect reported by VASIMR. The study generated positive results of the effect but incomplete result of the relationship within the plasma downstream because the mass ratio of ions to electrons is too significant so as to cloud out minute distinctions in velocity downstream of where the velocities of the two particles match.

5. Design Iterations on VASIMR

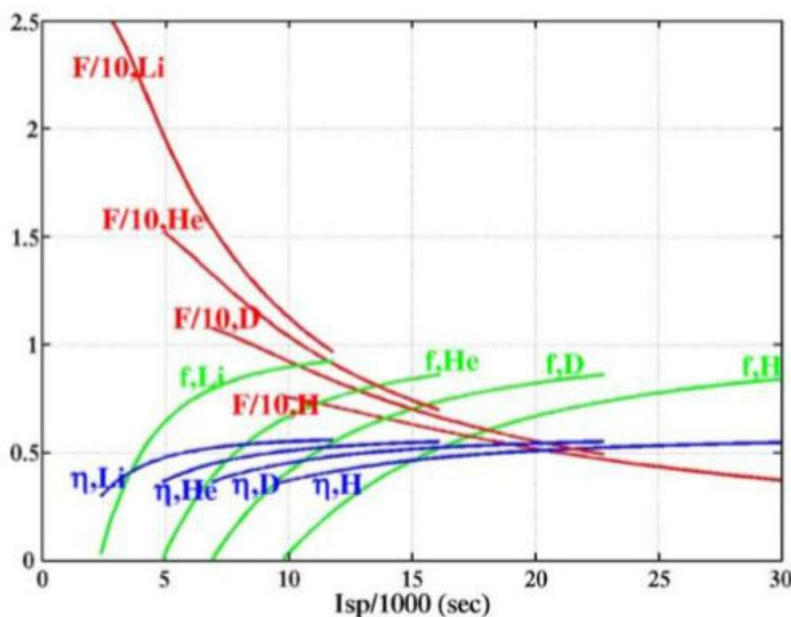
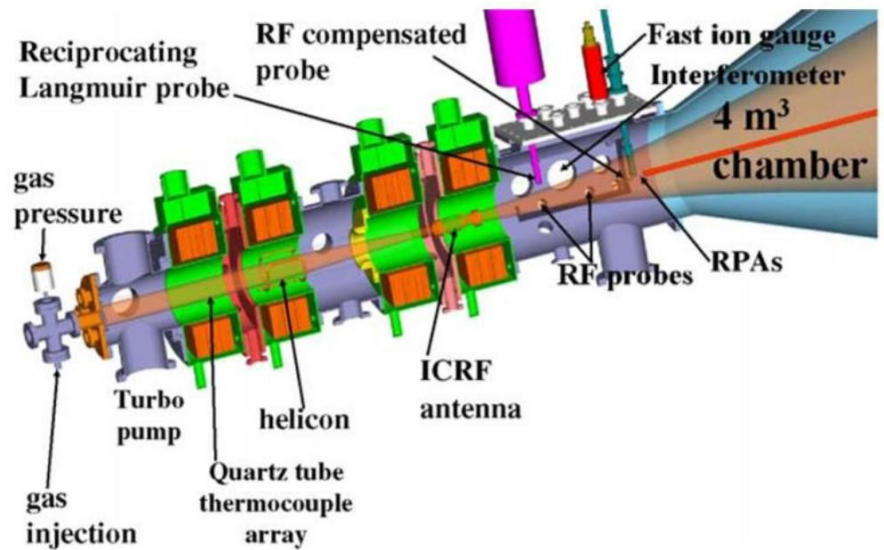
The VASIMR concept is traced back to MIT in Massachusetts in the mid 1980's, however credit for its conception is typically given to its development by NASA's Advanced Space Propulsion Labs (ASPL) because the key feature of RF ionization which enabled the engine to no longer require the use of electrodes, was developed there.

5.1 VASIMR iteration VX-10

The Vx-10 featured the signature magnetic mirror-field at the upstream end of the Helicon Antenna to trap the plasma and confine it to the region of greatest resonance (the central axis) within the Helicon. The Helicon first stage is critically important to access the range of desired from the VX-10 (5,000 to 30,000 seconds) for operation.

.Figure 5.1 (right); VX -10 design schematic from ASPL [40]

Experiments using multiple propellants were done on the VX – 10. In previous chapters the need for large ions was laid out for the two other electric propulsion systems discussed, Ion and Hall thrusters; however, while this is still the case with those thrusters, the target of the VASIMR engine is higher and delivering more thrust is the task of the RF ionizing antenna via rapid plasma production.



It is for these reasons that advantage can be taken of the increased that comes with using lighter propellants. These properties of molecular weight versus and that relationship to thrust are clearly made identifiable in the figure below where system efficiency can be seen to remain constant with increasing molecular weight while is shown to be inversely proportional to increasing molecular weight.

Figure 5.2 (left); Performance parameters as functions of I_{sp} for Lithium, Helium,

Deuterium, Hydrogen & other unnamed elements. The system efficiency η , the RF booster power partition f are dimensionless, the thrust F has units of Newtons [40]

A secondary benefit of using a lighter propellant for the VASIMR engine is that lighter propellants with fewer subatomic particles can be accelerated more efficiently than heavier particles such as Deuterium or Xenon, which are common propellants of other electric propulsion systems which operate at lower values. Later versions of the VASIMR such as the VX 50 and above do not use lighter propellants because, as is especially the case with hydrogen, they have low specific gravities (low energy density). Another reason is that these four fuels are expensive. The latest iteration of VASIMR, the VX-200 uses Argon expressly because of its high performance to cost ratio.

Nearly complete gas burn up in the helicon tube has been measured. This result relates to the propellant utilization efficiency of the engine and is shown in the figure below as ion output versus neutral particle input. The figure illustrates the observed one to one correlation in the range between $2 \cdot 10^{19}$ - $4 \cdot 10^{19}$ particles/second, indicating RF ionization efficiencies approaching 100% [40].

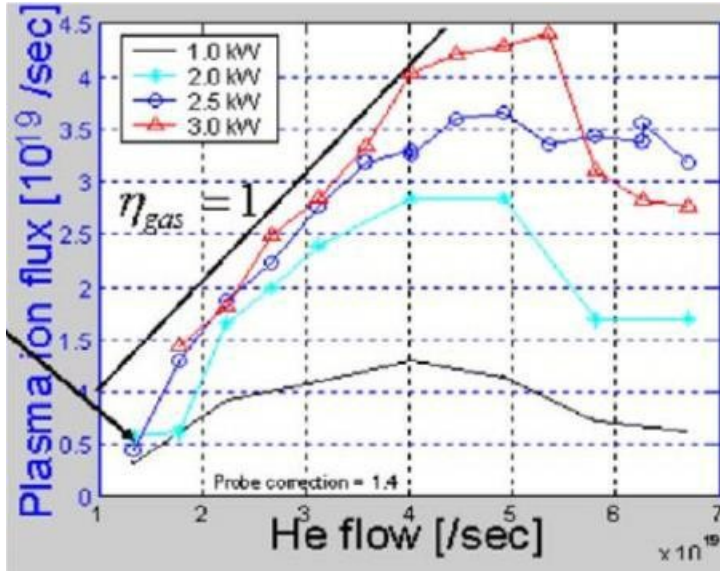


Figure 5.3 (left); plasma ion flux versus helium flow rate [40]

Efficient propellant utilization is important in the VASIMR application of plasma because the presence of non-ionized molecules in the RF booster stage (heating stage) would lead to unacceptable power losses and molecule to wall bombardment (atoms without charge can be not contained by magnetic field lines) causing corrosion and possibly critical failure if not at the very least life-cycle shortage for the engine [40].

The critical characteristic of the RF booster stage is the ability of the plasma flow to absorb RF waves. Unlike in Tokomaks the flow only passes beneath the antenna once so it is critical that absorption be both rapid and efficient. As of 2006 rapid absorption has been predicted and confirmed [40] via measurement using a potential analyzer placed in the exhaust field. The figure below illustrates the effect of the RF booster stage upon plasma velocity. The velocities in the figure are scaled by the gravitational constant 9.81 m/s [40].

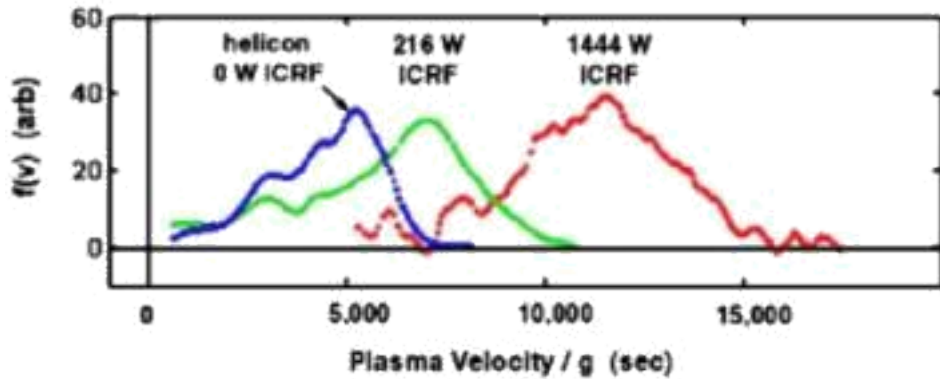


Figure 5.4 VX-10 ion velocity exhaust distributions for 0,216 & 1444 W of RF booster power [40]

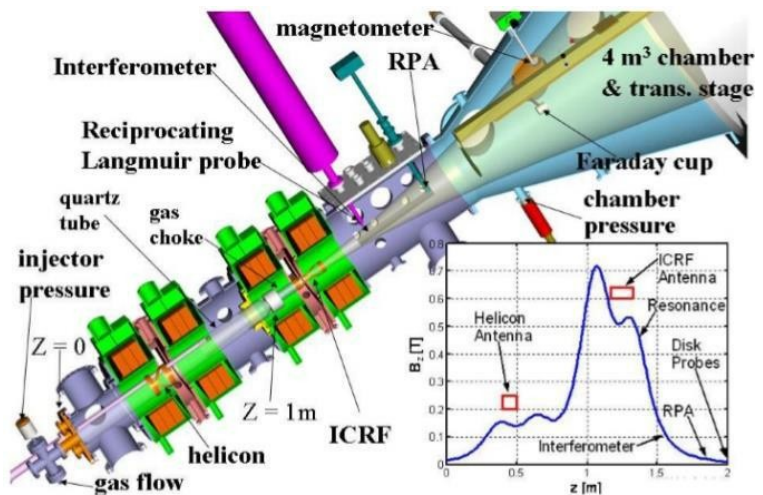
The Vx-10 achieved a maximum thrust of 100 mN [40].

5.2 VASIMR iteration VX-50

The VX -50 was the third iteration of the VASIMR engine and its goal was to function as a proof of concept of full/efficient plasma production and simultaneously attempt to achieve an low ionization cost of 100 eV.

The VX-50 was designed to process 50 kW of total RF power. In this experiment [41], power capability of up to 30 kW was documented in the plasma source and over 30 kW within the ICRH. Efficient plasma production was achieved with an ionization cost of just 100 eV. Measured plasma flux exceeded 1021 ions/sec and ion acceleration was observed using deuterium, neon and argon. Ion velocities were calculated between 30 and 150 km/s. A key result from testing was the confirmation of previous results on ionization efficiencies achieving greater than 90 % energy efficiency during ionization of the propellant & the maximum measured thrust was 0.5 N. [41]

Figure 5.5 (right); isotropic of the VX-50 showing key component parts and magnetic field flux as a function of distance along the thrusting axis [41]



This experiment was operated in vacuum and operated on Deuterium, Neon and Argon. These three propellants were likely chosen because they are slightly heavier than Hydrogen but still result in the same number of ions and electrons and identical charges as hydrogen (post-ionization). The magnetic field was generated by four, independently driven, superconducting electromagnets with a peak field strength of 1.4 Tesla. The Helicon Plasma section has a magnetic field of up to 0.4 Tesla and it peaks downstream and then comes

down to 1 Tesla where the ICRH is located before expanding out the aft end of the rocket to generate the shape of the magnetic rocket nozzle. The inert gas is injected into the rocket nozzle via a 9-cm diameter quartz tube which passes through the helicon antenna so as to confine the propellant to the ionization region within the helicon antenna and the quartz tube ends before the plasma reaches the ICRF antenna and creates a “magnetic choke”, to act as a limiter preventing too much plasma from reaching the ICRF antenna at one time.

The total RF power capability of the system is over 50 kW. The helicon plasma source was operated on 25kW at 13.56 MHz. Two different setups were chosen. One for Deuterium and one for both Argon and Neon. Deuterium experiments drove the ICRF on 25 kW operating between 2 – 4 MHz and a drive frequency of 3.6 MHz. For Argon and Neon experiments the ICRF was operated at 300 and 550 kHz and driven by a 50 kW solid-state transmitter. A couple of the instruments used to conduct measurements are a 70 GHz density interferometer located 20 cm downstream of the ICRF antenna and two retarding potential analyzers for ion energy measurements.

For a typical discharge the discharge-pulse length lasts for not longer than one second to mitigate the effects of neutral pressure buildup on the expansion chamber. RF power is applied once the gas flow reaches a set point. After a discharge is established the pressure at the injection point increases by over a factor of 10 to 0.3 Torr. The ICRF pulse typically lasts for 300 and power to the ICRF is only applied once the discharge reaches a steady state. [41]

The ICRF was the subject of the experiment which used deuterium for propellant and operated in excess of 20 kW to measure significant ion flow exceeding 200eV. Two separate Gridded RPA’s are used to measure the ion flow for verification. The calculated flow velocity was well in excess of 100 km/s corresponding to an in excess of 10,000 seconds. The Thrust was calculated from mass flow estimates to be between 0.15 and 0.2 Newtons.

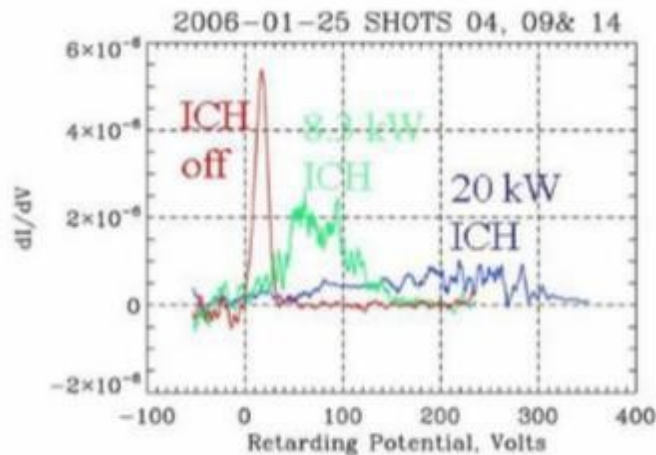


Figure 5.6 (left); The derivative of the RPA characteristic for three different ICRF power levels. This indicates the ion energy distribution acceleration. Preliminary impact target experiments confirm a significant momentum flux in the flow due to the action of

The plasma loading as a function of frequency (figure below) near the resonant frequency was used to optimize the plasma coupling performance to achieve RF wave absorption greater than 90%.

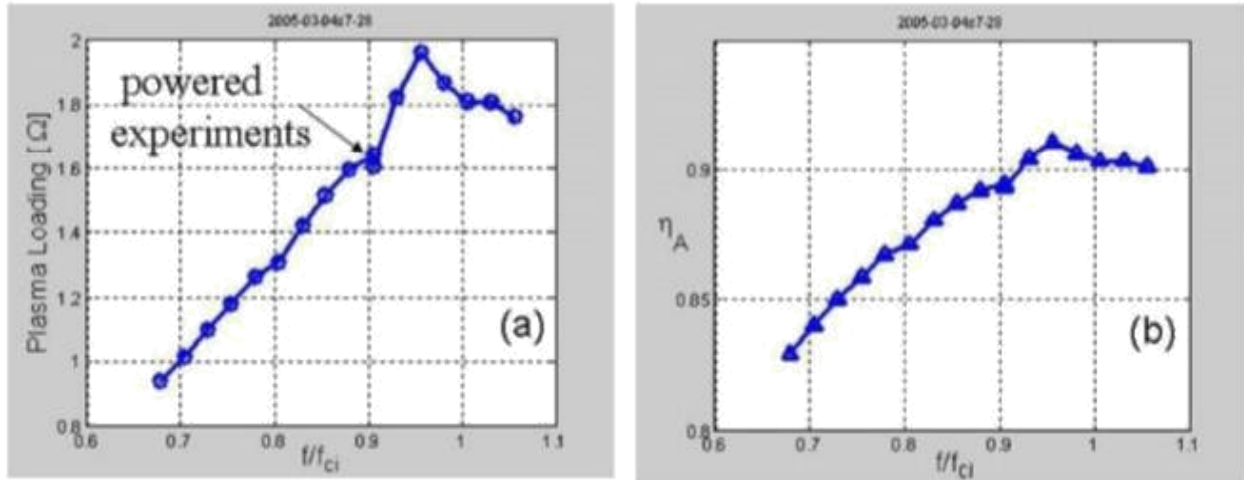


Figure 5.7 a) ICRF antenna plasma loading measurements for a range of frequencies, 4 MHz at the center of the antenna. Indicates the loading point where high power was applied. b) Antenna circuit efficiency for coupling power to the plasma, exceeding 90 %.

To understand the figures above: — < 1 places the resonance downstream of the antenna center.

The peak loading indicates that the RF power is propagating downstream and taking axial distance to penetrate into the plasma. From the figures above it is shown that peak resistance occurs when the resonance is located at the aft most end of the ICRF antenna which is consistent with computational modeling. Figure (a) shows plasma loading as a function of drive frequency normalized to the ion cyclotron frequency (·) located at the center of the antenna. Figure b displaying plasma coupling efficiency shows that the normalized relationship operates at a peak efficiency (·) of 0.92, $\gamma = 0.9$ and $f = 5.6$ MHz.

5.3 VASIMR iteration VX-200

On October 24, 2008 Ad Astra announced that the plasma generation component of their latest iteration, the VX-200 engine, crossed the 98% efficiency threshold; reaching operational status. Based on testing of the previous model, the VX-100, the thrust level of the VX-200 was estimated to be 5 N, have an operational efficiency of 65 % and produce an of 5,000 seconds when the ionization and RF heating components were given 30 & 170 kW, respectively [42].

The VX-200 uses Argon as propellant for maximum cost/performance. Results from 2009 [42] have shown a thruster efficiency of 72% and an of 5000 seconds and a thrust of 5.7 N. The optimum ionization cost is now as little as 80 eV/ion. The VX-100 and the VX-200 both demonstrated ionization costs below 100 eV/ion. The ionization cost is a measure of the engine's plasma production efficiency with values below 100 being required to ensure efficient operation [42].

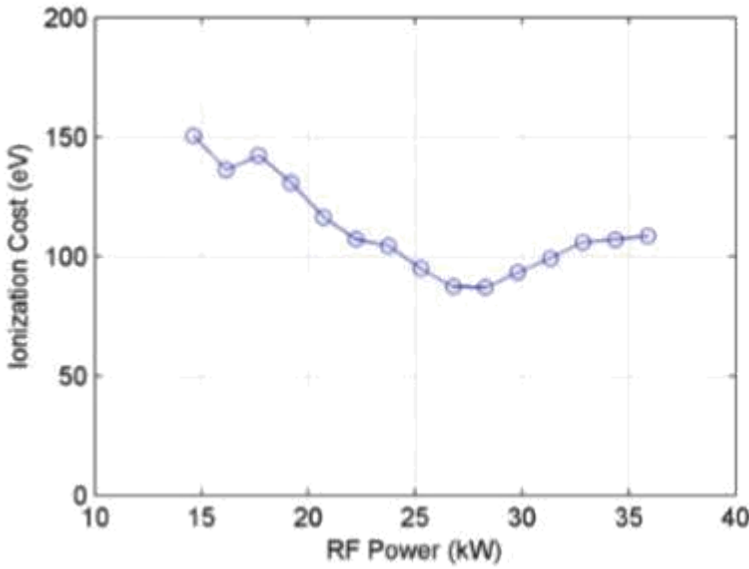


Figure 5.8 (left); optimization of ionization cost versus RF power input [42]

In 2011 additional testing of the VX-200 was done, this time with a magnetic field optimized around thrusting efficiency. Experimental results were obtained for plasma flux, RF power and neutral gas flow rate; which was used to determine the ionization cost of argon and krypton plasmas. Experimental results were also obtained for the exhaust plume in a vacuum up to 5 m from the exit plane of the

VASIMR engine. Finally, the ICH RF power coupling efficiency was determined by fitting a semi-empirical model of thruster efficiency as a function of to the experimental data, to be 89%. At a maximum power setting of 200 kw the thruster efficiency was determine using an identical analysis to be $72\% \pm 9\%$ and an $= 4900 \pm 300$ [44].

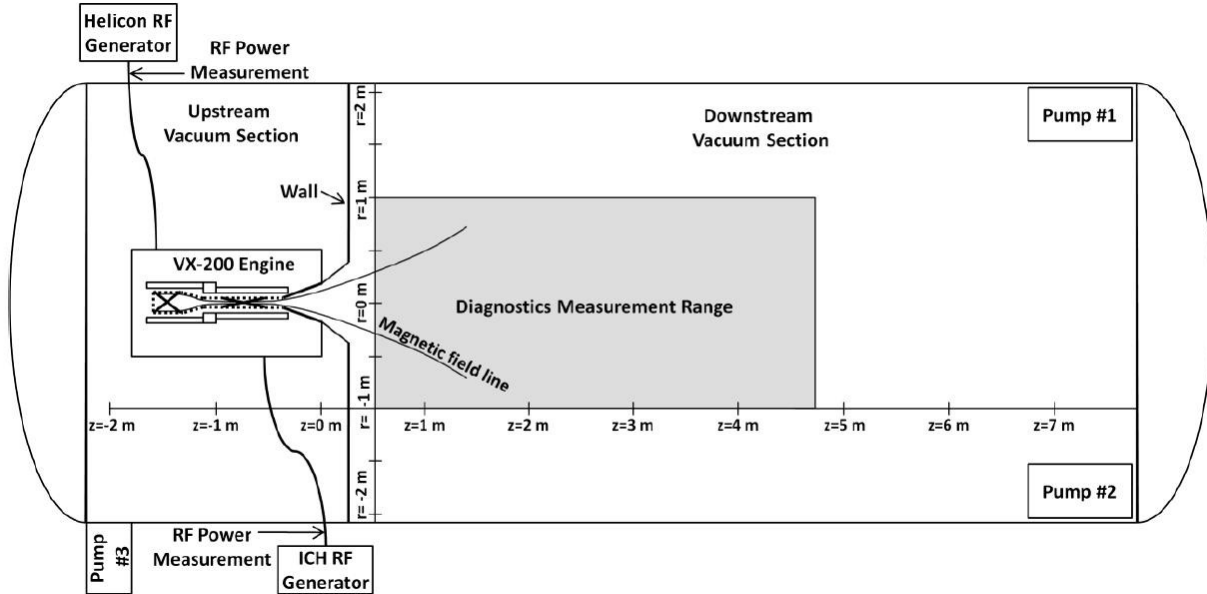


Figure 5.9 Schematic of the test section from the 2011 analysis. [44]

The RF helicon generator is rated to operate on 48 ± 1 at $91 \pm 1\%$ efficiency and a specific mass of 0.85 ± 0.02 / . The ICRH generator is rated to operate at 172 ± 1 and $98 \pm 1\%$ efficiency for a specific mass of 0.306 ± 0.003 / . Both of the generators functioning properties were determined via independent testing. The efficiency was determined to be 96% for both the helicon and ICH RF circuits when operated in junction, [44]. The superconducting magnets are kept at 6 K by operating a refrigeration cycle on 15 kW of power and drive a maximum magnetic field strength of 2 Tesla. In space, where the ambient temperature is significantly lower than a lab on the earth's surface, estimates for kW power consumption by

the cooling mechanism for the superconducting magnets is approximately 3 kW kept at 50 K. Ambipolar ion acceleration was expected and observed, confirming previous observations mentioned in preceding sections. This acceleration is again believed to be the result of the plasma interaction with the magnetic field gradient created in the expanding magnetic nozzle section. The ambipolar ion acceleration is attributed with an additional velocity gain of

5 to 10 / . The energy for this process is believed to be attributed to the electron energy distribution function as a result of electron-ion interaction and it was observed to range from between 10 and 20 V/m.

The testing duration for all of the data from the 2011 analysis of the VX – 200 was 30 s and steady-state operation was observed achieved in 0.8 s. The propellant mass flow rate if argon was varied between 50 and 160 mg/s and between 100 and 2250 mg/s when using krypton. [44]

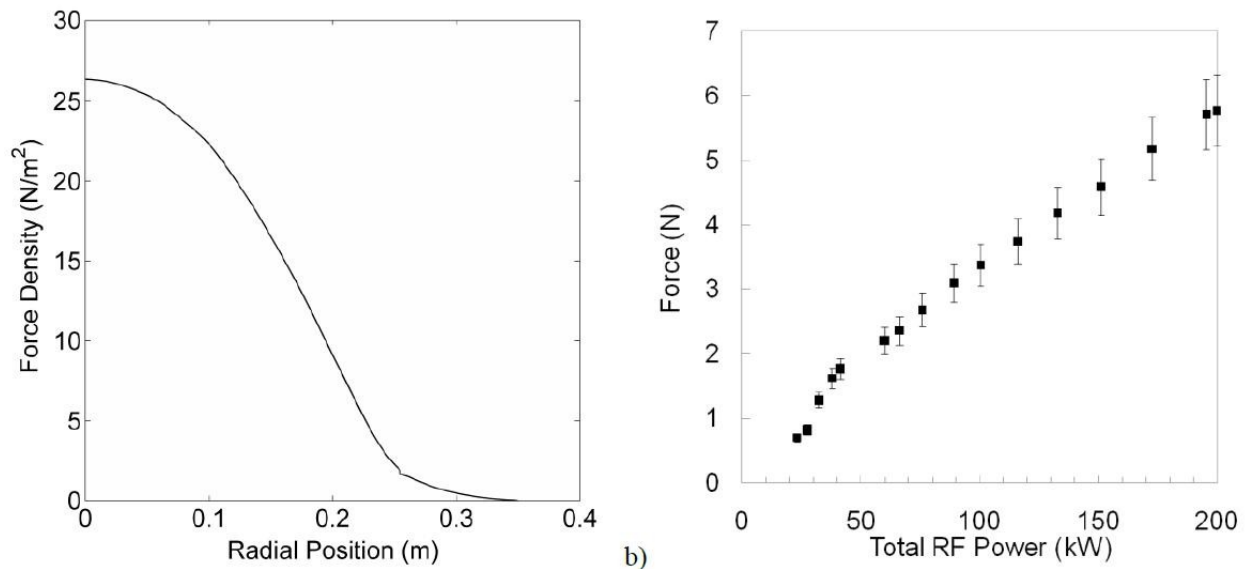


Figure 5.10 (left) force density measured as a function of radial distance. (right) confirmation of the linear relationship between total power and total thrusting force. [44]

The ion density within the plasma and the momentum (force) density of the exhaust plume 22.6 meters downstream of the end of the engine to observe the three-dimensional flow field. This testing was performed at a coupled RF power of 118 kW. The data gathered from this experiment displayed a “well-defined” edge for both ion exhaust density and momentum density. The experimentally determined boundary line defined by the exhaust plume relative to the engine axis, provided an estimate of the exhaust plume divergence half angle. This half angle was estimated at 30 ± 2 degrees, while the momentum density divergence half-angle was estimated to 24 ± 2 degrees. These half angles were found by integrating radially over the boundary of the exhaust plume. The error of 2 degree for each arises because the PMF’s were oriented normal to the engine axis while the contour clearly shows the height of the exhaust plume diminishing radially with increasing axial distance from the engine. The measured value of is used to determine nozzle efficiency,

$$= \frac{1}{2} (1 + \cos \theta) \quad (5.3.1) \quad [44]$$

The nozzle efficiency was calculated to be between 93% and 96% for the ion density and momentum density, respectively [44]. = 93% was used for all future system efficiency analysis from the 2011 report, because it is closer to the expected value of 90% taken from computer analysis. The nozzle efficiency discrepancy may be the result of the propellant being used; a conclusion of the analysis in regards to this nozzle efficiency discrepancy was that the separation of the plasma from the magnetic field when using argon, may be higher than anticipated meaning that the ions are being “held-back” by

the magnetic field less and are thus separating more efficiently. There has been no published data on this effect since the 2011 report. The jet power was determined by;

$$P_{jet} = \frac{1}{2} \rho v^2 A \tag{5.3.2} [44]$$

And was summarily used to determine thrusting efficiency as follows; where the terms in the denominator are the power supplied to the helicon and the ICRH, respectively:

$$\eta = \frac{P_{jet}}{P_{ICRH} + P_{HEL}} \tag{5.3.3} [44]$$

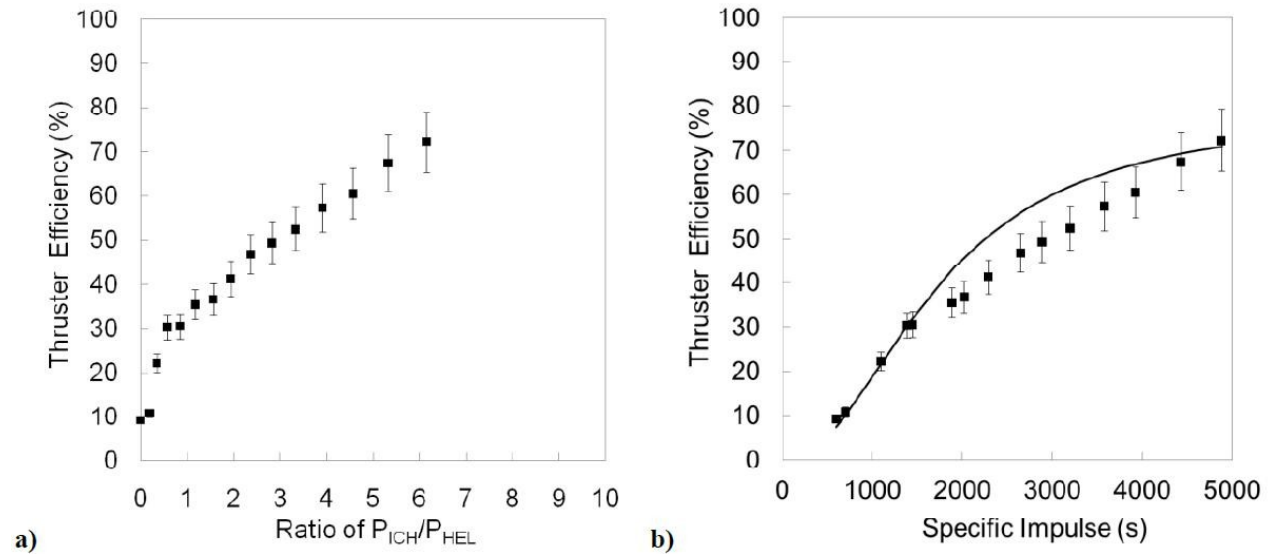


Figure 5.11 Thrusting efficiency as a function of power ratio(a) and as a function of specific impulse (b). Figure b uses a superimposed, least-squares fit. [44]

This iteration of the VASIMR engine was designed for a thruster efficiency of 60% at 5000 seconds. The measured performance of the VX-200 from the 2011 report revealed = 72% at = 4900 ± 300 s. [44] The likely reason for the engine outperforming its design specifications is the result of underestimation of the nozzle efficiency as stated earlier.

5.4 Mars Mission profile utilizing VASIMR engines

As shown the VASIMR's thrust output has, so far been experimentally shown to be linearly proportional to electrical energy input. With this in mind development of a nuclear-powered thermoelectric generator has been of much interest. The benefits of the current method of solar energy capture has its limits due to increased cost and size of solar cell arrays. Nuclear would provide energy on the order of MW. Figure 4.2 illustrates the linear relationship between input power and output thrust and it is expected that as long as the electrical components of VASIMR can be upgraded to tolerate the increasing power then the system will not have a thrusting limit; although this becoming a reality is decades in the future if not more since the electrical components in the VX-200 are currently at their respective limits.

In 2004 a Mars mission profile was proposed for a VASIMR earth to mars Crew Transfer Vehicle (CTV) operating 4 VASIMR engines on 4MW/engine (total 12 MW) nuclear powered engines and a 115 day launch to landing profile for the CTV. Hydrogen propellant tanks would surround crew for radiation protection. A payload of 190 mT into low Martian orbit. Exhaust velocities varying between 30 and 500 km/s. The first robotic vehicle leaves the cargo including food and scientific experiments on the Martian surface and it will leave the earth return vehicle (ERV) fully fueled in low Martian orbit. The outbound CTV would deliver the crew, lander and habitat and on return the CTV would propel the ERV with the crew back to earth.

The first robotic payload consisting of 30mT return habitat, 30 mT return propellant and 60 mT of cargo destined for the surface of Mars was set to depart LEO on August 3rd. The departure path consists of a 154 day spiral orbit out of the earths sphere of influence into a mars intercept trajectory via a Hohmann transfer. The Hohmann transfer orbit trip time would have to be 288 days to reduce required propellant. Propellant would be saved because the engines would operate at a high efficiency/low thrust setting.

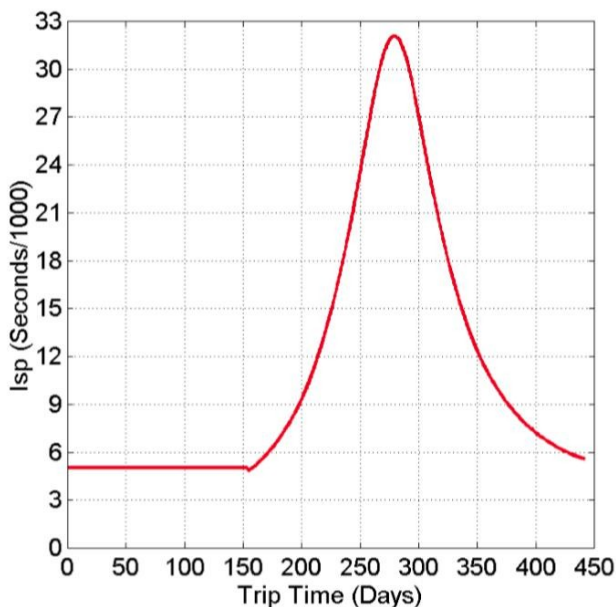


Figure 5.12 (left); Mission duration I_{Sp} profile [43]

5,000 s for the spiral orbit to get to a mars injection orbit. The profile was selected to maximize optimize the spacecraft for maximum payload; since there is no constraint on delivery time for the first mission profile. The payload mass fraction of this first mission is approximately 60%.

The outbound piloted mars mission profile is optimized around minimum flight duration for human considerations such as reducing risk by minimizing life support systems and materials operational life cycles. The piloted mission would depart on May 6th, 2018. The spacecraft would also utilize a spiral orbit to

leave earths sphere of influence and enter a mars injection orbit. The spiral orbit for the piloted mission, however, operates 4 VASIMR engines at a total of 12 Mw (3 times greater than the cargo delivery mission) and takes a 30 day spiral orbit. The injection orbit is not a Hohmann transfer but an 85-day heliocentric transfer for a total of a 115-day mission profile.

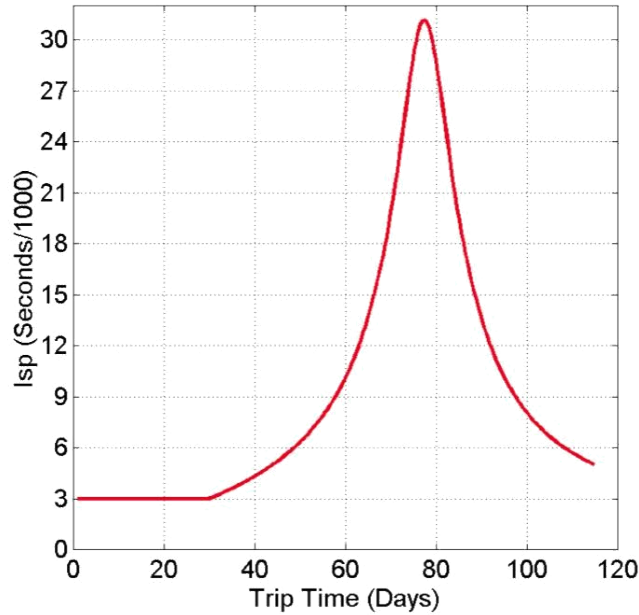


Figure 5.13 mission duration I_{sp} profile [43]

The profile is determined by the inputs of payload mass and transit time. There is a 61 mT payload and a 32% payload mass fraction. Noticeably the values for the initial spiral orbits are different for the two mission profiles. The lower in the second profile is on account of the increased thrust being generated by the engines which requires more propellant and reduced available heating adding to inefficiencies and required propellant mass but decreasing transit time; thus, resulting in a reduced payload mass fraction.

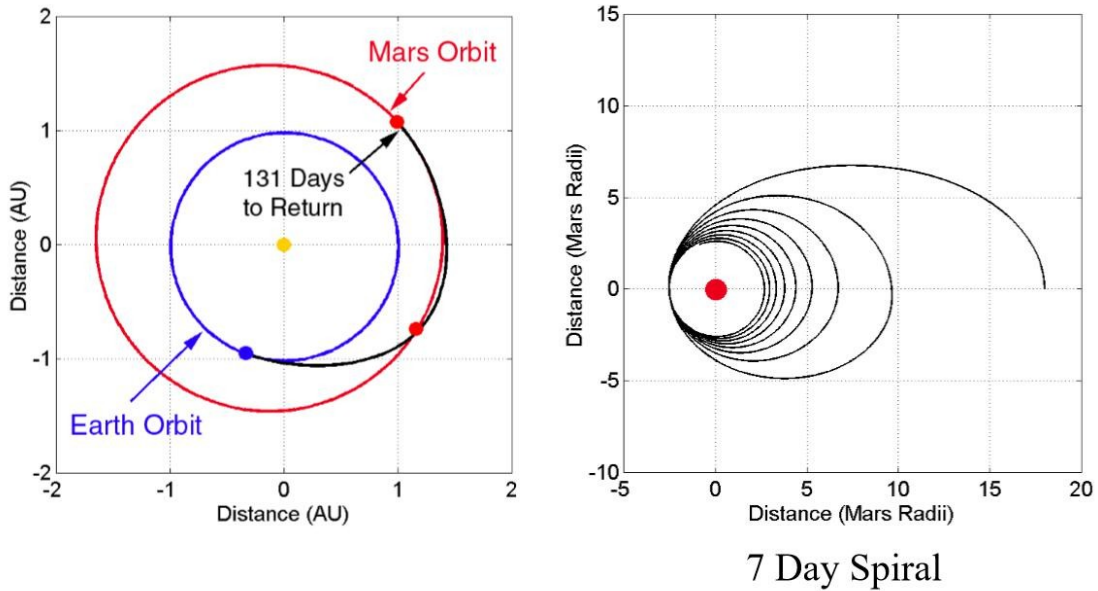


Figure 5.14 Mission profile for the CTV (left), 7 day spiral orbit Martian capture of the CTV[43]

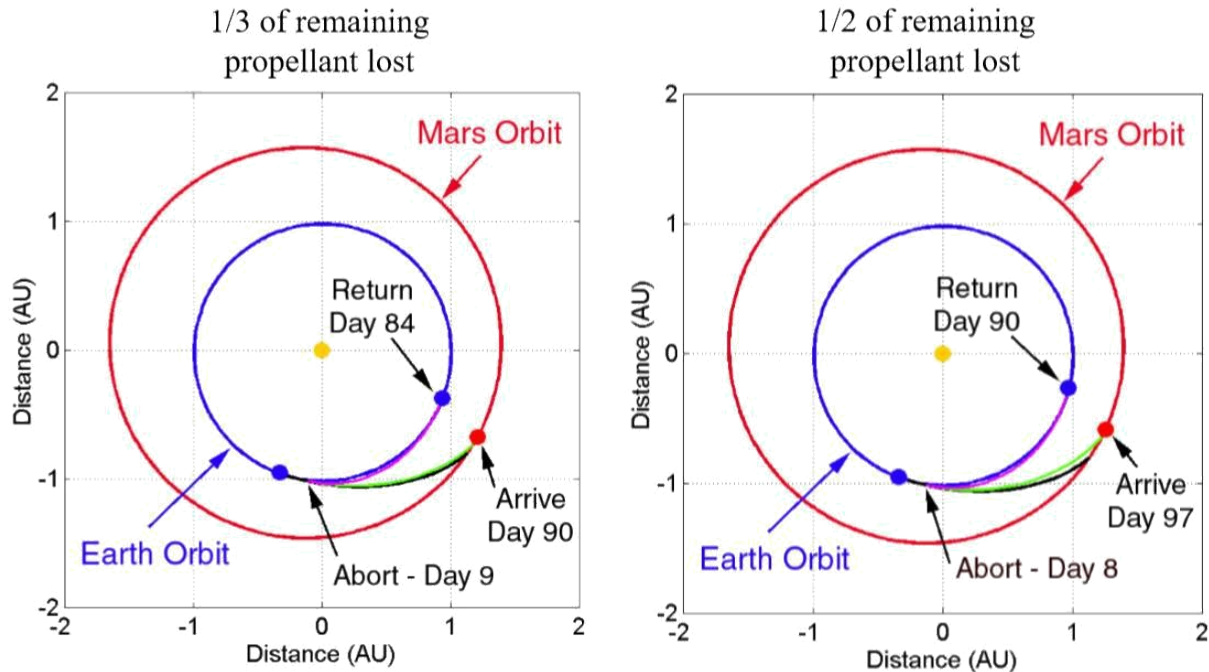


Figure 5.15 Two abort mission profiles for aborts on days 8 and 9 respectively. [43]

The Earth return on the ERV attached to the CRV is estimated to take 90 days [43].

6. Theory

6.1 Ionization methods & Electro - magnetism

The purpose of this investigation of ionization methods is to develop an expression for ionization cost. Ionization Cost, which is defined as the amount of energy (translational & potential) of the primary emission electrons emitted by a cathode, is a key design parameter of electric propulsion systems. Therefore, the ionization cost, more than anything else, drives the entire developmental design of any novel spacecraft using electric propulsion since the energy put into the primary electrons is directly related to the power requirement of the propulsion system.

Ionization is the process by which an atom acquires a positive or negative charge by losing (creating a positively charged ion) or gaining an electron (creating a negatively charged ion). In ion propulsion systems ions are produced by freeing, “loose” electrons in stable propellant atoms free of their host atoms, thereby producing positively charged ions and a bunch of negatively charged electrons. In regards to space propulsion there are the two methods of doing this. The first involves stripping atoms of electrons (Hall thrusters and Ion thrusters) and the second involves bombarding the atoms with large amounts of energy in the form of radio waves to “shake” the loosest electron free, so-to-speak.

In a plasma, most of the free electrons are secondary emission electrons. Secondary emission electrons are so named because they are the result of secondary collisions of electrons with the non-ionized atoms within a gas. In both electron and RF bombardment processes this same situation presents itself for high primary emission energies (>1000 eV) where the high-energy primary electrons compose a small percentage of the plasma while the majority of the plasma is composed of secondary emissions

[46]. This fact is central to the computation of Paschen's equation which relates the ionization cost in a gas as a function of the breakdown voltage.

6.2 RF bombardment

The paper *Plasma Ionization by Helicon Waves* by FF Chen goes into depth on the derivation of the equations listed in this section where I have summarized them for clarity. Equations 6.2.1 through 6.2.3 are Maxwell's equations for a charged particle in the presence of electric and magnetic fields. They are presented here for note. Maxwell's equations are developed further in section 6.5 to obtain a path function for a charged particle in both uniform and non-uniform magnetic fields. In Chen's experiment Argon was the test-gas, likely because of optimal ionization cost at low pressures (0.6 Torr) and the RF waves generated were sufficient to cause ionization. The magnetic field induced was sufficient to trap the electrons but not sufficient to trap the larger ions. The electrons built up along the main axis of the containment cylinder where they gradually created an ambipolar potential sufficient in charge to contain the ions.

In this way, a plasma could be created consisting of largely distinct regions of electrons and ions while operating on a lower power setting of the induced magnetic field compared with VASIMR which is sufficient in magnetic field strength to trap, easily, both particles.

RF bombardment rapidly imparts energy to atoms within a confined space by "delivering" that energy to all of the subatomic particles via RF waves in the GHz range. The specific bombardment frequency depends on the eigenmode of the propellant for the outermost suborbital electrons. By imparting energy to all of the subatomic molecules directly rather than relying on secondary or tertiary inelastic collisions, RF bombardment is intuitively a more efficient process of ionization. Its main drawback is the high input power requirement to drive the ionizing antenna necessary to achieve ionization costs of less than 100 eV. RF bombardment inevitably results in a heated plasma on the order of 5800 K, which is still relatively cold at about the same temperature within the combustion chamber of the Saturn V. The energy absorbed excites the electrons and causes them to break free once they have reached a minimum potential level resulting in a plasma of approximately equal numbers of free electrons and free ions.

The equations governing Helicon RF waves in a contained cylinder are derived from the following 3 linearized equations taken from Maxwell's equations and solved using Stoke's Theorem[46];

$$\begin{aligned} \nabla \times \mathbf{E} &= -\dot{\mathbf{B}} & (6.2.1) \\ \nabla \times \mathbf{H} &= \mathbf{J} + \dot{\mathbf{D}} & (6.2.2) \\ \nabla \cdot \mathbf{D} &= \rho_{ext} & (6.2.3) \end{aligned}$$

The purpose of these equations is to determine equations of motion of charged particles in the presence of induce magnetic and induced electric fields. These equations are used to theoretically predict the exhaust field characteristics such as ion and thrust density, of a plasma engine. These equations are also solved for the eigen values which are the harmonic frequencies of the molecules to be ionized within the ICH, but not within the Helicon RF emitter. The RF fundamental frequencies are determined from Ionization potential, which is a function of the mass of the atom and the strength of its attraction to its electrons and the explicit solution of Schrodinger's-wave equation [46].

To solve Schrodinger's wave equation set the n energy levels of the wave equal to the n ionization potentials of the molecule and solve for the resultant fundamental frequency(ν). The value h is Planck's constant ($6.62607004 \text{ E} - 34 \text{ m}^2 \text{ kg / s}$). The resultant frequencies then form the eigen frequencies of the propellant atoms.

Power dissipated in the process of RF bombardment is described as the product of the z-components of the electric field and the current. This is expressed below in equation 6.2.5 as the rate of change of the power supply with respect to time. [46]

Expanding this equation results in equation 6.2.6 from the general solution of equations 6.2.1 – 6.2.3 for the electric and magnetic fields within a plasma as a function of time after the assumption is made that the electron cyclotron frequency is significantly larger than the fundamental frequency of the ions contained by the electron sheath, equation 6.2.6 is obtained for the electric potential in the axial direction within a mirrored plasma.

$$\frac{dP}{dt} = \int_{-a}^a E_z J_z dz \quad (6.2.5)$$

$$E_z = -\frac{\partial \phi}{\partial z} \quad (6.2.6)$$

Integrating 6.2.5 and assuming a stable plasma (such as exists for small time intervals in the ionization helicon of VASIMR) yields equation 6.2.7

A definition of a stable plasma is a plasma which, as a control-mass, does not lose energy over some finite time. Obvious sources of energy loss in plasmas are heat and light, emitted by ions returning to stable states. Equation 6.2.6 is useful then for determining the ionization cost of a non-adiabatically created plasma within a contained volume such as can be modelled within the space of the helicon RF component.

6.3 Electron bombardment

In electron bombardment, an easily conducting surface such as iron or magnesium is given a large potential voltage and electrons are emitted from it as the potential difference between that surface and ground becomes significant enough to free the electrons trapped there. These high-energy electrons are then directed via some mechanism such as a magnetic field or a series of electric potentials into an ionization chamber where they will eventually collide with an inert gas population causing secondary electron emissions again and again until they run out of energy.

In general, the ionization cost in all such plasma operations is (and must be) typically many times greater than the minimum ionization potential energy because so much energy is lost due to secondary electron emission. For example, in Argon, the minimum ionization potential is known to be 15.76 eV [47], yet Chen reports that it was frequently measured at as much as 200 eV [46]. And further atmospheric-based measurements have ionization costs of as much as 10,000 eV [44]. Adastra claims to have demonstrated an ionization cost of less than 100 eV for Argon propellant. Published data measured at the maximum efficiency setting of 45 kW diverted to the RF magnetizing coil and ionizing antenna shows an ionization cost of 98 eV.

6.3.1 Ionization cost

Ionization cost is essential to the comparison of electric propulsion systems in the same way that is essential to the comparison of chemical propulsion systems. It is abbreviated in this report as *IC* and is defined, for weakly ionized plasmas, as the energy required therein to create each electron-ion pair. *IC* has units commonly given in electron-Volts (1 eV = 1.60218E-19 Joules).

$$= * (6.3.1)$$

The derivation of equation 6.3.1 is simple and has the key assumption that the electrons are moving from the cathode to anode potential surfaces adiabatically. The figures;

, , , , , 0 & are defined in the nomenclature section after the table of contents but for convenience are defined here as: the average time for each electron to move from anode to cathode, the spacing between the anode and cathode, the average velocity of the primary electrons, potential energy, kinetic energy, electron charge, electron mass, number of ions & potential voltage, respectively.

$$= \frac{E}{v} \quad (6.3.2)$$

$$= * \quad (6.3.3)$$

$$- * (6.3.4)$$

$$= \frac{1}{n} \quad (6.3.5)$$

Following Thomson's equation for a charge between two potential surfaces (derived from LaGrange's equation) in an adiabatic system;

$$= \frac{1}{\ln \left(\frac{A}{B} \right)} \quad (6.4.1)$$

The constants A & B are defined below by the Boltzmann constant (k), Neutral atom temperature (T), collisional cross-section (σ) and the ionization potential (I).

$$= \frac{1}{\ln \left(\frac{A}{B} \right)} \quad (6.4.2)$$

(6.4.3)

The term is the secondary electron emission coefficient and is determined experimentally. Equation 6.4.1 was not Paschen's original law. Paschen conducted his experiments under relatively higher pressures (above 100 torr) where this "curve" is linear. For air and gaps of about a millimeter (on the order used in the experiment in Chapter 7.1) the breakdown voltage is approximately given by equation 6.4.4[48], which is also Paschen's original expression determined experimentally.

$$= 30 + 1.35 \left(\right) \quad (6.4.4)$$

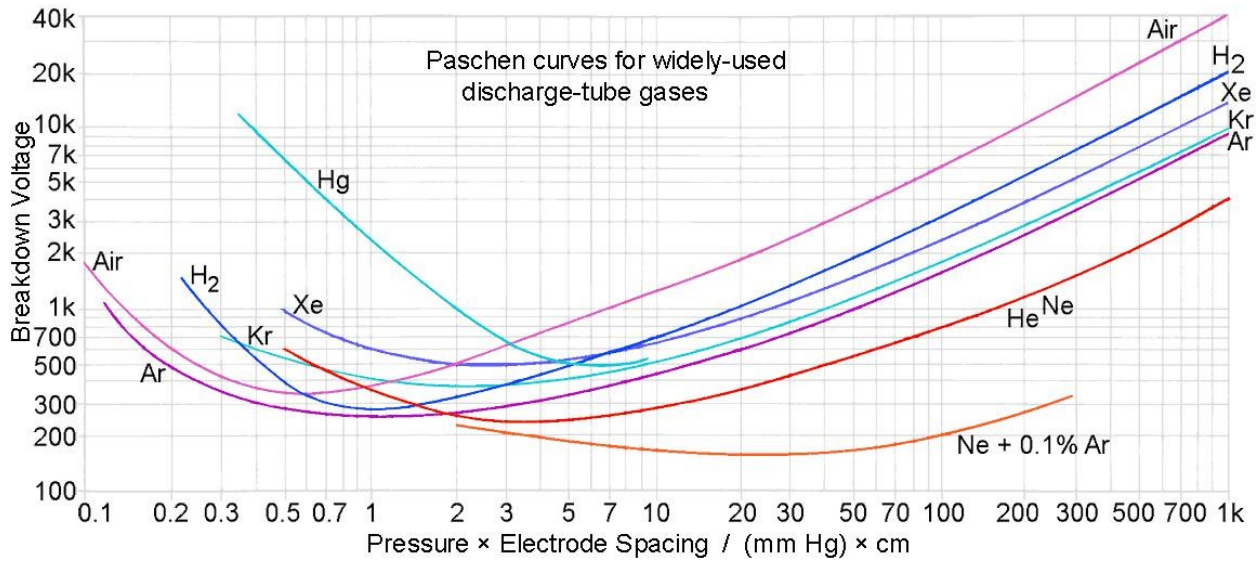


Figure 6.1 Theoretical Paschen curves for various elements [49].

The figure above illustrates the importance of the Paschen curve in estimating ionization cost as a function of pressure while the figure 6.2, below, illustrates the minimum ionization potential of various elements as a function of increasing atomic mass. Figure's 6.1 and 6.2 can be used to select an optimal propellant for electron bombardment propulsion set ups. For an RF bombardment propulsion set up, figures 6.1 & 6.2 are guiding metrics, but experimental data is required. The reason for this comes down to efficiency. Atoms of Kr and Xenon exist in more than one stable isotope resulting in a shifting of the region of maximum ionization efficiency in both RF bombardment regions. As of right now VASIMR uses Argon, despite having published better ionization results when operating using Krypton. The reason given for this is a lack of experimental test data from the ICRH portion of the engine, and conversely good results so far using Argon of over 70 % total efficiency. The presence of isotopes in krypton and xenon is estimated to move the optimal ionization and ICRH regions by less than 5 mm, but no data could

be found on the effects of this. I'm sure they've tested them or attempted to develop Xe and Kr versions of the VX-200i, but they haven't published any data pertaining to it.

Propellants are selected from figure 6.2 on the basis of their ionization potential to atomic mass ratio. In order to produce more thrust a heavier propellant is desired. The selection list is illustrated by figure 6.2 as He, Ne, Ar, Kr & Xe. I haven't come across anyone using Rn.

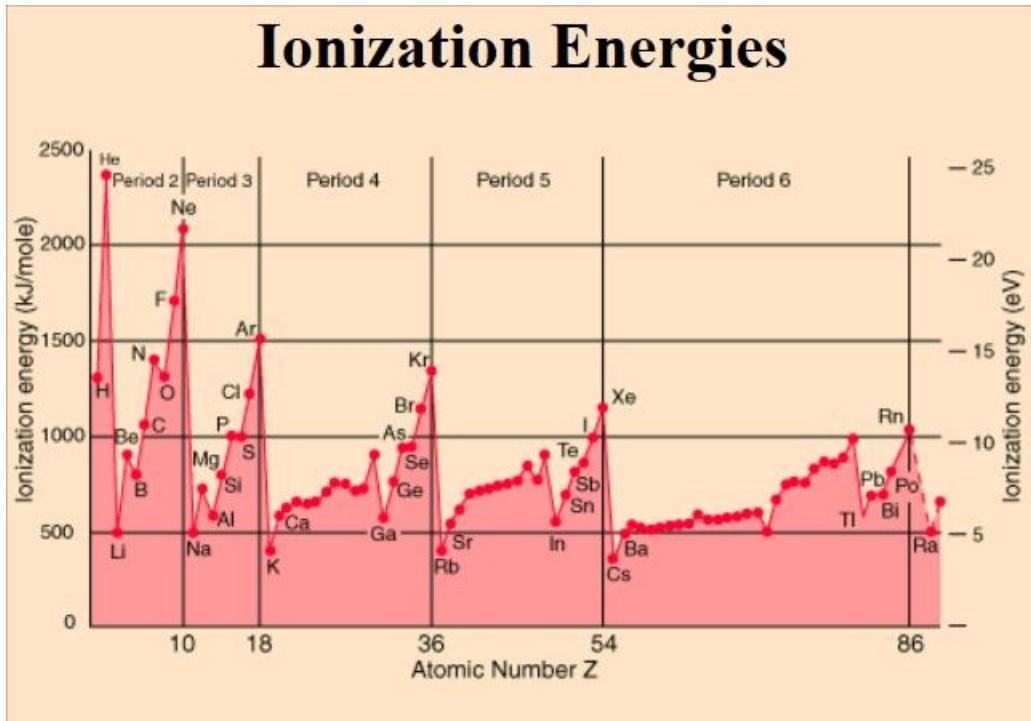


Figure 6.2 Minimum ionization potential of elements a function of increasing atomic mass.

An added complication in attempting to just use the Paschen curve is that for VASIMR, which involves an ICRH, new Paschen curves would have to be taken for the elevated neutral atom temperature (), and it is possible that Paschen's law may not apply for temperatures on the order of thousands Kelvin. Currently there is no information on this specifically published by Adastral or Paschen curves for gases hotter than the surface of the sun. There is only the fact that the VX-200i uses Argon.

6.5 Electro - magnetism & electro - magnetic interaction

Electro-magnetism was first observed by Hans Christian Oersted in 1820 when he noticed that a current carrying conducting wire caused the deflection of a nearby compass needle. The fundamental governing equations of electro-magnetism are known as Maxwell's equations and they describe the motion of a charged particle in vacuum under the influence of magnetic and electric potential fields. The four Maxwellian equations are;

$$\nabla \cdot \vec{E} = \rho \quad (6.5.1)$$

$$\nabla \cdot \vec{B} = 0 \quad (6.5.2)$$

In the above equations ρ is the density of electric charge, ϵ_0 & μ_0 are positive constants and \mathbf{j} is electric current density. Integration of equation 6.5.1 over a volume V with surface S and applying the divergence theorem results in Gauss's law of electric flux; which states the total electric flux out of a closed surface is proportional to the electric charge contained within the bounds of the closed surface.

From equation 6.5.2,

$$\nabla \cdot \mathbf{B} = \mu_0 \mathbf{j} \cdot \hat{n} = 0 \quad (6.5.6)$$

The above equation states that the net flux of magnetic field through any closed surface is zero. Intuitively this is obvious when considering that point magnetic sources do not exist in nature so that any magnet contained within a closed surface would have the same amount of magnetic flux "leaving" as "entering". Using Stokes theorem and integrating equation 6.5.6 results in Faraday's law for electromagnetic induction, which, for time-independent systems reduces nicely to Ampere's law.

$$\text{Stoke's Theorem: } \oint \nabla \times \mathbf{A} \cdot d\mathbf{l} = \oint \mathbf{B} \cdot d\mathbf{l} \quad (6.5.7)$$

$$\text{Faraday's Law: } \oint \mathbf{E} \cdot d\mathbf{l} = - \frac{d\Phi_B}{dt} \quad (6.5.8)$$

$$\text{Ampere's law: } \oint \mathbf{B} \cdot d\mathbf{l} = \mu_0 \int \mathbf{j} \cdot d\mathbf{a} \quad (6.5.9)$$

An important derivation of ampere's law for long straight current carrying conductors is the Biot-Savart law because it is integrated to determine the magnetic field vector at any particular point some distance from a stationary, current-carrying circular loop a distance from the origin.

$$\mathbf{B} = \frac{\mu_0}{4\pi} \int \frac{\mathbf{j} \times \hat{r}}{r^2} dV \quad (6.5.10)$$

The above equation, the Biot Savart law, is given as the magnetic field due to a current-carrying conductor of infinitesimal length dl . This equation can be solved for a situation such as a solenoid, involving a loop of radius a which is axisymmetric about the x-axis. Solving the resultant relation then for the magnetic field as a function of x along the axisymmetric axis of a single loop in the (x, y, z) as well as directions along the same axis results in the following two expressions.

$$= \frac{0}{4} \left(\frac{\quad}{(a^2 + x^2)^{3/2}} \right) \quad (6.5.11)$$

$$= \frac{0}{4} \left(\frac{\quad}{(a^2 + x^2)^{3/2}} \right) \quad (6.5.12)$$

x & y in equations 6.5.11 & 6.5.12 are oriented in the axis-symmetrical direction to the right and the vertical radial direction, respectively. and are magnitudes of vectors defined by the cross product of the conductor length vector and a position vector at which the magnitude is to be measured. The vector is defined in terms of a & x in all the equations in this section. It is important to note that these solutions are for a constant value of conducting loop radius (a) and a variable distance from the solenoid x . [50]

The local minimum strength of a magnetic field within a solenoid occurs at all locations along the symmetric X axis, as shown in the below derivation of equation 6.5.11. [50]. Integrating for a single loop then multiplying by N loops gives equation 6.5.13 which is equation 6.5.11 evaluated for N circular loops.

$$= \frac{0}{2} \quad (6.5.13)$$

6.5.1 Trapping charged particles in a mirrored magnetic field

To trap a charged particle in a mirrored magnetic field sufficient force is required in the perpendicular direction to a charged particles' velocity vector to force the charged particle into assuming a closed-loop path (equation 6.5.14).

$$= \times \quad (6.5.14)$$

Charged particles can be trapped within a potential well created by magnetic field lines strong enough to capture them into an orbit. The orbital radius of a particle inserted into a uniform magnetic field will obey the following relation derived from equation 6.5.14.

$$= \quad (6.5.15)$$

The obvious issue with 6.5.15 is that magnetic fields are rarely uniform. For non-uniform magnetic fields the orbital radii of charged particles have to be determined using vector calculus and Maxwell's equations from the previous section. Dividing equation 6.5.14 by the mass of the current-carrying electron results in an expression for the resultant acceleration on a charged particle q as a function of the instantaneous velocity and magnetic field strength B .

$$= () \times \quad (6.5.16)$$

One moving point charge is placed a distance a above the origin along the z axis and is oriented in the negative y axis direction and another opposing it a distance $-a$ along the negative z axis oriented in the positive y axis direction. The following 4 equations are the accelerations produced by on a charged

particle q in a magnetic field induced by the two moving point charges just described. The EOM derived from equation 6.5.3 are;

$$\begin{aligned} \ddot{x} &= \frac{q}{m} \left(E_x - v \frac{dB_x}{dt} \right) \quad (6.5.17) \\ \ddot{y} &= \frac{q}{m} \left(E_y - v \frac{dB_y}{dt} \right) \quad (6.5.18) \\ \ddot{z} &= \frac{q}{m} \left(E_z - v \frac{dB_z}{dt} \right) \quad (6.5.19) \end{aligned}$$

Maxwell's equations are now solved for \mathbf{E} and \mathbf{B} and then the above 4 equations can be solved for the equations of motion of a charged particle under the influence of a magnetic field produced by two moving point charges. The situation being developed here is similar to what would exist at the exit plane of a solenoid or the exit plane of the VX-200.

Setting 6.5.14 equal to zero, using Stokes theorem and integrating the Biot-Savart law (6.5.10), and using a bit of algebra an expression for \mathbf{B} can be obtained. Where A is a constant

$$\mathbf{B} = \frac{A}{r^3} \mathbf{x} \quad (6.5.20)$$

Resulting in the following equations for the induced magnetic field;

$$\begin{aligned} B_x &= \frac{A}{r^3} x \\ B_y &= \frac{A}{r^3} y \\ B_z &= \frac{A}{r^3} z \end{aligned} \quad (6.5.21)$$

Converting r distances to one cartesian coordinate system;

$$\begin{aligned} r_1 &= \sqrt{x^2 + y^2 + z^2} \quad (6.5.24) \\ r_2 &= \sqrt{x^2 + y^2 + z^2} \quad (6.5.25) \end{aligned}$$

And the observation that;

$$\frac{1}{r_1} = \frac{1}{r_2} \quad (6.5.26)$$

Combining the results gives a dynamical system expression, obtained from the derivations of the Maxwellian equations and the definition of the force on a charged particle in the presence of a magnetic field, (6.5.17,18,19). Into these expressions are substituted our expression for \mathbf{B} given by the following 6 expressions, and recalling that 1 amp = 1 coulomb/ second, to convert q in the above expressions to an appropriate current value.

$$= \sqrt{\Sigma B_x^2 + \Sigma^2 + \Sigma^2}; \quad (6.5.28)$$

$$\begin{aligned}
 & \text{(6.5.29)} \\
 & \text{(6.5.30)} \\
 & \text{(6.5.31)} \\
 & \text{(6.4.32)}
 \end{aligned}$$

Performing a simple test on the above 6 equations; subbing in $z=v=0$ and solving indeed does result in $v_1 = v_2$. Finally, setting the vector from the integrated form of equation 6.5.7 equal to the above expressions allows for a solution to the equation of motion for a charged particle in a non-uniform magnetic field.

These equations are integral to the magnetic nozzle analysis of section 8.2.

7. Experiment: Ionization Cost and Voltage breakdown in air at Sea Level

The specific purpose of this experiment was to determine the ionization cost of standard atmosphere. In general, it's purpose was to serve as a first step toward the design of an apparatus for trapping charged particles in a magnetic field and highlight key aspects of the propellant selection process as the first step in the design of any electric propulsion engine.

7.1 Investigation of ionization cost in standard atmosphere

The purpose of this experiment was to determine both whether or not voltage breakdown in standard atmospheric conditions of 20% 760 could be determined reliably and if so for what gap distances was it accurate to the theoretical prediction of Paschen's law. The results could then be applied to similar experiments for other gases and aid in propellant selection between Ar, Xe, Kr, Ne & He. The results were able to show a 2mm region of <15% error to Paschen's theoretical predictions for air where Ionization Cost could be reasonably accurately known.

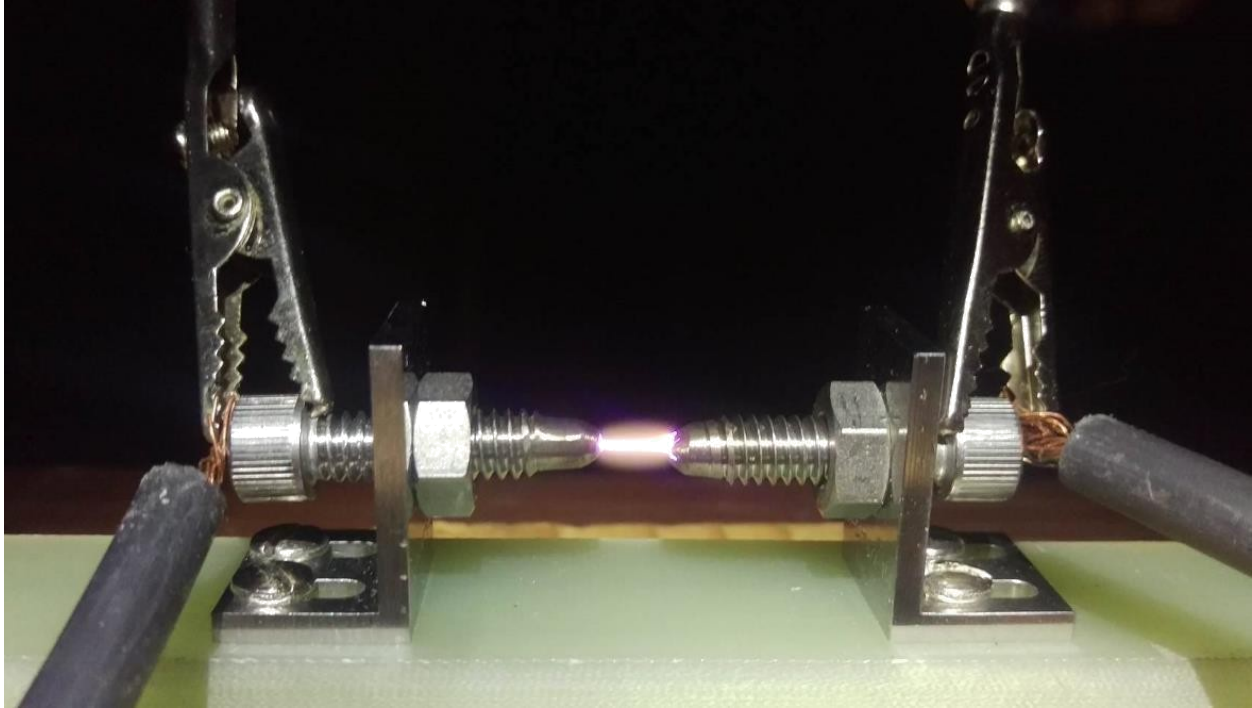


Figure 7.1 Experimental apparatus set up (shown for a gap of 3 mm), the purple-ish glow given off is created by Argon returning to a stable state.

The assumption was made that the primary electron emissions were adiabatic. This assumption is appropriate for small gaps of less than 1 cm because these electrons will not exist long enough to lose substantial energy due to thermal processes. Ionization cost was calculated from equation 6.4.1 multiplied by a conversion factor of $6.2415 \times 10^{18} \text{ (e}^{-}/\text{J)}$ to convert joules to electron-volts.

This experiment was set up in standard atmospheric conditions at an indoor lab facility provided courtesy of L3 Communications located in Redwood City, California. The necessary equipment including a 60,000 Peak- transformer, anode, cathode & high-resistance oscilloscope were also all obtained from L3 Communications in Redwood City. Breakdown Voltages were measured on an Oscilloscope as peak to peak values. Current was measured by using a 10:1 toroid attached to the cathode lead wire on a separate, low-resistance oscilloscope.

Paschen's equation (6.4.1) served as a theoretical basis for breakdown voltages against which was compared measured breakdown voltages. Areas of convergence to within $\pm 10\%$ have been said to be reasonably accurate for further analysis. It has been documented that convergence of measured breakdown voltages and theoretical breakdown voltages should exist in standard atmosphere for gap distances of less than 1 cm [49]. For gaps of beyond 1 cm it is thought that the quantities A & B (equation's 6.4.2 & 6.4.3, respectively) would vary too widely between anode and due primarily to lower secondary emission electron energies (<40% [47]) causing too many non-adiabatic collisions.

The published data featured in figure 6.1 was compared to the theoretical voltages obtained at 76 Torr ($h_p(760) * .1 \approx 76$) by equation 6.4.1. A breakdown voltage of approximately 5000V [49], was expected and the theoretical calculated breakdown voltage for 0.1 cm was 5034V [49]. Verification of a second point using the same process and a gap of 1 cm from the published

data is between 30 & 35 , compared to the theoretical value of 35.509 *kV*. It was assumed that the accuracy of these results to experimental data for error<15% would lend some credibility to the Ionization Cost calculation of equation 6.3.1.

Paschen curves for constant pressure proved difficult to find so care was taken to first validate the theoretical voltages obtained from equation 6.4.1. before proceeding with analysis.

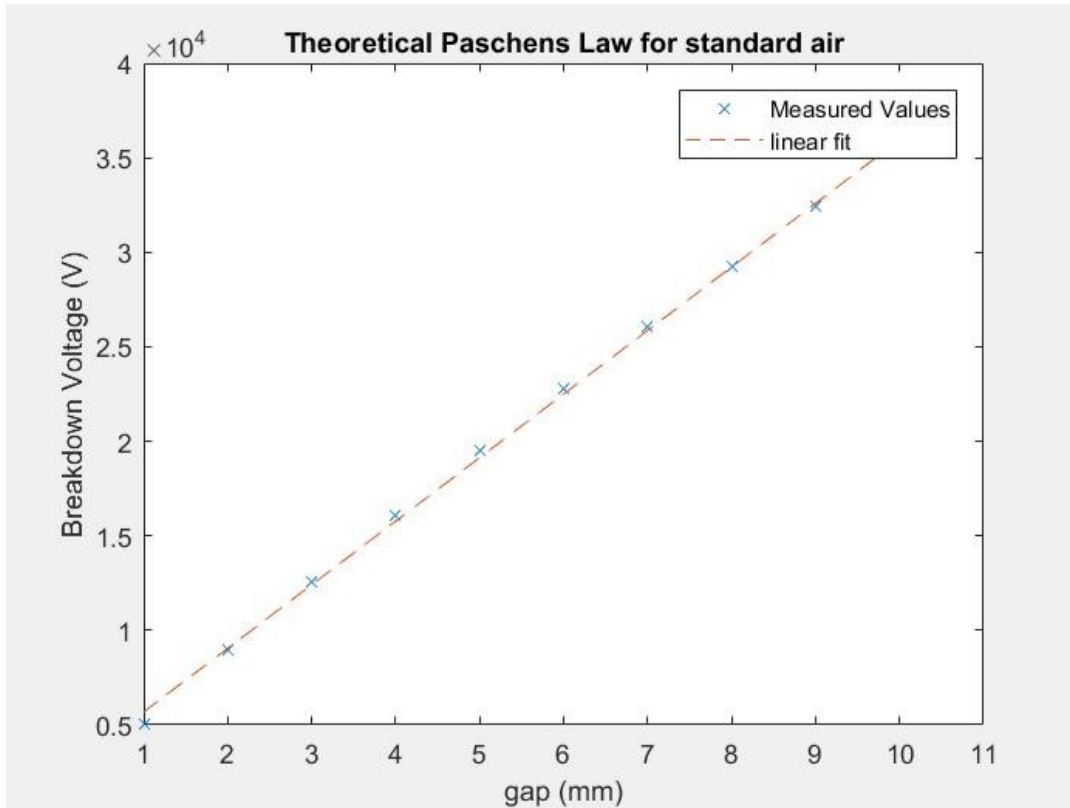


Figure 7.2 theoretical Paschen prediction, atmospheric air. The linear fit equation $y = 3363 \cdot d + 2319$ was solved for in MATLAB, utilizing $y = mx + b$ to generate the linear fit curve.

The assumption stated by equation 6.4.4 [49], that for air gaps of less than 1 cm at standard pressure a Paschen curve can be accurately approximated by a straight line, is illustrated by figure 7.2 where a linear fit was applied in MATLAB to theoretical data from equation 6.4.1. The average deviation of the theoretical value from this linear approximation was 2.13% but ranges between 0.076 % → 11.38

% The upper limit of this range is the reason the linear approximation of 6.5.4 was not used for this experiment. 5% was arbitrarily selected as a maximum acceptable deviation and 1 % for a maximum acceptable average deviation for the linear fit model and neither equation 6.5.4 nor a linear fit model satisfied either completely for the reasons just stated.

The minimum ionization potential of a molecule is the minimum amount of energy that molecule needs to lose the most “loosely” bound electron and become an ion. These quantities for all the elements of the periodic table are approximately known values for stable isotopes. The equation below is the expression for a rough estimate of ion population caused by secondary emission.

$$\frac{\#}{*} = 40\% \quad (7.1)$$

The percentage of secondary emission energies is given as 40% for high primary emissions on the order of multiple thousand electron volts. This is simply because higher energy collisions will result in higher ionization potentials for each primary electrons' first few collisions [49]. The average ionization potential of air at standard conditions is estimated at 30eV.

7.2 Results

The measurements between 0 & ≈2mm were taken at the end of the experiment, whereas the rest of the measurements were taken in increasing gap distances beginning with the 3rd data point.

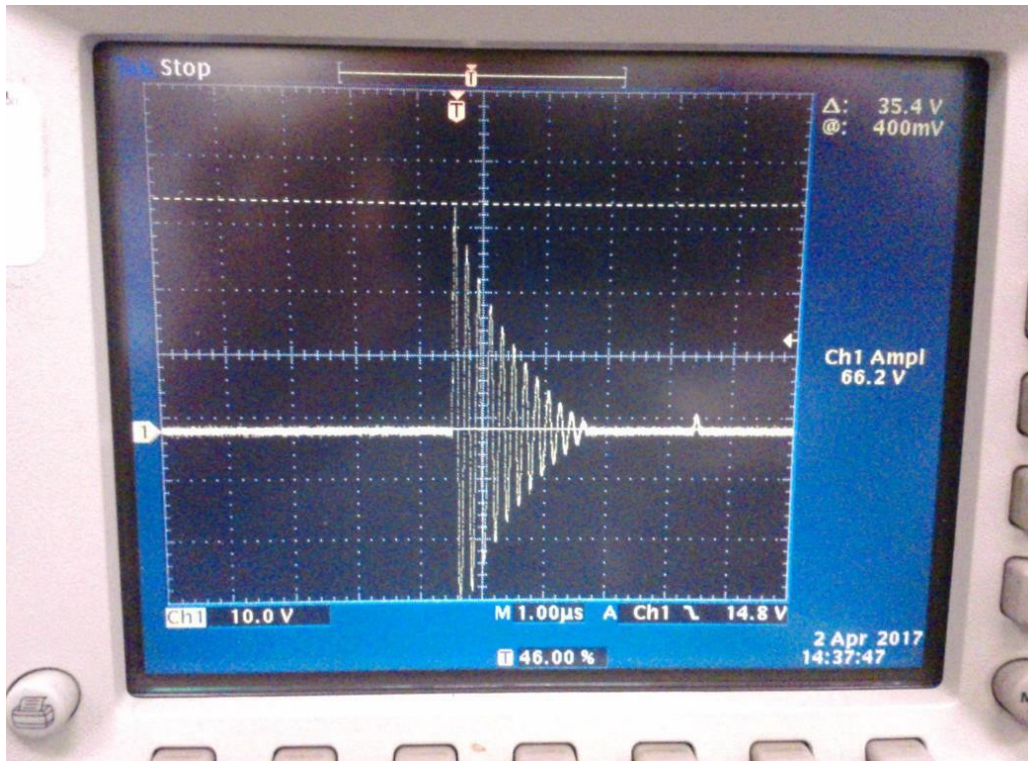


Figure 7.3 measurement, oscilloscope, for breakdown voltages. Equipment owned by L3 Communications.

The measured ionization cost () was determined from equation 6.3.1, while the values are from the linearly fit line in figure 7.1 and the gap positions in table 7.1.

Table 7.1 Ionization Cost, experimental and theoretical results

		Measured Ionization cost and corresponding gap distance										UNITS
gap	.2032	.7620	1.016	1.9812	2.413	3.302	9.9822	12.7	19.05	22.86		mm
	1500	3700	4700	8000	9500	12000	15999	20499	25799	29999		eV
	3002	4881	5735	8981	10,433	13,422	35,885	45,024	66,376	79,188		eV

% deviation	50.04	24.20	18.05	10.92	8.94	10.60	55.41	54.47	61.13	62.12	%
--------------------	-------	-------	-------	-------	------	-------	-------	-------	-------	-------	----------

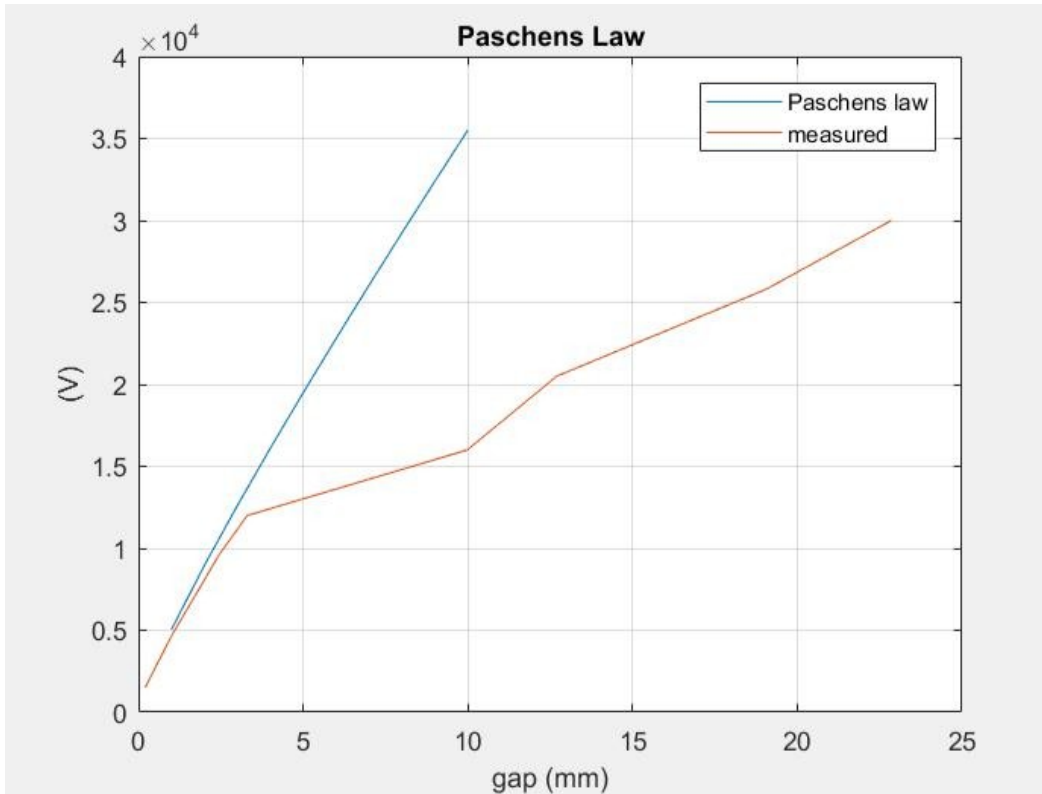


Figure 7.4 Paschen curve for atmosphere at 760 Torr

Moderate correlation (error <15%) to theory for the Paschen curve results listed in table 7.1 and displayed in figure 7.4 between gap distances of 2 & 4 mm. The second-degree polynomial curve fit displayed as the red line in figure 7.5 exhibited a mean deviation from the measured values of 7.26%. Deviation from theory at gaps above 1 cm in standard atmospheric conditions was expected although not at values of 1 cm, for which deviation of over 50% was observed.

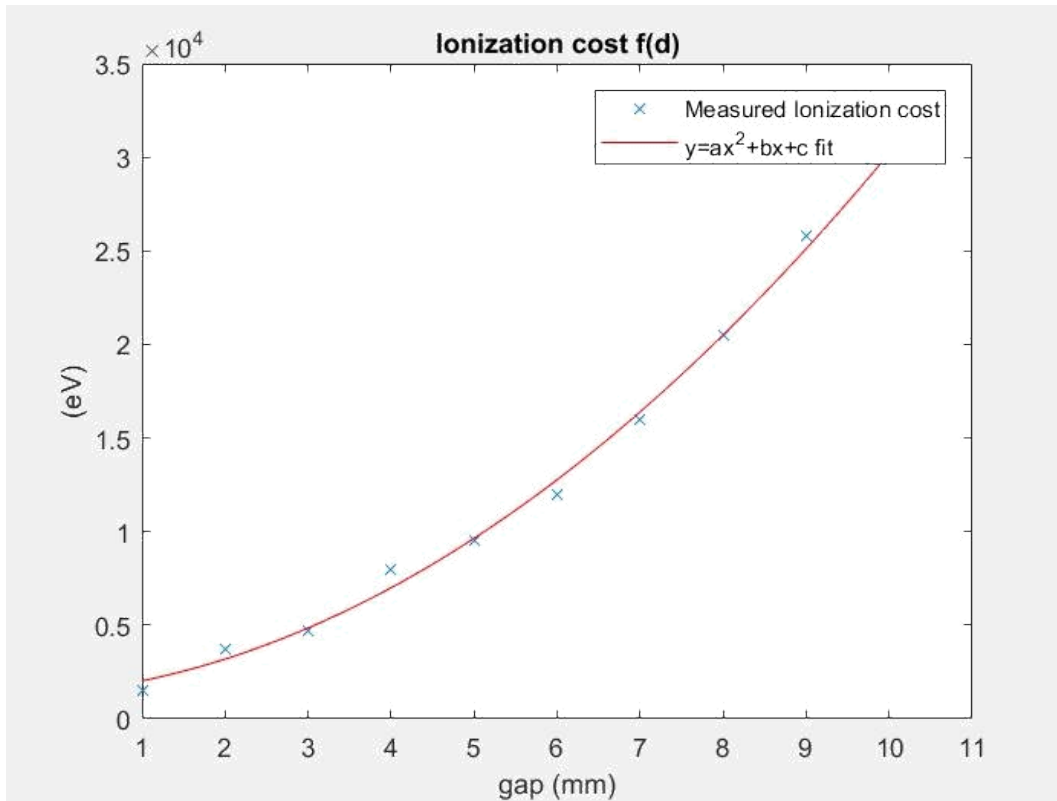


Figure 7.5 ionization cost vs. gap distance, second degree polynomial curve fit

7.3 Discussion

A minimum gap, which was unexpected, was observed at (where error is greater than 15%) ≈ 2 . The measured error in the breakdown voltage cannot be caused by heating because Ampere's law states that voltage potential is linearly proportional to internal resistance.

$$= (7.3.1)$$

The only way the results for could become 50% or so less than theoretical analysis (assuming no human error) were if the air became conducive to electricity over time. My conclusion, however, is that the result is probably due to human error. Additional testing is required to prove this, however, access to the necessary instruments is no longer available.

The atmospheric values of breakdown voltage are documented at values inconsistent with Paschen's law above 1 cm for previously published data as well although, most results cohere to theory up to 1 cm. As for the minimum gap, as mentioned this was previously unexpected. I could find no mention in any relevant published data of significant deviation for small gap distances of $\ll 2$ mm. The reason for the minimum gap error is unknown, but it can probably be attributed to human/instrument error since it is unlikely that a law used so reliably in industry would be wrong. This lab was conducted in an unfamiliar place on unfamiliar equipment meaning that significant human error is not unlikely.

Unfortunately, I do not have the ability to repeat the experiment a second time so I cannot know for sure what caused the error.

This analysis has provided a range of anode-cathode gap distances (2 → 4) for further investigation, which might yield consistent results in ionization cost analyses over a range of propellants being considered for ion thruster development.

Compared with the ionization cost of <100eV for VASIMR means that the most efficient ionization of air at sea level conditions would result in a propulsion system operating on at least 15 times the Energy cost of the VX-200i. The VX-200i claims to operate at under 100 eV for some specific low thrust regimes where propulsive efficiency is greatest at over 10,000 seconds [43]. The minimum ionization potential of Argon is 43 eV, and that increases in the ICRH section when the ions are heated to nearly 90,000 K. Total efficiency in the ionization process for the VX-200i is 93%[47], which is two to three times as efficient as currently operating ion and hall thrusters operating on between 2 and 3 hundred eV.

This analysis has provided a range of anode-cathode gap distances (2 → 4) for further investigation which might yield consistent results in ionization cost analyses over a range of propellants being considered for ion thruster development. By determining ionization cost as a function of gap distance this experiment has also laid out a foundation for studying ionization cost which can now be used to design an investigation of charged particle trapping in a mirrored magnetic field.

8. Electromagnetism

This chapter deals with Electromagnetism and serves as a theoretical basis for future experimental analyses studying ion behavior in an expanding magnetic nozzle. An expanding magnetic nozzle is a key feature of the VASIMR engine and an important feature of all electric propulsion systems.

8.1 Investigation of charged particle trapping within the ICRH of VASIMR modeled by a uniform magnetic field

For this analysis equation 6.5.14 was solved in MATLAB using ode45 and the results were compared with the theoretical radius predicted for a charged particle in a uniform magnetic field (6.5.15).

$$= \times^{(6.5.14)} \quad (6.5.15)$$

The fundamental quality of the VASIMR engine is its mirrored magnetic field which traps both the ions and the freed electrons in a restricted space small enough for efficient ionization and heating. To simulate this effect, consider an Argon ion in the VX-200i after it has left the RF antenna and before it enters the ICRH where magnetic field strengths have been reported as high as 2 Tesla. Within the ICRH is it necessary that the location of the ion not be allowed to vary by more than 1 mm from the central heating axis in order to achieve efficiencies >70%. This simulation was completed by assuming the minimum charge case for an argon ion, since this would correlate to a maximum orbital radius according to equation 6.5.15.

Table 8.1 Simulation input parameters

<i>Name</i>	<i>Value</i>	<i>units</i>
B	2	Tesla
	6.6335209 e-26	Kg
	1.602 e-19	Coulomb(s)
	5,000	m/s
Time Step	0.8 e-5	s

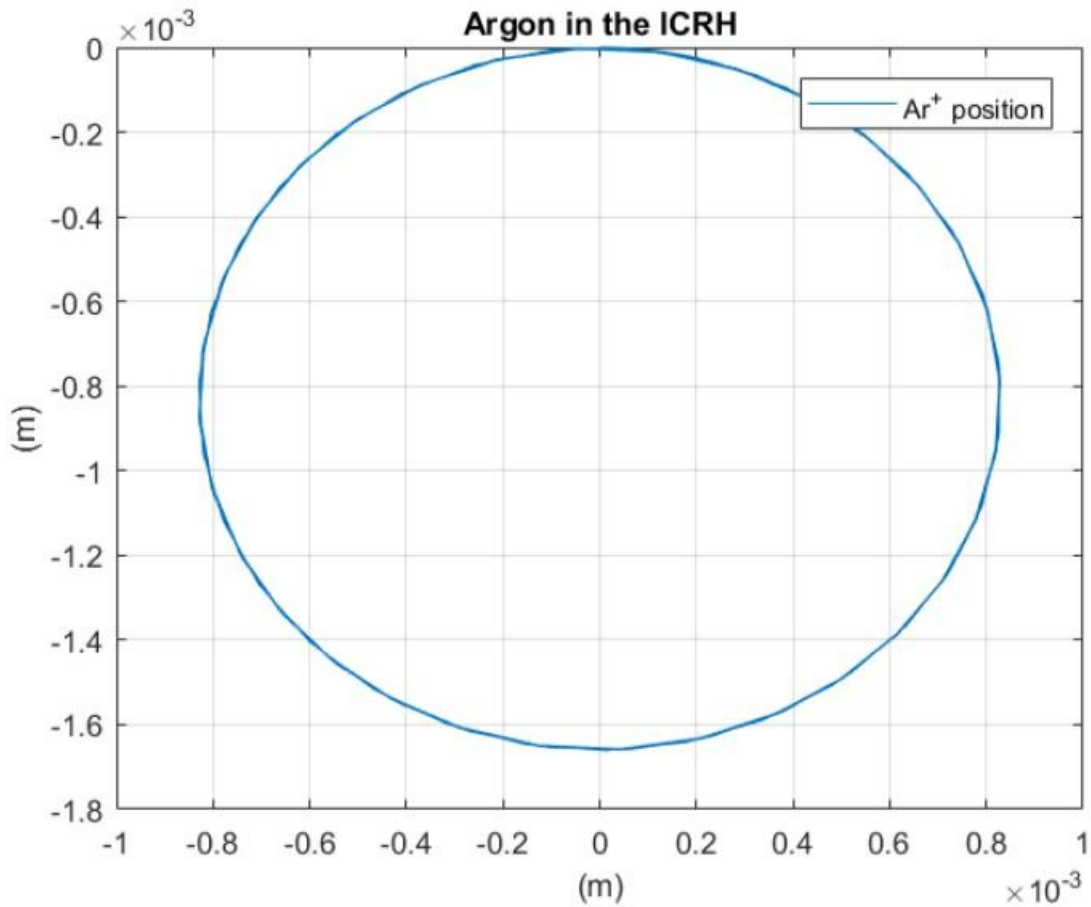


Figure 8.1 2Dimensional Path of Argon within VASIMR's ICRH

The equations of motion for this particle result in an orbital radius which matches the predicted orbital radius of equation 6.5.15 within a percent error of <1%.

Table 8.2 Simulation results

<i>Parameter</i>	<i>Value</i>	<i>Units</i>
	.00083	m
	.0008303	m

This was a simple illustration of charged particle trapping for the main purpose of demonstrating the orbital nature of the path of the charged particles trapped in a uniform magnetic field and lead into the next experiment which is modelling of the particle as it leaves the ICRH. The results for this chapter were that there was <1% error as well as confirmation, from a general and theoretical point of view, the behavior of argon ions within the ICRH to remain within 1 mm of the symmetry axis.

From this analysis, a possible reason for the selection of Argon rather than Krypton or Xenon arises from equation 6.5.15. Although the ionization potentials are lower for Xe & Kr and their masses both greater than Argon making them increasingly ideal for momentum exchange, their orbital radii may be too large for efficiency losses to offset the positive effects of newtons second law. This combined with the fact that both Krypton and Xenon have multiple stable isotopes means that not only will the orbital radii for these propellants in the ICRH be larger, but there will be multiple orbital radii for each case resulting in even greater losses in efficiency.

8.2 Investigation of charged particle trapping in a non- uniform magnetic field

BOOM

As stated earlier, the behavior of a plasma in an expanding magnetic nozzle can be approximated most accurately by using Maxwell's equations (6.5.1 → 6.5.4). It was generally felt that solving Maxwell's equations for a complex 3-dimensional plasma was beyond the scope of this report. However, the motion of a single charged particle in an expanding magnetic nozzle could be investigated using Maxwell's equations and a few appropriate assumptions. First, the assumption must be made that all external sources of electric potential gradient are negligible. That there is no affecting electric field present in the nozzle is an appropriate assumption because the source of the electric field in the plasma comes from the plasma itself and so without multiple charged particles there is no internal electric field. Second, the process is adiabatic. This is appropriate because the model is theoretically in vacuum and the particle is insulated from sources of inelastic collision by a conservative magnetic potential field.

This analysis was completed by orienting two point sources of magnetic induction a distance ' a ' above and below the origin in the $-y$ and $+y$ directions, respectively and then scaling up the induction of those points until a magnetic field of 2 Tesla could be calculated at the origin. The combined effect of the 'fixed' charges at locations a & $-a$ along the z -axis are to compound to induce a magnetic field in the positive direction (no Oz component) while within the YZ plane. The component of the magnetic field decreases in proportion to the square of the x distance from the origin as the magnetic equipotential lines wrap around the two point sources until they eventually intersect the point sources again, thus satisfying Stokes Theorem. See figure 8.2 for cartesian coordinate system layout.

There had to be an assumption made about the cartesian velocity of the ions leaving the ICRH and that was that \gg . This assumption is appropriate since translational velocity dominates ionic motion, yet cannot be zero because this would result in ions without orbits in the simulation as well as be unrealistic to the ions and electrons comprising the plasma which have 6 degrees of freedom.

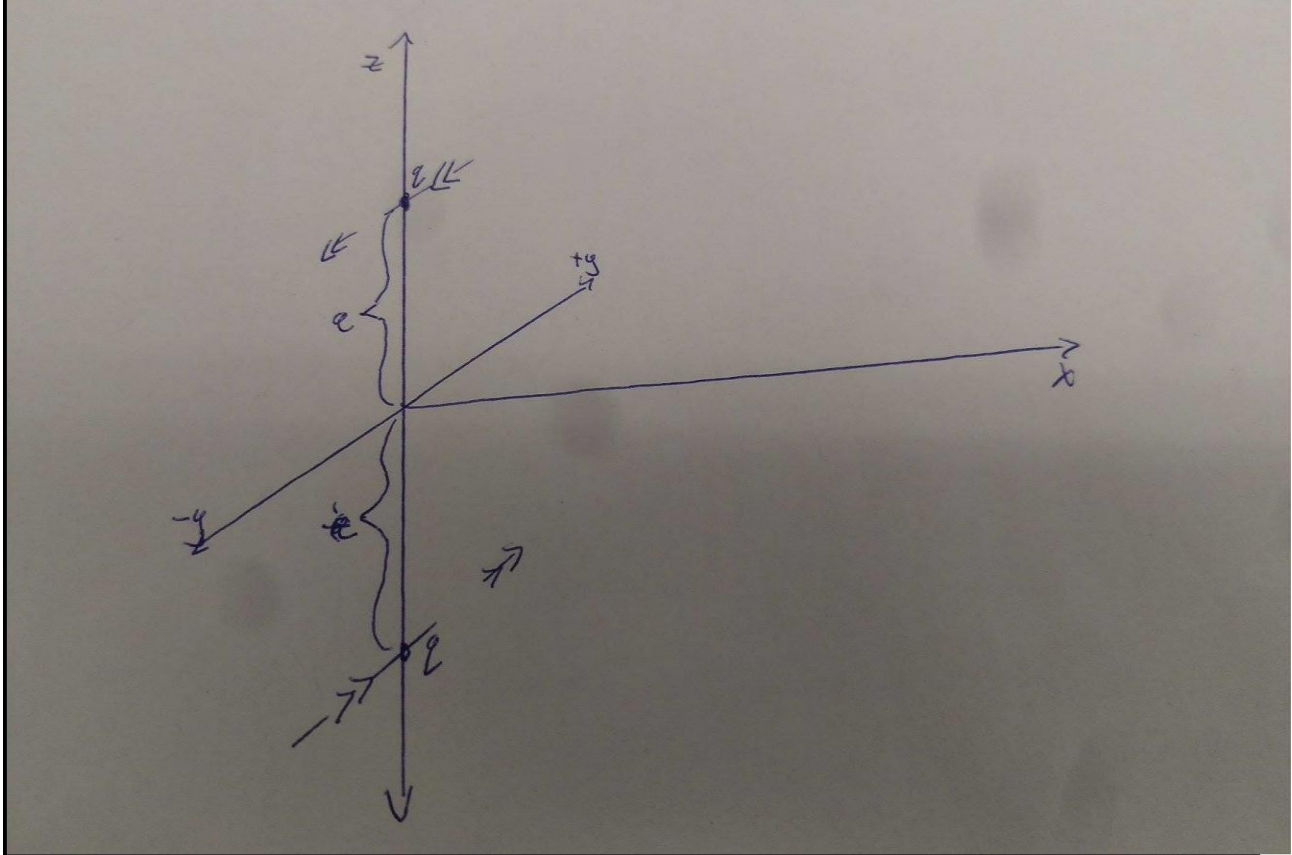


Figure 8.2 Cartesian coordinate system showing magnetic inductance locations in relation to the origin. The double arrows indicate the direction of the “moving” charged particles.

For this analysis, the components of the magnetic field in the cartesian directions x , y , & z , equations 6.5.20 through 6.5.32, for all points within the exhaust region of the flow for 2 point sources of magnetic induction, were substituted into the cartesian acceleration equations 6.5.17 through 6.5.19 and solved using ode45 in MATLAB. The results of this path simulation are displayed in figures 8.3 & 8.4. The simulation parameters and initial conditions were pulled from published data pertaining to the state of the Argon ions in the flow at the exit plane of the VASIMR rocket engine. The model performs a path estimation of a single charged particle in an expanding magnetic nozzle.

[44]. 50 iterations were done of exhaust field trajectories for an of 5,000 seconds. This value corresponds to the maximum of VASIMR for $a = 6.1$, according to figure 5.11

Table 8.3 Simulation Constants

Symbol	Value	Units
A	2.6e-33	Kg*Wb*m/A
q	1.609 e04	Coulombs
	2350	m/s
a	1	m
	6.6335209 e-26	Kg
B (0,0,0)	2.0	Tesla
Iterations	50	

Table 8.4 Initial Conditions & iterative time constants

Condition	Value	Units
	0	m
	49,050	m/s
	Variable	m/s
	Variable	m/s
time final	1e-4	s
Time step	1e-7	s

According to equation 6.5.15 the orbital radius expected at the beginning of the simulation should be smaller than at the end. According the equation 6.5.14 the resultant path should be be circular about the x axis and positive in the x-direction for positive & initial conditions, a fact which is observable by figure 8.3. According to the Biot Savart law (6.5.10) the radius should increase as the cube of the distance from the origin. The following plots verify these results thus confirming the accuracy of the equations derived in chapter 6.5 and their implementation.

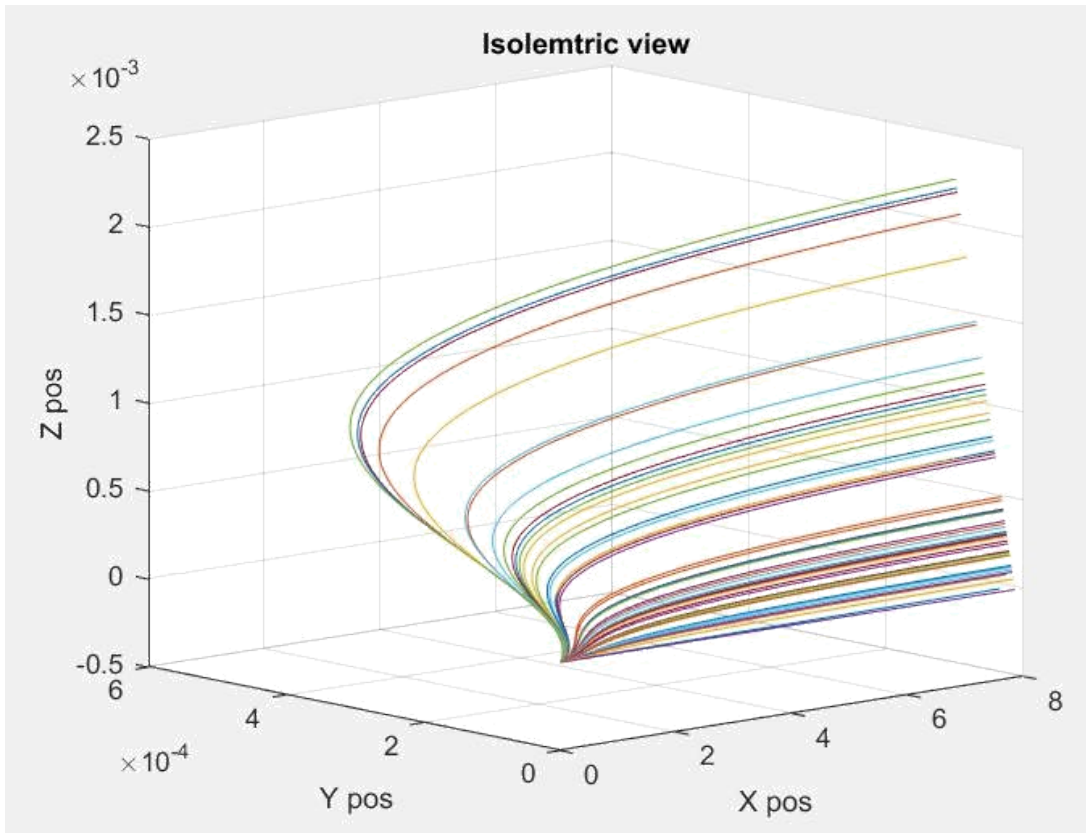


Figure 8.3 Isometric View. All ions begin at the origin and progress in the positive x direction.

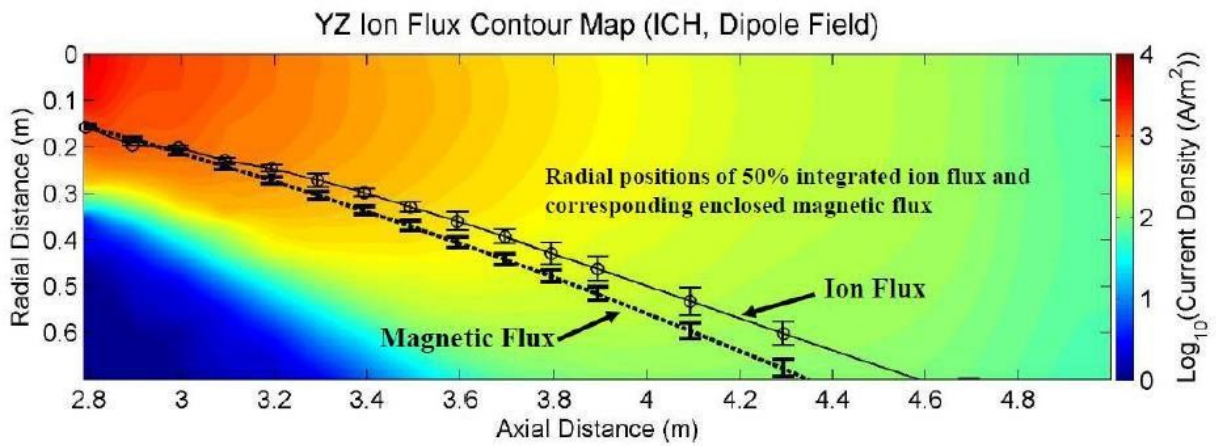


Figure 8.4 Published data. Ion density within the ICRH exhaust field. [44]

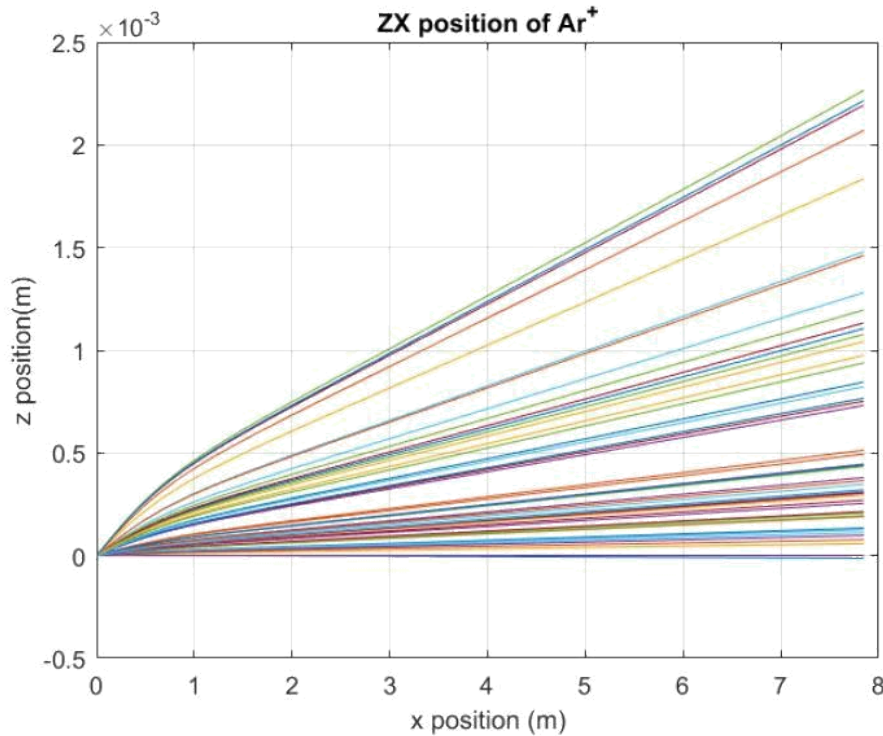


Figure 8.5 Exhaust field trajectories for Argon ions with constant x-direction exhaust velocities and 10% variable y & z velocities.

From the comparison of figures 8.4 & 8.5 it is apparent that there is considerable error between the particle trajectories being simulated and the trade study results that the simulation is based on. This is believed to be the result of intermolecular forces including inelastic collisions & ambipolar acceleration discussed earlier. A final source of error may result from the point charge modeling approach taken in the simulation. Future refinement of this analysis may be able to determine to what extent, exactly, each is affecting the flow field trajectory.

Sampling at 3 m “downstream” of the exit the simulation flow field radius maximum is ≈ 1 meter. This is a 60% error from the measured flow field radius of the VX-200i.

The simulation results show no additional acceleration in the x-direction for particles subjected to an expanding magnetic nozzle. This is not the case with VASIMR but it is the expected result of this solution. This is because in VASIMR the charged plasma particles affect each other internally per Maxwell’s equations. The effects of electric and magnetic fields on a plasma from internal and external forces utilizes all of Maxwell’s equations and therefore is beyond the scope of this report.

A plasma as a gas is approximately inert (containing equal numbers of positive ions and negative electrons), and so, will accelerate; as such will any supersonic rocket exhaust subjected to an increasing cross sectional area. However, individually the charged particles will obey Maxwell’s equations when subjected to electric & magnetic fields. For this reason, the analysis in this section is inaccurate; and that is the point. In order to understand the effects of the plasma and the expanding magnetic nozzle a basis must exist and be shown to be accurate for their effect on a single particle.

This chapter has investigated methods of ion trapping to serve as a basis for both understanding in VASIMR and future experimental investigations into the behavior of a plasma in an expanding magnetic field.

9. Novel Design

9.1 Purpose

The purpose of this chapter is to develop an electric propulsion concept which fills the design space between the small Hall & Ion thrusters and the large VASIMR engine. Then, compare it to a chemical method tasked with the same velocity budget. The concept calls for essentially taking a VASIMR engine, removing the ICRH half and using the remaining ionization half to power satellite missions to nearby orbiting bodies such as Venus, the moon or Mars.

The broader goal of this project was to incorporate the mirrored magnetic field already developed and in use on small, earth-orbiting satellites and the rapid RF ionization antenna developed by AdastrA into a novel design of a smaller propulsion system of greater relative thrust. By doing so, future satellites could take advantage of the benefits of the highly efficient RF bombardment process such as greater mass flow rate and thruster efficiency without the drawbacks of the weight and size of VASIMR.

Such a system would be capable of downsizing satellite missions to other planets, but it does not come without restrictions. Absorption efficiency is a function of propellant density so that in order to attain over a 70% absorption efficiency a mass flow rate of 0.0612 g/s [44] must be used in the RF antenna region. However, this efficient mass flow rate only results in a 10% thrusting efficiency [44]. One way of solving this problem would be to insert an electric potential gradient into the plasma exhaust region. Then the issue would be that the free electrons and ions, having opposing charges, would end up accelerating in opposing directions. This is a fact taken advantage of by the ionization process of hall thrusters discussed in chapter 3. As long as the spacecraft is insulated from damage that might be caused by the interaction of these increasingly large numbers of free electrons there isn't a problem until the cathodes decay to a failing point or the electric charge builds up enough to pull the ions back into the thruster resulting in exactly zero thrust and general mayhem for the spacecraft's electric components.

The main issue with using cathodes and anodes is that the decay related to these components is currently the main limiting factor of electric propulsion systems because of their rate of decay resulting from high energy interactions with charged particles. For these reasons, it is unlikely that such a system could be designed and continuously operated over a burn time of 100^+ days necessary to reach nearby orbiting bodies at constant thrust of $\approx 1 \text{ N}$, without experiencing critical failure. The cathodes and anodes currently operating on Ion and Hall thrusters max out at about 0.1 N of thrust making the prospect of using anodes and cathodes unlikely. Although, NASA's NEXT thruster promises almost half a Newton of thrust so perhaps it might not be so unreasonable in the near future to get closer to a whole Newton.

9.2 Novel Solution Design Analysis

The velocity of the ions exiting the helicon on the Vx-200i is in the vicinity of 10^4 m/s , according to AdastrA, resulting in an τ of 1019 seconds, according to equation 9.4.1.

$$\tau = \frac{1}{\omega} \quad (9.4.1)$$

Since ω is a fixed value in order to attain 72% absorption efficiency, τ is determined from equation 9.4.2.

$$\tau = \frac{1}{\omega} \quad (9.4.2)$$

The results of table 9.1 are the parameters taken from Ionization experiments done on the VX-200i and the equations featured in this chapter. The maximum payload mass is taken to be a scaled value of the VASIMR estimated payload mass on the basis of thrust, i.e solve equation 9.3 for m_p ($m_p = 400,000$) [44].

$$I_{sp} = \frac{F}{\dot{m} g_0} \quad (9.4.3)$$

Table 9.1 Preliminary design analysis values; from published RFHelicon experimental data and the featured equations in this chapter. Data from MATLAB file solarray.m

Parameter	Value	Units
C	10,000	m/s
(Argon)	1019	S
	0.0612	mg/s
F	0.6118	N
requirement	= 25	kW
	= 99	eV
	72% ± 9%	%
	= 10%	%
	41,067	kg
B	2.0	Tesla
Propellant	Argon	

In table 9.1 the design feature which stands out the most has to be the 25-kW power requirement. Assuming that this rocket will not be using a small nuclear based power plant the size requirement of the EPS power supply will most likely be limiting. The company MadeInSpace has developed a factory satellite capable of assembling large solar arrays from compactible storage, so, perhaps such a system could be deployed effectively if used for this purpose.

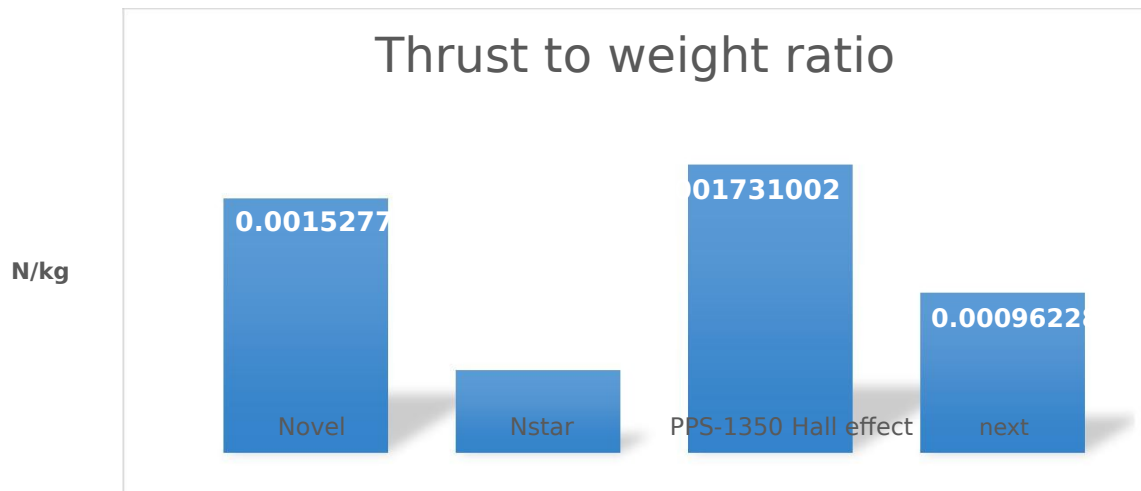


Figure 9.1 Thrust to weight ratio of the EPS; comparison between the Novel solution and 2 other flight tested thrusters. The "NEXT" thruster is in development.

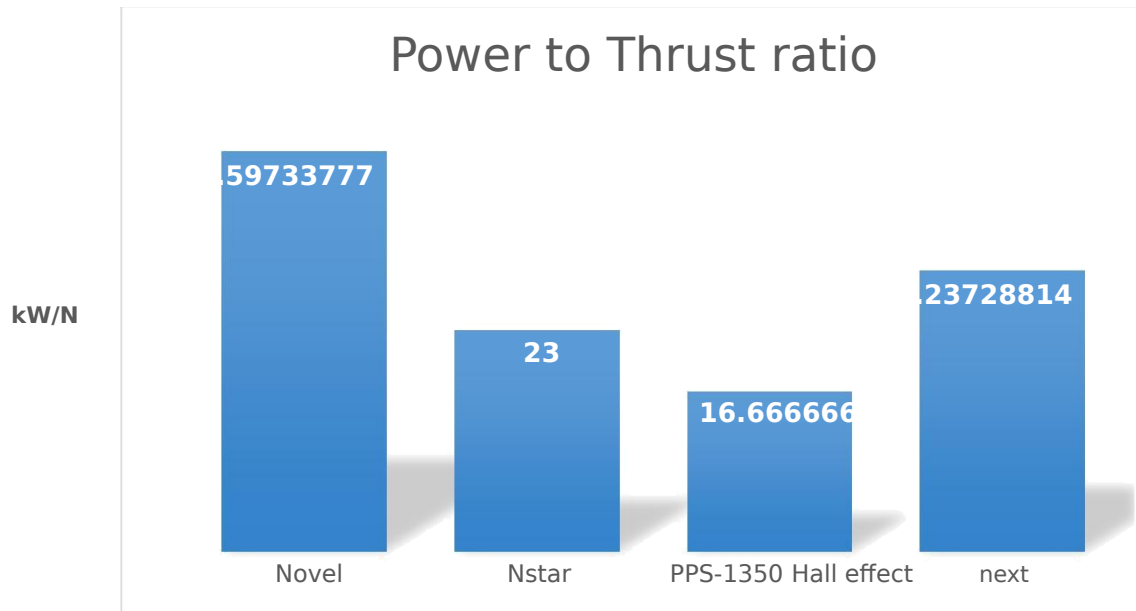


Figure 9.2 Power to thrust ratio of the EPS; comparison between the Novel solution and 2 other flight tested thrusters. The "next" thruster is in development.

Figure 9.2 outlines the effect of both not having an ICRH component and the high magnetic field requirement necessary to sustain >70% absorption efficiency of the propellant in the RF antenna.

9.3 Mission profile Design

This design process is for a three stage to orbit chemical rocket followed by a single electrical “burn” to reach an escape trajectory towards Mars followed by a single chemical stage for Mars orbit insertion (MOI). The purpose being that this novel solution would operate within the realm of possibility of chemical methods, so what would be the cost/benefit analysis of using it, what are the weight and cost savings of doing so and can the design be altered in any way to improve performance parameters.

The design process begins by selecting a payload mass and a delta V budget, then solving equation 2.1.3 to determine mass ratio and so on until you have your rocket design. The advantage thus far is that all electric propulsion systems in use today that I am aware of are single stage so equation 2.1.3 remains algebraically simple, having only one mass ratio.

$$\frac{m_0}{m_f} = \frac{1}{1 - \frac{F}{g_0 m_f}} \quad (2.1.3)$$

9.4 Novel solution comparison

The design space of the novel solution is defined by the estimated thrust (F) in table 9.1, scaled down from a previously published flight profile for a manned mission to Mars utilizing the VX-200i. This solution is for a design comparison between two mission profiles, each delivering a 1,000-kg payload to 300 km LEO. Then a single stage comparison is done between the novel electric propulsion solution and a chemical solution. In this way, an accurate cost comparison can be made between the two systems by incorporating their effects on the design of the ground to LEO stages.

9.4.1 Propellant selection

The propellant could be selected as Krypton or Xenon or Argon, but the bulk of published data deals almost exclusively with Argon, and since this solution has to be based on something concrete, the selection to use Argon is made. Comparison with Xenon in the cost analysis section is featured. Testing would likely yield the selection of a different propellant, either Krypton or Xenon, since a study published by Adastral has already demonstrated a higher thrusting efficiency (>80%) utilizing Krypton and possibly higher (estimating the trend between thrusting efficiency and atomic number) utilizing Xe. The catch will be the tradeoff these propellants provide with absorption efficiency, however VASIMR insists on using Argon so for now in this analysis I am going to assume they know what they are doing and do the same.

9.4.2 Design

Solving the equation below requires the assumption that either the mass ratios are all identical or that the initial individual stage masses are equal in order to result in one equation with one unknown, where the unknown parameter (propellant mass) is solved for in terms of the payload mass ().

$$\Delta V = v_1 \log \left(\frac{m_1}{m_1 - m_{p1}} \right) + v_2 \log \left(\frac{m_2}{m_2 - m_{p2}} \right) + v_3 \log \left(\frac{m_3}{m_3 - m_{p3}} \right) \quad (9.4.1)[3]$$

The VX-200i currently operates beyond the upper limit of power available in space. There simply does not exist an independent platform in earth orbit capable of the VASIMR engine's 200 kW power requirement. The power available to the International Space Station is only 90 kW highlighting the importance of having a high thrust to power ratio.

To determine the propellant mass & spacecraft stage mass for a range of delta V budgets from LEO equation 9.4.1 was solved where system mass was a known parameter for the electric system and the system mass from the ground to LEO stages was set to 7% of propellant mass and 14% of propellant mass for the ground to LEO and LEO burns, respectively (a metric borrowed from Sutton's Elements of Rocket propulsion text [3]). After some algebra equations 9.4.2 & 9.4.3 are derived for the single stage.

$$m_{p1} = \left(\frac{m_1}{m_1 - m_{p1}} \right)^{\frac{\Delta V}{v_1}} - 1 \quad (9.4.2)$$

$$m_{p2} = \left(\frac{m_2}{m_2 - m_{p2}} \right)^{\frac{\Delta V}{v_2}} - 1 \quad (9.4.3)$$

Now, equation 9.4.4 gets plugged into equation 9.4.1 and everything is solved for in terms of . The complete analysis is in MATLAB file "DSA.m".

9.4.3 Solution

To reiterate, this analysis was a cost comparison between the novel solution and traditional chemical methods for a LEO to outward burn. The results of the tables and figure(s) are for a velocity step of 3.5 km/s, which is the velocity budget between LEO and a mars transfer orbit.

Table 9.2 The results of this table were obtained from MATLAB file DSA.m

Parameter	Electric Value (Ar)	Chemical Value	Units
Initial mass	81870.7	177148.1	kg
Total cost	127,990	275,510	\$
LEO burn	431.92	2022.19	Kg
DV budget	3500	3500	m/s
	1000	1000	Kg

Table 9.3 Solar array sizing from MATLAB file solararray.m for dv= 3.5 km/s (MOI dv)

Parameter	Value	Units
Power Requirement	25	kW
Array mass	1522.9	kg
Panel surface area	121.83	.
Electrical system mass	1,563	Kg
.	3,637.1	Kg
	1,074.1	Kg

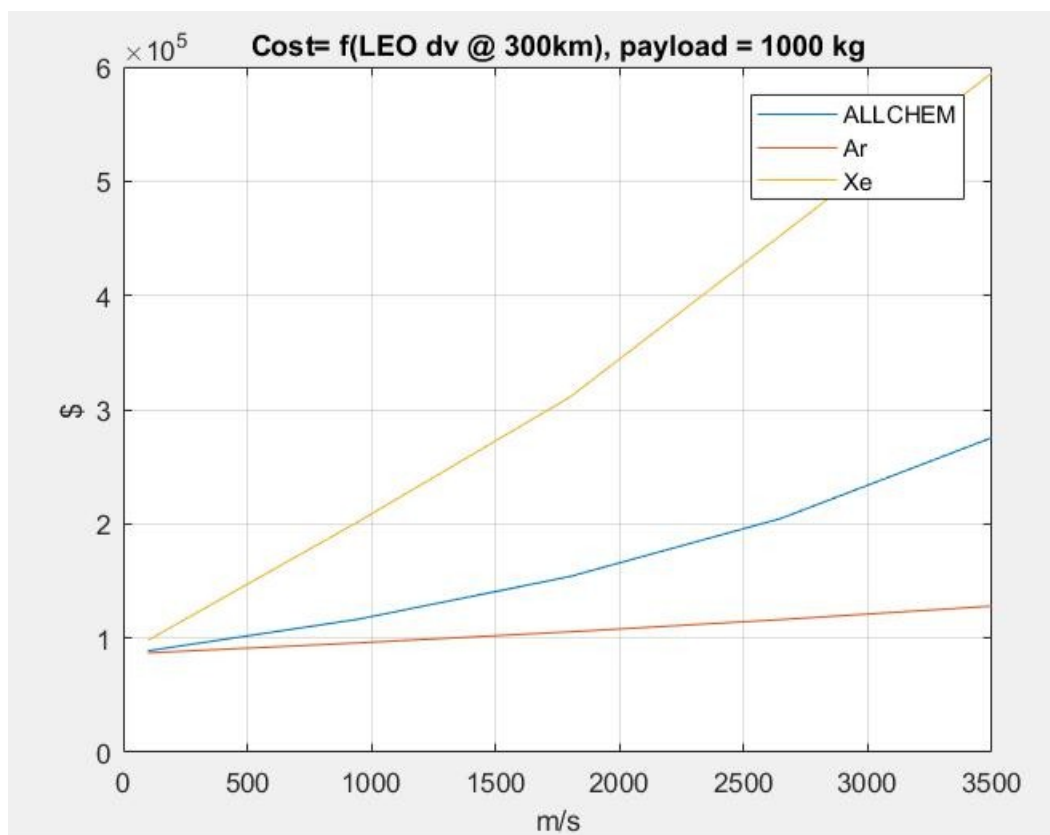


Figure 9.3 Cost comparison from MATLAB DSA.m

Xenon would be chosen as long as an gain of about 80 seconds is considered absolutely necessary, which it likely is. However, still the selection was with Argon for now for the reasons previously listed.

When cost is more of a concern and burn time is not I would go with Argon. The reason the delta V budget analysis stops at 3500 m/s is because from 300 km altitude a dv budget of 3.5 km/s is what is required for a trans Martian insertion orbit. As long as cost is not being considered, an all chemical design is also a plausible choice, yet recall that mission profile is set up so that the final stage burns out in LEO and in order to do anything like a mars orbit insertion at least one chemical stage would be required if not two, (one more for the trans orbit burn and another for Martian orbit capture) adding significantly to cost and weight.

10. Conclusive Remarks

10.1 Project Conclusion

I set out with the daunting task of designing a smaller Variable Specific Impulse Magneto Plasma Rocket engine for satellite payloads that are a bit larger and require more thrust for orbit maintenance than a small satellite; or for smaller satellites attempting to maneuver to nearby orbiting bodies.

The initial prospect was a VASIMR engine of a smaller diameter and a lower power requirement, capable of still attaining these goals. The lower power was going to be the result of using electron bombardment rather than RF bombardment and the higher efficiency was going to come from an ICRH section and an expanding magnetic nozzle. The results of the Paschen's Law analysis of chapter 7, where experimental investigation led to independent verification of a regime of gap distances coherent to Paschen's Law for voltage breakdown in air of between 2 → 4 cm, and ionization costs for this regime of from 8,000 → 13,500 eV meant that the RF bombardment scheme had to be abandoned. An ionization cost of just 8,000 eV per primary emission electron translates to a power requirement of ≈ 1.5 +

4 / , not including the inducting magnetic coils or the ICRH power requirements. So, obviously for a propulsion system desiring to operate near 1 N that scheme wasn't going to work.

The idea then occurred that the issue with ion propulsion (limited by cathode/anode decay) is not so much the which sometimes can get decently above 3,000 seconds, but to a decent extent, is the restriction by the cathodes and anodes on the mass flow rate. If the cathodes and anodes could be removed from ion and hall thrusters then there wouldn't be anything preventing them, theoretically, from being able to produce more thrust.

Chapter 9 details the design process of a compromise in thrust along those lines between the original intent of the project which was variable and a thrust of 1 to 2 Newtons, and the much more practical .6 N and "low" ($\approx 1,019$). By not being so concerned with specific impulse I was able to realize that the true advantage of using RF bombardment was not just its efficiency but it's capacity to ionize larger volumes of propellant. This idea led to the development of the thruster in chapter 9, for which the design parameters have been summarized below in table 10.1

Table 10.1 summarized results of the novel design of table 9.1

Parameter	Value	Units
(Argon)	1019	S
.	0.0612	mg/s
F	0.6118	N
requirement	≈ 25	kW
	≈ 99	eV
	72% \pm 9%	%
	$\approx 10\%$	%

	41,067	kg
B	2.0	Tesla
Propellant	Argon	

This design was then used to come up with a cost analysis for comparison to chemical methods as well as using Xenon instead of Argon in an identical electric set up. The result of that analysis was that Xenon was expensive but where cost is less important than it might be preferable over Argon. See figure 9.3 for details.

Much is made in this report of the choice by AdastrA to use Argon. The exact reason for this selection is not published but from the time I have spent on this report I get the feeling that the reason has nothing to do with cost. The reason seems to be more related to the absorption efficiency of Argon within the ICRH of VASIMR as possibly compared to Xenon or Krypton. The VASIMR project vastly out paces the cost of Xenon gas by billions of dollars and published data for the Helicon RF shows positive results for a correlation between increasing atomic mass to ionization cost ratios among the noble gases where that such ratio is largest. Yet, there was one report dealing with Krypton and Argon in the Helicon RF which cited concern over multiple stable isotopes of Krypton which might cause unsteady absorption efficiencies in the ICRH. It was for this reason and the lack of published data that I selected Argon and not Krypton or Xenon in the propellant selection process.

This Novel design requires a few more years of development at least, but I believe I have accomplished my task of providing a fundamental understanding of electric propulsion and laying out a design basis for future investigations into the performance trade-off's in terms of thrust and power required for the three propellants, Argon, Krypton & Xenon within the presented novel design.

10.2 Future Plans

The next step is to get enough funding to be able to experimentally investigate the concepts outlined in chapter's 7 through 9 and the conclusion. Investigation would begin by constructing Paschen curves for the 3 Nobel gases (Xe, Ar & Kr) at near-vacuum pressures and temperatures. These results would contribute to propellant selection based on maximizing by minimizing ionization cost.

Following this, experimental investigations would pertain to the characteristics of charged particle trapping in a magnetic mirror to further optimize electrical efficiency. In addition, investigation of the propellant atoms in order to understand the role the multiple stable isotopes of Xe & Kr play in the movement of the optimal absorption location within the ICRF antenna, needs to be done to maximize optimality.

Investigation of these performance parameters is key in developing this novel thrusting apparatus because the of the novel solution presented in chapter 9 barely exceeds 1000 seconds and operates at a relatively high mass flow rate for comparable ion thrusters. This fact is demonstrated by figure 9.2 in the preceding section. Improvements need to be made to the power to thrust ratio by both bringing down operational power costs and improving thruster efficiency beyond 10%, in order to boost the total thrust of the novel design to the eventual goal of 1 N.

11. Citations

[1] Diaz, F. R. C. (2000). The VASIMR rocket. *Scientific American*, 283(5), 90-97.

- [2] Squire, J. P., Chang, F. R., Jacobson, V. T., McCaskill, G. E., Bengtson, R. D., & Goulding, R. H. (2000). Helicon plasma injector and ion cyclotron acceleration development in the VASIMR experiment.
- [3] Sutton, G. P. (1986). *Rocket propulsion elements: An introduction to the engineering of rockets* (8th ed.). New York: Wiley.
- [4] Mattingly, J. D. (1996). *Elements of gas turbine propulsion*. New York: McGraw-Hill.
- [5] VASIMR Laboratory Experiment [Digital image]. (n.d.). Retrieved September 28, 2016
- [6] Squire, J. P., Olsen, C. S., Chang Díaz, F. R., Cassady, L. D., Longmier, B. W., Ballenger, M. G., ... & Bering III, E. A. (2011, September). VASIMR® VX-200 operation at 200 kW and plume measurements: future plans and an ISS EP test platform. In *32nd International Electric Propulsion Conference, Weisbaden*.
- [7] Bering, E., Chang-Díaz, F., Squire, J., Brukardt, M., Glover, T., Bengtson, R., . . . Cassady, L. (2008). Electromagnetic ion cyclotron resonance heating in the VASIMR. *Advances in Space Research*, 42(1), 192-205. doi:10.1016/j.asr.2007.09.034
- [8] Northern Lights. (n.d.). Retrieved September 30, 2016, from <http://www.northernlightscentre.ca/northernlights.html>
- [9] Fiehler, D., & Oleson, S. (2003). A comparison of electric propulsion systems for Mars exploration. *American Institute of Aeronautics and Astronautics*.
- [10] Our Engine. (n.d.). Retrieved September 30, 2016, from <http://www.adastrarocket.com/aarc/VASIMR>
- [11] Layers of the sun. (n.d.). Retrieved September 30, 2016, from http://www.nasa.gov/mission_pages/iris/multimedia/layerzoo.html
- [12] Krider, E. P., NOOGLE, MA UMAN, M. C., & ORVILLE, R. (1974). Lightning and the apollo 17/saturn V exhaust plume. *Journal of Spacecraft and Rockets*, 11(2), 72-75.
- [13] F-1 Engine. (n.d.). Retrieved September 30, 2016, from https://history.msfc.nasa.gov/saturn_apollo/documents/F-1_Engine.pdf
- [14] Brophy, J. R., Kakuda, R. Y., Polk, J. E., Anderson, J. R., Marcucci, M. G., Brinza, D., ... & Sovey, J. (2000). Ion propulsion system (NSTAR) DS1 technology validation report. *JPL Publication 00-10, October*.
- [15] A step forward in heating technology | EUROfusion. (n.d.). Retrieved September 30, 2016, from <https://www.euro-fusion.org/newsletter/a-step-forward-in-heating-technology/>
- [16] Longmier, B. W., Bering III, E. A., Carter, M. D., Cassady, L. D., Chancery, W. J., Glover, T. W., ... & Squire, J. P. (2011). Ambipolar ion acceleration in an expanding magnetic nozzle. *Plasma Sources Science and Technology*, 20(1), 015007.
- [17] S. (n.d.). Nuclear Test Ban Treaty. Retrieved November 10, 2016, from
- [18] S. (n.d.). What is chemical propulsion? - Northwestern University. Retrieved November 10, 2016,
- [19] S. (n.d.). Electromagnetism. Retrieved November 18, 2016, from <http://siarchives.si.edu/history/exhibits/henry/electromagnetism>
- [20] Benson, T. (2014, June 12). Brief History of Rockets. Retrieved November 18, 2016, from https://www.grc.nasa.gov/WWW/K-12/TRC/Rockets/history_of_rockets.html

- [21] Dunbar, B. (n.d.). Hermann Oberth. Retrieved November 18, 2016, from <https://www.nasa.gov/audience/foreducators/rocketry/home/hermann-oberth.html>
- [22] Verein für Raumschiffahrt (VfR). (2012, June 4). Retrieved November 18, 2016, from <http://weebau.com/history/vereinfurraumschiffahrt.htm>
- [23] 20. HISTORIC VIEW OF THE VEREIN FUER RAUMSCHIFFAHRT, 1930. LEFT TO RIGHT: RUDOLF NEBEL, FRANZ RITTER, UNKNOWN, KURT HEINISCH, UNKNOWN, HERMANN OBERTH, UNKNOWN, KLAUS RIEDEL, WERNHER VON BRAUN, UNKNOWN, KLAUS RIEDEL HOLDS EARLY VERSION OR MODEL FOR THE MINIMUM ROCKET, 'MIRAK'. - Marshall Space Flight Center, Redstone Rocket (Missile) Test Stand, Dodd Road, Huntsville, Madison County, AL. (n.d.). Retrieved November 18, 2016, from <http://www.loc.gov/pictures/item/al1184.photos.047001p/>
- [23] Konstantin Tsiolkovsky - Alchetron, The Free Social Encyclopedia. (2014). Retrieved November 18, 2016, from <http://alchetron.com/Konstantin-Tsiolkovsky-1198740-W>
- [24] Take A Vacation to Mars (Or an Intro to Rocket Science). (n.d.). Retrieved November 18, 2016, from <http://www.occupiedmars.com/science/2016/04/02/take-a-vacation-to-mars.html>
- [25] Hermann Oberth Space Travel Museum. (n.d.). Retrieved November 18, 2016, from <http://www.atlasobscura.com/places/hermann-oberth-museum>
- [26] Wernher von Braun. (n.d.). Retrieved November 19, 2016, from <https://www.britannica.com/biography/Wernher-von-Braun>
- [27] Національний технічний університет України "Київський політехнічний інститут імені Ігоря Сікорського" (n.d.). Retrieved November 19, 2016, from <http://kpi.ua/en/node/9398>
- [28] Rockets and Missiles. (2012, January 1). Retrieved November 19, 2016, from <http://spaceline.org/rocketsum/jupiter-c.html>
- [29] *The Race for space* [Video file]. (n.d.). Retrieved September 09, 2016.
- [30] Mitchell, D. P. (n.d.). Lunar Impact. Retrieved November 20, 2016, from http://mentallandscape.com/L_Luna2.htm
- [31] A. (2011, October 10). Sputnik and The Dawn of the Space Age. Retrieved November 22, 2016, from <http://history.nasa.gov/sputnik/>
- [32] Silva, G. D., Rufino, S. C., & Iha, K. (2013). Green Propellants - Oxidizers. *Journal of Aerospace Technology and Management*, 5(2), 139-144. doi:10.5028/jatm.v5i2.229
- [33] Guery, J. F., Chang, I. S., Shimada, T., Glick, M., Boury, D., Robert, E., ... & Glick, R. (2010). Solid propulsion for space applications: An updated roadmap. *Acta Astronautica*, 66(1), 201-219.
- [34] Nance, J. C. (1965). Nuclear pulse propulsion. *IEEE Transactions on Nuclear Science*, 12(1), 177-182.
- [35] Dunbar, B. (2016, January 11). Ion propulsion. Retrieved November 27, 2016, from <https://www.nasa.gov/centers/glenn/about/fs21grc.html>
- [36] Rayman, M. D., Varghese, P., Lehman, D. H., & Livesay, L. L. (2000). Results from the Deep Space 1 technology validation mission. *Acta Astronautica*, 47(2-9), 475-487. doi:10.1016/s0094-5765(00)00087-4
- [37] Murphy, E. L., & Good Jr, R. H. (1956). Thermionic emission, field emission, and the transition region. *Physical review*, 102(6), 1464.

- [38] The Physics of Rockets. (n.d.). Retrieved November 27, 2016, from http://genesmission.4t.com/Physics/Laws_of_Motion/Rockets.html
- [39] Goebel, D. M., & Katz, I. (2008). Fundamentals of Electric Propulsion. doi:10.1002/9780470436448
- [40] Chang-Díaz, F. R. (2006). Plasma propulsion for interplanetary flight. *Thin Solid Films*, 506, 449-453.
- [41] Squire, J. P., Chang-Díaz, F. R., Carter, M. D., Cassady, L. D., Chancery, W. J., Glover, T. W., ... & Deline, C. A. (2007, September). High power VASIMR experiments using deuterium, neon and argon. In *30th International Electric Propulsion Conference* (No. 2007-181).
- [42] Longmier, B. W., Ballenger, M., Olsen, C. S., Squire, J. P., & Díaz, F. R. C. Performance studies of the VASIMR® VX-200.
- [43] Glover, T. (2004, April). VASIMR: Express Flight to Mars. Cambridge, MA: Mars Week Conference, MIT.
- [44] Longmier, B. W., Squire, J. P., Cassady, L. D., Ballenger, M. G., Carter, M. D., Olsen, C., ... & Bering, E. A. (2011, September). VASIMR VX-200 performance measurements and helicon throttle tables using argon and krypton. In *32nd International Electric Propulsion Conference*.
- [45] Aflori, M., Ivan, L. M., Mihai-Plugaru, M., & Dimitriu, D. G. (2006). Estimating electrons and ions energies in an RF capacitively-coupled argon discharge. *Romanian Journal of Physics*, 51(1/2), 225.
- [46] Chen, F. F. (1991). Plasma ionization by helicon waves. *Plasma Physics and Controlled Fusion*, 33(4), 339.
- [47] Argon. (n.d.). Retrieved April 06, 2017, from https://chemglobe.org/ptoe/_/18.php
- [48] Lux, J. (2004, February 9). Paschen's Law. Retrieved January 5, 2017, from <http://home.earthlink.net/~jimlux/hv/paschen.htm>
- [49] Knight, D. W. (2013). Gas Discharge Tubes. Retrieved Feb. & march, 2017, from http://www.g3ynh.info/disch_tube/intro.html
- [50] Young, H. D., & Freedman, R. A. (2004). *University physics: with modern physics*. San Francisco: Pearson Addison Wesley.
- [51] Kremer, P. (n.d.). ChemGlobe. Retrieved Feb. & march, 2017, from https://chemglobe.org/ptoe/_/18.php

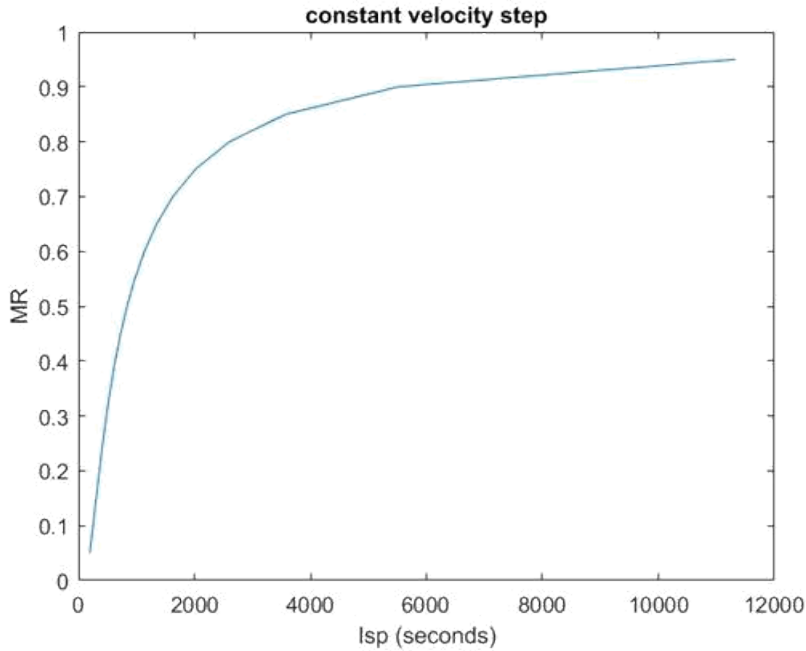
APPENDIX A

```

clear all; close all; clc

% isp = 200:50:10000;
MR = .05:0.05:0.95;
g = 9.81;
du = 5700;
%-----
isp = du./(g*log(1./MR));
% du = -isp./g * log(1/MR);
plot(isp,MR)
title('constant velocity step'); xlabel('Isp (seconds)'); ylabel('MR')

```



The ICRF on the VX-200i consists to two high power applications, the magnetic coils and the helicon RF antenna. The power ratio between these two components varies but for high efficiency it is approximately 4:1 (20% to the antenna and 80% to the magnetic coils). This makes a lot of sense considering the magnetic field strength at the ionization point within the antenna is 2.0 T and the radius of the coils themselves is relatively large at 0.65 meters meaning a lot of power is required to drive them.